

*The Generation & High Resolution
Spectroscopic Detection of Free
Radicals in the Gas Phase*

A Thesis submitted by
NEIL ALAN ISAACS
for the degree of
DOCTOR OF PHILOSOPHY
in the
FACULTY OF SCIENCE
of the
UNIVERSITY OF LEICESTER

Department of Chemistry,
The University,
LEICESTER. LE1 7RH

February 1986

UMI Number: U360126

All rights reserved

INFORMATION TO ALL USERS

The quality of this reproduction is dependent upon the quality of the copy submitted.

In the unlikely event that the author did not send a complete manuscript and there are missing pages, these will be noted. Also, if material had to be removed, a note will indicate the deletion.



UMI U360126

Published by ProQuest LLC 2015. Copyright in the Dissertation held by the Author.
Microform Edition © ProQuest LLC.

All rights reserved. This work is protected against
unauthorized copying under Title 17, United States Code.



ProQuest LLC
789 East Eisenhower Parkway
P.O. Box 1346
Ann Arbor, MI 48106-1346



Dedicated to my Parents

for understanding

and to

Sally my fiancée

for waiting

STATEMENT

The majority of the experimental work described in this thesis was carried out by the author, except where otherwise stated in the text, in the Department of Chemistry of the University of Leicester during the period September 1981 and September 1985. The experimental work contained in Chapter V was performed by the author as a guest worker of Dr. P.B.Davies in the Department of Physical Chemistry of the University of Cambridge.

The work in this thesis is not being currently presented for any other degree.

All work recorded herein is original unless otherwise stated in the text or by reference.

February 1986

Signed: _____

ACKNOWLEDGMENTS

I would like to thank Dr.D.K.Russell for all his help, patience, guidance and encouragement during the course of this work, particularly when results seemed elusive. I would also like to thank Dr.P.B.Davies for both his hospitality and his guidance and Simon Johnson for proving to be such an amicable colleague during the experiments performed at Cambridge. I am also extremely grateful to all the Department of Chemistry's workshop staff without whose skill, advice and co-operation this thesis would not have been possible. I would also like to thank Ann Crane for turning my scribbles into intelligible figures and Philip Acton for his help with the electronics.

LIST OF CONTENTS

LIST OF CONTENTS

<u>LIST OF CONTENTS</u>	5
<u>LIST OF CONTENTS OF FIGURES</u>	11
<u>GENERAL INTRODUCTION</u>	14
<u>CHAPTER I - THEORETICAL BACKGROUND</u>	21
I.1 Introduction	21
I.2 The "effective" Hamiltonian	21
I.3 Atoms	22
I.4 Molecules	27
I.5 References	38
<u>CHAPTER II - GENERATION BY MICROWAVE DISCHARGE</u>	39
II.1 Introduction	39
II.2 Review of Species Generated by Microwave Discharge	39
II.3 Experimental	44
II.3 (i) The Iodine Atom System	44
II.3 (ii) The Fluorine Atom System	45
II.4 Results and Discussion	46
II.4 (i) The Iodine Atom System	46
II.4 (ii) The Fluorine atom System	48
II.5 Conclusions	52
II.6 References	53
<u>CHAPTER III - GENERATION BY GLOW ELECTRICAL DISCHARGE</u>	59
III.1 Introduction	59
III.2 Review of Species Generated by Electrical Discharge	59
III.3 Developmental	62

LIST OF CONTENTS

III.3 (a) Within the EPR Spectrometer Cavity	64
III.3 (b) Within the MMR Spectrometer Cavity	66
III.3 (c) Within the IDL Absorption Tube	66
III.4 Experimental	66
III.4 (a) Within the EPR Spectrometer Cavity	66
III.4 (a) (i) The Oxygen Atom System	66
III.4 (a) (ii) The Fluorine Atom System	67
III.4 (b) Within the MMR Spectrometer Cavity	69
III.4 (b) (i) The Sulphur Monoxide Radical System	69
III.4 (c) (i) The Silicon Hydride and Silylene Radical Systems	69
III.5 Results and Discussion	70
III.5 (a) Within the EPR Spectrometer Cavity	70
III.5 (b) Within the MMR Spectrometer Cavity	71
III.5 (c) Within the IDL Absorption Tube	71
III.6 Conclusions	71
III.7 References	73

CHAPTER IV - GENERATION BY CARBON DIOXIDE LASER AND
SULPHUR HEXAFLUORIDE PHOTSENSITISATION

<u>SULPHUR HEXAFLUORIDE PHOTSENSITISATION</u>	76
IV.1 Introduction	76
IV.2 Review	76
IV.3 Experimental	81
IV.3 (a) The Silicon Containing Intermediates for Detection by IDL Spectroscopy	81
IV.3 (a) (i) The 1,1-Dimethylsilacyclobutane System	82
IV.3 (a) (ii) The Vinyl dimethylcarbinoxydimethylsilane System	82
IV.3 (a) (iii) The Dihydridosilacyclobutane System	82

LIST OF CONTENTS

IV.3 (b) The Potential Atom and Radical Sources for High Resolution Spectroscopic Detection	82
IV.3 (b) (i) The Methyl Iodide System	82
IV.3 (b) (ii) The Acetone System	83
IV.3 (b) (iii) The Acetaldehyde System	83
IV.3 (b) (iv) The Iron Pentacarbonyl System	83
IV.3 (b) (v) The Sulphur Hexafluoride System	84
IV.3 (c) The Informative, Indirect and Direct Generation Systems	84
IV.3 (c) (i) The Oxygen Atom Effective Temperature System	84
IV.3 (c) (ii) The Sulphur Monoxide Radical System	85
IV.3 (c) (iii) The Nitrogen Difluoride Radical System	87
IV.3 (c) (iv) The Iodine Atom System	89
IV.3 (c) (v) The Selenium Chloride Radical System	89
IV.4 Results and Discussion	90
IV.4 (a) The Silicon Containing Intermediates for Detection by IDL Spectroscopy	90
IV.4 (a) (i) The 1,1-Dimethylsilacyclobutane System	90
IV.4 (a) (ii) The Vinyltrimethylcarbinoyldimethylsilane System	91
IV.4 (a) (iii) The Dihydridosilacyclobutane System	92
IV.4 (b) The Potential Atom and Radical Sources for High Resolution Spectroscopic Detection	93
IV.4 (b) (i) The Methyl Iodide System	93
IV.4 (b) (ii) The Acetone System	94
IV.4 (b) (iii) The Acetaldehyde System	96
IV.4 (b) (iv) The Iron Pentacarbonyl System	98
IV.4 (b) (v) The Sulphur Hexafluoride System	98

LIST OF CONTENTS

IV.4 (c) The Informative, Indirect and Direct Generation Systems	101
IV.4 (c) (i) The Oxygen Atom Effective Temperature System	101
IV.4 (c) (ii) The Sulphur Monoxide Radical System	105
IV.4 (c) (iii) The Nitrogen Difluoride Radical System	105
IV.4 (c) (iv) The Iodine Atom System	106
IV.4 (c) (v) The Selenium Chloride Radical System	107
IV.5 Conclusions	107
IV.6 References	109

CHAPTER V - DETECTION BY ELECTRON PARAMAGNETIC

<u>RESONANCE SPECTROSCOPY</u>	111
V.1 Introduction	111
V.2 Historical Review	111
V.3 Developmental	118
V.4 Experimental	126
V.4 (i) The Nitric Oxide System	126
V.4 (ii) The Oxygen Atom System	127
V.4 (iii) The Hydrogen Atom System	127
V.4 (iv) The Nitrogen Atom System	127
V.4 (v) The Chlorine Atom System	127
V.4 (vi) The Fluorine Atom System	131
V.4 (vii) The Hydroxyl Radical System	131
V.4 (viii) The Sulphur Monoxide Radical System	131
V.4 (ix) The Methoxy Radical System	131
V.4 (x) The Fluorosulphite Radical System	132
V.4 (xi) The Phosphorus Oxide Radical System	133
V.4 (xii) The Arsenic Oxide Radical System	135

LIST OF CONTENTS .

V.4	(xiii) The Selenium Oxide Radical System	135
V.4	(xiv) The Selenium Nitride Radical System	137
V.4	(xv) The Selenium Chloride Radical System	137
V.5	Results and Discussion	139
V.5	(i) - (vi) The Atom Systems	139
V.5	(vii) - (viii) The Hydroxyl and Sulphur Monoxide Radical Systems	140
V.5	(ix) The Methoxy Radical System	140
V.5	(x) The Fluorosulphite Radical System	140
V.5	(xi) The Phosphorus Oxide Radical System	141
V.5	(xii) The Arsenic Oxide Radical System	143
V.5	(xiii) The Selenium Oxide Radical System	143
V.5	(xiv) The Selenium Nitride Radical System	143
V.5	(xv) The Selenium Chloride Radical System	144
V.6	Conclusions	144
V.7	References	144

CHAPTER VI - DETECTION BY DIODE INFRARED LASER

	<u>ABSORPTION SPECTROSCOPY</u>	149
VI.1	Introduction	149
VI.2	Review	149
VI.3	Experimental	151
VI.4	Results and Discussion	154
VI.5	Analysis	160
VI.6	Conclusions	164
VI.7	References	165

LIST OF CONTENTS

<u>CHAPTER VII - DETECTION BY MILLIMETER WAVE MAGNETIC</u>	
<u>RESONANCE SPECTROSCOPY</u>	167
VII.1 INTRODUCTION	167
VII.2 Developmental	167
VII.3 Experimental	176
VII.4 Results and Discussion	176
VII.5 Conclusions	176
VII.6 References	181
<u>GENERAL CONCLUSIONS</u>	183
<u>APPENDIX I</u> - EQUIPMENT AND CHEMICALS	187
<u>APPENDIX II</u> - OASPEC: Computer program to calculate effective temperatures in the carbon dioxide laser and the sulphur hexafluoride photosensitisation generation method	192
<u>APPENDIX III</u> - NAI2PIV: Computer program to predict and statistically fit vibration-rotation transitions in a $^2\Pi$ molecule	202
<u>APPENDIX IV</u> - QCALC: Computer program to calculate the Q within a Fabry-Perot semi-confocal resonator	223

LIST OF CONTENTS OF FIGURES

LIST OF CONTENTS OF FIGURES

I.3.1	The energy level diagram of the low and high field couplings and EPR transitions in the fluorine atom	25
I.3.2	The energy level diagram and EPR transitions of the oxygen atom	28
I.4.1	The energy level diagram and MMR transition in molecular oxygen	32
I.4.2	The energy level diagram and EPR transitions in a $^2\Pi$ molecule	35
II.4.1	Part of the EPR spectrum of iodine atoms from the products of a 2450 MHz discharge of O_2 mixed with CH_3I	47
II.4.2	Part of the EPR spectrum of fluorine atoms at 8710 and 9409 MHz	49
IV.3.1	The SO radical EPR signal arising from CO_2 laser deposited sulphur and the products of a 2450 MHz discharge in O_2	86
IV.3.2	The NF_2 radical EPR signal from 10.0 mBar of N_2F_4 and 3.0 mBar of SF_6 and a 1.0 Hz chopped laser beam	88
IV.4.1	Pre and post laser pyrolysis infrared spectra of $(CH_3)_2CO$	95
IV.4.2	Pre and post laser pyrolysis infrared spectra of CH_3CHO	97

LIST OF CONTENTS OF FIGURES

IV.4.3	Pre and post laser pyrolysis infrared spectra of Fe(CO) ₅	99
IV.4.4	Pre and post laser pyrolysis infrared spectra of SF ₆	100
IV.4.5	A plot of CO ₂ laser power output versus ln (calculated effective temperature) at incremented O ₂ pressures	104
V.3.1	Schematic diagram of a Varian V-4535 Zeeman cavity containing a quartz pill-box	121
V.3.2	The TE ₀₁₂ mode pattern produced by a quartz pill-box inside a Varian V-4535 Zeeman cavity	123
V.3.3	A scale drawing of the modified Zeeman cavity	124
V.3.4	The TE ₀₁₂ mode pattern produced by the modified Zeeman cavity	125
V.4.1	The EPR spectrum of NO	128
V.4.2	The EPR spectrum of O atoms	129
V.4.3	The EPR spectrum of ³⁵ Cl and ³⁷ Cl atoms	130
V.4.4	An EPR spectrum tentatively assigned to the PO radical	134
V.4.5	Part of the EPR spectrum of the SeO radical showing two signals of differing parities of different phase due to the DC bias	136
V.4.6	Part of the EPR spectrum of the OH radical showing resolved Λ -doublets of differing parities split out by the applied D.C. bias	138
VI.3.1	A schematic block diagram of the experimental arrangement of the absorption cell and infrared diode laser spectrometer	153
VI.4.1	A frequency scan through the Q ₁ (0.5) and Q ₂ (1.5) components of SiH	158

LIST OF CONTENTS OF FIGURES

VI.4.2 A frequency scan through the $R_1(5.5) (2 \leftarrow 1)$ hot band showing the three transient absorptions tentatively assigned to the SiH_2 radical	159
VI.4.3 The graphical output from the asymmetric rotor program predicting the transition and relative intensities of the SiH_2 radical	161
VI.5.1 Graphical output of the predicted transition frequencies and strengths of the SiH radical	162
VI.5.2 Graphical output of the predicted transition frequencies and strengths of the SiH Q-branches	163
VII.2.1 The Variation of (a) power and (b) frequency of output of the IMPATT oscillator as a function of cavity size	169
VII.2.2 A typical plotted trace from the storage oscilloscope arising from the defective IMPATT power supply when connected to the zena diode circuit	170
VII.2.3 Schematic block diagram experimental arrangement of the millimeter magnetic resonance wave spectrometer	172
VII.2.4 Scale drawing of the Fabry-Perot cavity used in the spectrometer	174
VII.4.1 Millimeter wave magnetic resonance spectrum of the $m_j = 0 \leftarrow m_j = -1$ component of the $N = 1, J = 0 \leftarrow J = 1$ transition in O_2	177

GENERAL INTRODUCTION

In many chemical reactions, the observed products, from known reactants, can only be understood by the postulation of some form of mechanism. In such cases, various reactive intermediates, charged species, atoms and free radicals are used to explain the observed phenomena. The existence of these transient species is by inference rather than by actual experimental observation. It is therefore highly desirable to prove the existence of such species unambiguously, both to reinforce the postulated mechanism, and to subsequently predict the course of analogous chemical reactions.

The requirement that any transient production system being employed must be capable of generating a sufficiently high steady state concentration of the transients for even the very sensitive high resolution spectroscopic techniques to detect signals arising from transients has in many cases proved impractical to attain. Three production systems in which absorptions arising from transients were detected are discussed within Chapters II, III and IV of this thesis and the methods described in the first of these two chapters cover the vast majority of the species generated and subsequently detected by high resolution spectroscopic techniques. Other generation methods which also proved successful in producing detectable concentrations of transients have been UV photolysis¹, the application of an electron gun², direct thermal heating^{3,4} and the use of flames⁵. Another related technique is the formation of molecular beams of transients for subsequent detection, but no mention of this technique is made.

The microwave discharge breaks apart stable molecules

GENERAL INTRODUCTION

into transient fragments by the build up of high power microwave radiation within a cavity which contains large electric fields which ionise the gas and lead to plasma formation. This method of generating a detectable steady state concentration is discussed in Chapter II. Similarly, either an alternating or direct current discharge breaks apart stable molecules by electron collision with the gas causing plasma generation, and this method of generating a steady state concentration is discussed in Chapter III. The carbon dioxide laser and sulphur hexafluoride photosensitisation method breaks apart stable precursors by firstly the sulphur hexafluoride absorbing the laser radiation by virtue of an infrared coincidence in the carbon dioxide laser output frequency and a strong bending absorption in the sulphur hexafluoride, and secondly the vibrationally excited or "hot" sulphur hexafluoride molecules colliding with the precursor and imparting this energy to it and causing it to fragment. This method of generating a detectable steady state concentration of transients is discussed in Chapter IV.

The term high resolution spectroscopy encompasses many differing spectroscopic methods and it was neatly defined by Professor Hirota in his recent book⁶, 'A high resolution molecular spectrum denotes a spectrum which exhibits well-resolved rotational structures or it corresponds to the rotational transitions of a molecule (i.e. the pure rotational spectrum). Although direct transitions among fine and/or hyperfine structure components are rarely discussed, they are certainly classified as high resolution spectra.' The high resolution spectroscopic techniques which are

GENERAL INTRODUCTION

discussed in this thesis are electron paramagnetic resonance spectroscopy, infrared diode laser spectroscopy, millimeter wave magnetic resonance spectroscopy, laser magnetic resonance spectroscopy and microwave spectroscopy. The latter two techniques are discussed by reference only.

Electron Paramagnetic Resonance Spectroscopy (EPR) is the tuning of the energy levels within an atom or a molecule containing either electron spin or orbital angular magnetic moments into resonance with microwave radiation by the application of a magnetic field. If the molecule is in the gas phase then information pertaining to the spin-orbit interaction, the spin-rotation interaction and the electron-nuclear interaction can be obtained from its EPR spectrum. In general, the transitions which are observed are those between the magnetic sub-levels of a particular level, although other types of transitions have been observed. The molecule can interact with either the magnetic component (magnetic dipole transitions) or the electric component (electric dipole transitions) of the microwave radiation; the latter being considerably ($\times 1000$) stronger and consequently easier to observe.

For a magnetic dipole or an electric dipole transition to occur within a molecule certain conditions governed by selection rules must be satisfied. Different selection rules apply to the particular case under consideration. EPR spectroscopy as a detection system for transient species is considered in Chapter V.

Infrared diode laser absorption spectroscopy (IDL) is particularly useful for high resolution spectroscopy in the infrared region of the electromagnetic spectrum due to its

GENERAL INTRODUCTION

high sensitivity and high resolution relative to other infrared radiation sources. The diodes themselves can be tuned over about 100 cm^{-1} by altering their environmental temperature and current. Each diode is constructed to operate within a specific region and they emit of the order of milli-Watts of power. Their lasing action is due to a population inversion between the valence and conduction bands in the semi-conductor diode.

The high resolution results from the precision with which the diode's emission frequency can be controlled (0.0001 cm^{-1}) through the temperature and current stability. The high sensitivity arises from the fact that the milli-Watt power output occurs at a narrow, discrete frequency, consequently it only excites a discrete frequency transition viz. all the power goes directly into that one transition in the transient giving the diode source a relatively high spectral brightness. The more molecules that can be pushed into the higher state (the higher the power) the more intense the transition (the greater the chance of seeing a small absorption from a transient species in low concentration). The high power output of the diode also overcomes the detector noise problem, because all of the power is being emitted and detected at this discrete frequency allowing a larger signal to be generated within the detector. This makes IDL spectroscopy a very useful technique for the detection of transient species and this is borne out by the number of new species detected recently and these are cited in Section VI.2. IDL spectroscopy as a detection system for transient species is considered in Chapter VI.

Silane plasma glow discharges have been used as a source

GENERAL INTRODUCTION

of SiH , SiH_2 and SiH_3 radicals⁷⁻¹⁰ and it is believed that these radicals play a major role in the formation of amorphous silicon hydride films which are currently being employed in the development of solar cells. Interest has centered on the mechanism of the formation and the nature of these films, so a method of monitoring the relative concentrations of these species via their strong spectroscopic transitions may go some way to elucidating the mechanism of formation of these films and data of this type is contained in Chapter VI on the SiH radical. In addition, the carbon analogues of these radicals have now been well characterised in both the optical and high resolution regions of the electromagnetic spectrum and comparison of their molecular parameters should prove informative from a theoretical view point.

Transient species, such as SiH , are also known to exist in stars¹¹ and as non-transients in inter-stellar space, but there is a need for more accurate terrestrial laboratory data on new species to aid these searches, since the nature of the work requires very accurate predictions of the transition frequencies. This would allow the relative concentrations of such species within these environments be obtained.

A region of the electromagnetic spectrum of great interest to molecular spectroscopists is the millimeter wave region, defined roughly by the wavelengths 0.1 and 10 mm (30 - 3000 GHz). The reason for this is that many molecules exhibit their strongest rotational transitions in this range, with the result that the most extensive and accurate structural information may be obtained from observations in this region. However, as is well known, progress in this area

GENERAL INTRODUCTION

has been somewhat slow compared to other regions, largely because of the lack of convenient stable, powerful and tunable sources radiation sources, particularly above about 100 GHz (for an excellent account of the point, see Krupnov, Section VII.6, Ref.1). Among the methods used have been the generation of harmonics from lower frequency sources, usually klystrons, (Section VII.6, Ref.2) far-infrared lasers (Section VII.6, Ref.3) and wave mixing (Section VII.6, Ref.4). While these methods have gone some way to resolving these problems, there is still a need for further development in this area. Chapter VII reports the first use of a solid state oscillator in the millimeter wave region as a source in molecular spectroscopy using the millimeter wave magnetic resonance spectrometer. The technique is very similar to EPR spectroscopy except that the transitions observed occur between the magnetic sub-levels of different rotational levels whereas, generally, they occur within the same rotational level in EPR spectroscopy.

REFERENCES

1. S.Aditya & J.E.Willard, J. Chem. Phys., 44, 833 (1966).
 2. R.Panock, M.Rosenbluh, B.Lax & T.A.Miller,
Phys. Rev., 22A, 1050 (1980).
 3. P.B.Davies, B.J.Handy & D.K.Russell,
Chem. Phys. Letts., 68, 395 (1979).
 4. H.M.Pickett & T.L.Boyd, J. Mol. Spec., 75, 53 (1979).
 5. K.M.Evenson, H.E.Radford and M.M.Moran,
Applied Phys. Letts., 18, 426 (1971).
 6. "High-Resolution Spectroscopy of Transient Molecules",
Published by Springer-Verlag Chemical Physics 40, (1985).
 7. J.Perrin & E.Delafosse,
J. Phys. D: Appl. Phys., 13, 759 (1980).
 8. P.Kocian, Thin Solid Films, 80, L81 (1981).
 9. M.Taniguchi, M.Hirose, T.Hamasaki & Y.Osaka,
Appl. Phys. Lett., 37, 787 (1980).
 10. J.M.Jasinski, E.A.Whittaker, G.C.Bjorklund, R.W.Dreyfus,
R.D.Estes & R.E.Walkup,
Appl. Phys. Lett., 44, 1155 (1984).
 11. Bull. Astron. Inst. Neth., 17, 311 (1964).
-

CHAPTER I - THEORETICAL BACKGROUNDI.1 INTRODUCTION

In this chapter the relevant theoretical background to the following chapters is outlined. Initially, a qualitative description of the construction and application of the "effective" Hamiltonian is given. This is followed by a discussion of some of the more important aspects of the energy levels of atoms, with particular emphasis being paid to the spectra of atoms which are considered in this thesis. Finally, a similar discussion for molecules is presented.

I.2 THE "EFFECTIVE" HAMILTONIAN

The general approach to the assignment and analysis of spectroscopic observations is, of course, well known, and the details of this procedure can be found in a number of texts¹⁻³. The general procedure can be summarised as follows. Firstly, a Hamiltonian is constructed: for the present purposes it can be considered as a quantum mechanical operator equivalent of the classical energy. Secondly, a suitable basis set is constructed: this is a complete set of functions upon which calculations are performed, usually a set which are eigenfunctions of the major terms in the Hamiltonian. In practical spectroscopy, the Hamiltonian is usually reduced to an "effective" Hamiltonian working within a small basis sub-set of the total basis set. The effect of this reduction is to alter the interpretation of the parameters appearing in the Hamiltonian, and to introduce new terms. An example of the former effect is the variation of the spin-orbit coupling constant with vibrational level in SiH (Chapter VI), and of the latter effect is the Λ -doubling observed in the EPR spectrum of

SECTION I.2 - THE "EFFECTIVE" HAMILTONIAN

the NO (Chapter V). The matrix elements of the "effective" Hamiltonian within the chosen basis set (usually truncated to reduce computation time) are then calculated using standard techniques⁴. The resultant matrix is then diagonalised (transformed so that the off-diagonal elements are reduced to zero), and the eigenvalues which are subsequently generated are the energy levels of the system under consideration. Should the intensities of the transitions be required, the eigenvectors may also be returned from the diagonalisation procedure. A prediction of the general form of the spectrum can be obtained by an application of the selection rules pertinent to the system under consideration. These are the changes in the quantum numbers which describe the basis set. Transitions which obey these rules are "allowed", and are usually strong in intensity. Transitions allowed by terms in the Hamiltonian which mix the basis set are usually weaker and are known as "forbidden". There are of course transitions which are absolutely forbidden and these are never observed under any circumstances. The selection rules are generally derived from group theory.

I.3 ATOMS

The Hamiltonian appropriate to the energy levels within atoms in this thesis has been known for many years⁵. In general, the following terms are incorporated:

- (i) the electronic energy, sometimes calculated from SCF or other calculations, but more usually taken as an experimental parameter (if only the ground state of atoms is being considered this can be set to zero);
- (ii) the spin orbit-coupling, arising from the interaction

SECTION I.3 - ATOMS

between the magnetic moments associated with the electron spin (\underline{S}) and the orbital angular momentum (\underline{L}), and this is usually expressed in the form $A \underline{L} \cdot \underline{S}$ (where A is the spin-orbit coupling constant);

- (iii) the Zeeman effect, which arises from the interaction of the magnetic moments in the atom with an applied magnetic field (expressed in its simplest form as two scalar terms, $\mu_B (g_s \underline{S} + \underline{L})$, where μ is the Bohr magneton, and $g_s = 2.00232$;
- (iv) the nuclear hyperfine effects arising from the interaction of the nuclear magnetic moment with the electronic magnetic moments usually written as the sum of three terms (the Fermi contact interaction, the electron spin/nuclear spin dipole-dipole interaction and the electron orbital/nuclear spin interaction²);
- (v) the nuclear quadrupole interaction, arising from the non-spherical charge distribution in the nucleus with electric field gradients in the atom (this is a tensorial interaction).

The EPR spectrum of the fluorine atom, F, may serve as an example to illustrate some of these terms. The F atom has an electron configuration $(1s)^2(2s)^2(2p)^5$, leading to the ground state term of 2P (i.e. a state of spin multiplicity of $2S + 1 = 2$, and a total orbital angular momentum of 1). In the Russell-Saunders coupling scheme⁵, this leads to the states of total angular momentum described by the quantum number J , $J = 1 \pm 1/2$, i.e. $J = 1/2$, and $J = 3/2$. Since the unfilled 2p shell is more than half full the latter of these is the lower in terms of relative energy (i.e. this is an inverted as opposed to a regular doublet), the splitting being about

404 cm^{-1} ⁶. The F nucleus ($I = 1/2$), interacts with the electronic magnetic moments. At zero applied magnetic field, this coupling implies that an appropriate basis set for calculations is the coupled representation, described by the total angular momentum quantum number, F, where,

$$\underline{F} = \underline{J} + \underline{I} \quad (\text{I.3.1})$$

The possible values of F are therefore 2 and 1 for the $J = 3/2$ level, and 1 and 0 for the $J = 1/2$ level. At low magnetic fields, each F level splits out into $(2F + 1)$ magnetic sub-levels, labelled by the quantum number M_F ($M_F = -F, -F + 1, \dots, +F - 1, +F$). At high magnetic fields (where the coupling of the electron magnetic moment to the field exceeds the electron/nuclear coupling), a more appropriate description is the decoupled set, where each J level splits into $(2J + 1)$ magnetic sub-levels, and further into $(2I + 1)$ levels due to the hyperfine effect. Both these limits are illustrated in Figure I.3.1, which also shows the correlation between these two descriptions.

Also shown in Figure I.3.1 are the observed EPR transitions (Chapter II, Section II.4). These may be predicted by an application of the selection rules,

$$\Delta F = 0, \pm 1 \text{ and } \Delta M_F = 0, \pm 1 \quad (\text{I.3.2})$$

and,

$$\Delta J = 0, \pm 1, \Delta m_J = 0, \pm 1 \text{ and } \Delta m_I = 0 \quad (\text{I.3.3})$$

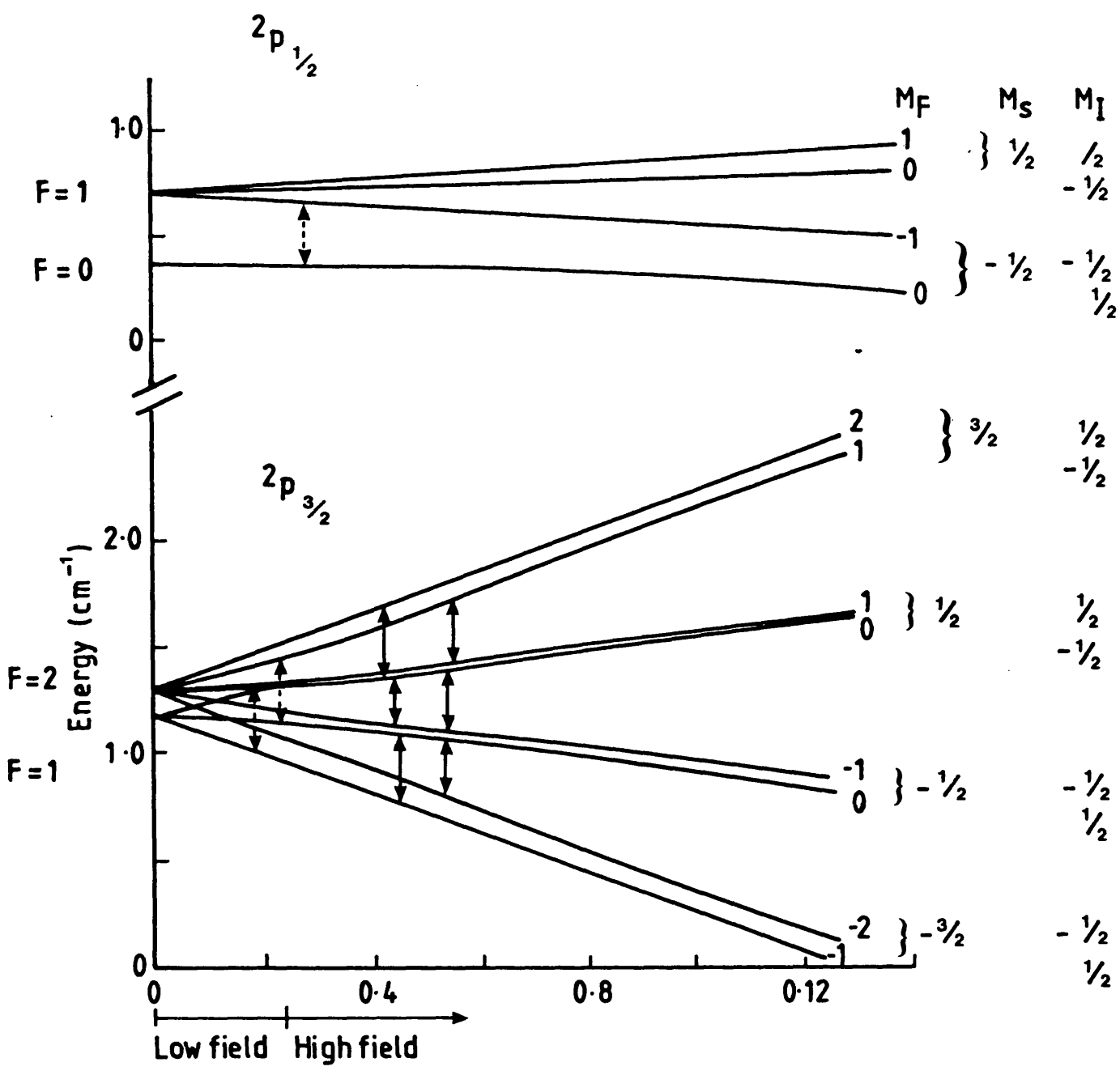


Figure I.3.1. The energy levels of the F atom as a function of magnetic field. Also shown are the low field (the dashed lines) and the high field (full lines) EPR transitions.

SECTION I.3 - ATOMS

appropriate to the low and high field cases respectively. In most EPR spectrometers, the magnetic component of the microwave radiation is perpendicular to the applied magnetic field, so that only transitions in which Δm_f (or Δm_j) = ± 1 are observed: in addition, the energy gap between the $J = 1/2$ or $3/2$ levels effectively eliminates the $\Delta J = \pm 1$ transitions. The low field transitions indicated by the dashed lines within the $^2P_{3/2}$ level in Figure I.3.1 are formally "forbidden" by the high field selection rules (I.3.2), and are indeed much weaker as is illustrated by the observed spectrum (Chapter II, Section II.3 (ii)). The approximate field of the strong transitions (the full lines in Figure I.3.1) may be predicted using the relation,

$$\Delta E = \mu B g_j \Delta m_j \quad (\text{I.3.4})$$

where the hyperfine effects have been neglected, and g_j is the well known Landé g -factor⁷,

$$g_j = 1 + \frac{S(S + 1) + J(J + 1) - L(L + 1)}{2J(J + 1)} \quad (\text{I.3.5})$$

With $\Delta E = 9000$ MHz, $\mu = 14$ MHz mT^{-1} , $g_j = 4/3$ this predicts a magnetic field of 0.48 T for the observed spectrum. In practice, the magnetic field also mixes in levels of different J , leading to a slight curvature of the magnetic sub-levels (known as the second-order Zeeman effect), and the prediction as a consequence is not exact. The relative intensities of the transitions indicated in Figure I.3.1 are governed by a

SECTION I.3 - ATOMS

combination of Boltzmann factors, angular momentum factors, and the extent of mixing between the various levels.

A second example also referred to in Chapters IV and V and Appendix II is that of the EPR spectrum of the oxygen atom, O. O has the electronic configuration $(1s)^2(2s)^2(2p)^4$, leading to a ground state term of 3P . The spin-orbit levels have a total angular momentum of $J = 2, 1, 0$, with a relative energy increasing as J decreases viz. an inverted triplet. The nuclear spin of ^{16}O is zero, so complications from hyperfine effects do not arise. These levels, and their behaviour in a magnetic field, are illustrated in Figure I.3.2 which also shows the observed EPR transitions, which are governed by the selection rules, $\Delta J = 0$, $\Delta m_J = \pm 1$. From Equations I.3.4 and I.3.5, the spectrum is predicted to occur near 0.4 T at a microwave frequency of 9000 MHz, for transitions within both the 3P_2 and 3P_1 levels. As was mentioned above the slight curvature of the levels due to the second order Zeeman effect produces a splitting of the predicted six line pattern: since the $^3P_0 - ^3P_1$ energy spacing is much smaller than the $^3P_1 - ^3P_2$ spacing this effect is larger in the 3P_1 magnetic sub-levels and the observed spectrum consists of a strong central quartet arising from the more populated 3P_2 levels, flanked by a weaker doublet from the less populated 3P_1 levels. This spectrum is described in some detail in Appendix II, which describes a computer program which simulates the observed spectrum (amongst other things).

I.4 MOLECULES

The most complete derivation of a Hamiltonian for molecules is that of Howard and Moss⁸. The situation here is

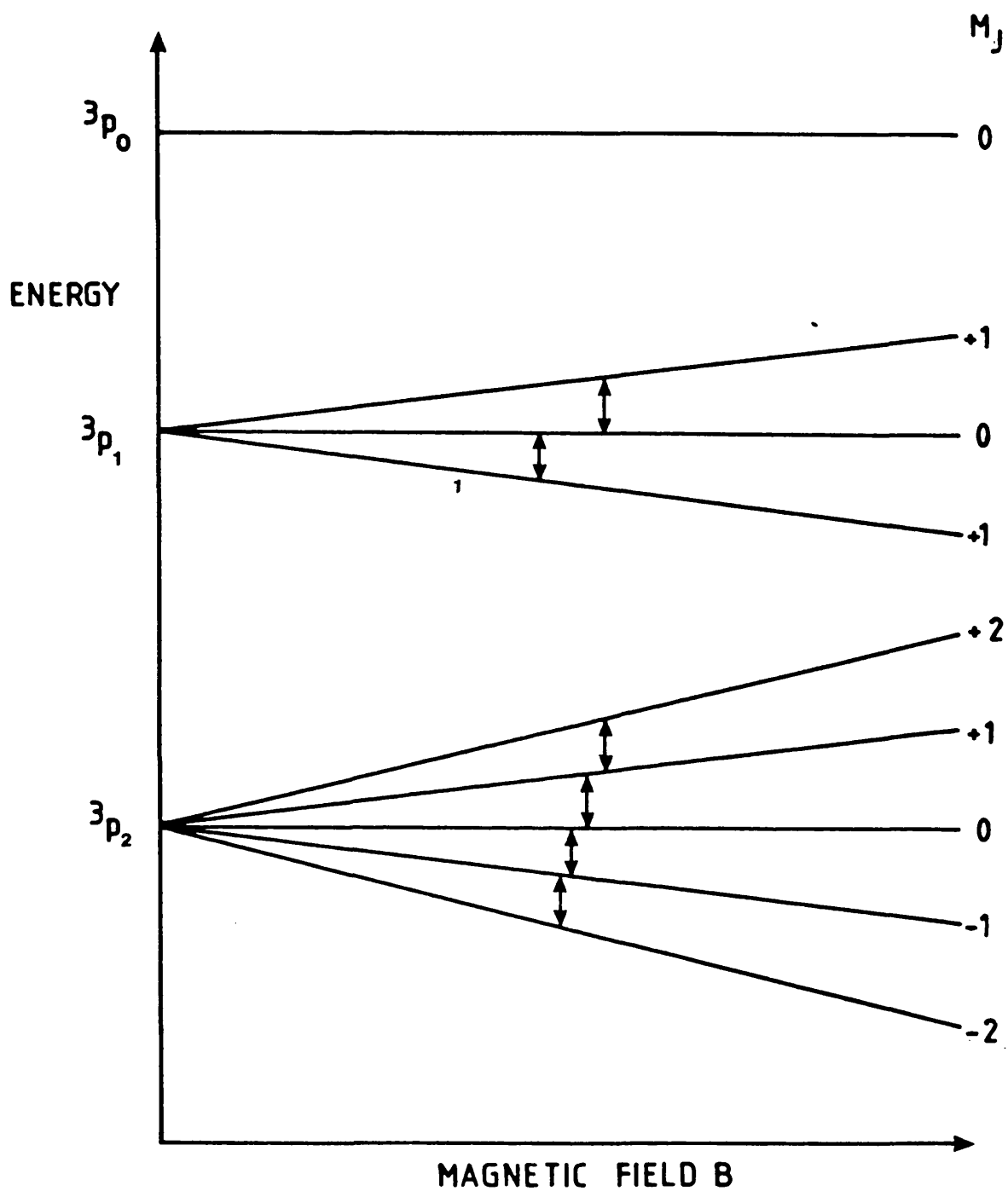


Figure I.3.2. The energy levels of the O atom as a function of magnetic field. The EPR transitions are also shown.

SECTION I.4 - MOLECULES

much more complex than for atoms due to the additional degrees of freedom of nuclear vibrations and rotations. Thus in addition to the terms described in Section I.3 there are expressions describing the following contributions,

- (i) nuclear vibrational energy which in the case of transitions occurring in the ground vibrational state is usually set to zero (e.g. most of the EPR spectra discussed in Chapter V). If a single vibrational transition is observed (e.g. the fundamental vibrational-rotational transitions in SiH described in Chapter VI), the band centre is usually taken as an experimentally determined parameter. In other cases the usual expression is,

$$E_{\text{vib}} = \omega_1(v_1 + 1/2) + \omega_2(v_2 + 1/2) + \dots \quad (\text{I.4.1})$$

where ω_i and v_i are the vibrational frequencies and quantum numbers of the normal mode i respectively. This expression may be used for non-degenerate vibrations, together with appropriate extensions for degenerate vibrations and anharmonicity where necessary⁹.

- (ii) Nuclear rotations. The general expression here is,

$$H_{\text{rot}} = 1/2(N_x^2/I_x + N_y^2/I_y + N_z^2/I_z) \quad (\text{I.4.2})$$

where N_x , N_y , and N_z represent the components of molecular rotational angular momentum around the molecular axes x, y and z , and I_x , I_y and I_z are the moments of inertia around these axes.

- (iii) where necessary, the effect of an applied electric field

(the Stark effect) may be added.

The process of reduction to an "effective" Hamiltonian introduces a number of new complications. For example, the reduction of the Hamiltonian to one which is operating within single vibrational level introduces the phenomenon of centrifugal distortion, and variation of the parameters within the vibrational level (e.g. as in the case of the SiH spectrum in Chapter VI). Reduction to a Hamiltonian operating within a single electronic state introduces such well known effects as the g-tensor anisotropy in solid state ESR¹⁰, and Λ -doubling in the case of some molecules discussed in Chapter V and in SiH in Chapter VI.

The presence of a large number of possible angular momenta within a given molecule leads to a number of different orderings of couplings, dependent upon their relative magnitude: these are commonly known as Hund's coupling cases (Ref.2, Vol.II). The two most commonly used, and the only cases necessary for the molecules discussed within this thesis, are Hund's coupling case (a) and (b) for diatomic molecules. In Hund's case (a) the spin-orbit coupling is large (applicable to $^2\Pi$ electronic states such as in NO and PO). In Hund's case (b), the spin-orbit coupling is assumed to be small or zero and this is used in the case of $^3\Sigma$ electronic states for molecules like O_2 and SO.

The oxygen molecule, with its ground state electron configuration of $(\Pi^*)^2$ (neglecting the filled molecular orbitals) has a ground electronic state of $^3\Sigma_g^-$ symmetry. In the ground state, the two unpaired electrons have parallel spin, and each electron occupies each of the doubly degenerate Π^* (i.e. the axial component of the orbital angular momentum

SECTION I.4 - MOLECULES

$\Lambda = \pm 1$) molecular orbitals, leading to a total spin $S = 1$ and electronic orbital angular momentum component $\Lambda = 0$. The energy levels for molecules in which Hund's case (b) is an appropriate description may be considered as similar to those of a closed shell molecule, but split by the interaction of electron spin and molecular rotation. For a diatomic molecule such as O_2 , the rotational energies are simply,

$$E_{rot} = BN(N + 1) \quad (I.4.3)$$

where the rotational constant, B , is given by,

$$B = \frac{h^2}{8\pi^2 I_x} \quad (I.4.4)$$

and the rotational quantum number, N , has values $0, 1, 2, \dots$. In O_2 , the nuclear spin statistics of the identical ($I = 0$) ^{16}O nuclei preclude the existence of even N rotational levels. The spin ($S = 1$) of the electrons then splits each rotational level, N , into three components labelled by J ,

$$\underline{J} = \underline{N} + \underline{S} \quad (I.4.5)$$

where J now takes the values $N - 1, N, N + 1$ for $S = 1$. In O_2 , the actual ordering of these levels is complicated by the interaction of the spins of the two electrons. At the left-hand side of Figure I.4.1 are shown the two lowest ($N = 1$ and $N = 3$) rotational levels in O_2 : in the centre of Figure I.4.1 are shown the resultant spin split rotational levels.

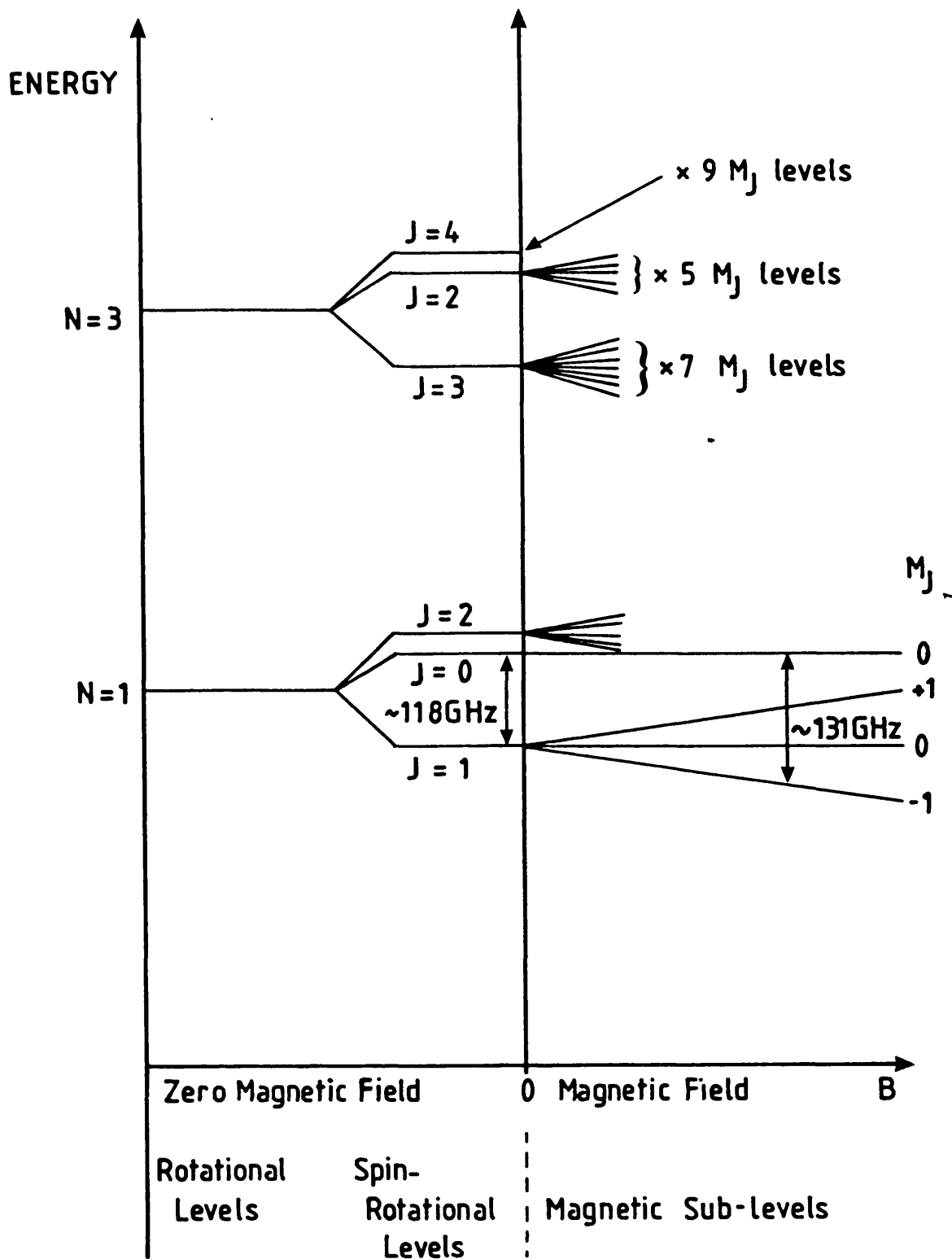


Figure I.4.1. The energies of the two lowest rotational levels in the O_2 molecule (not to scale). For details of the transition shown see text.

SECTION I.4 - MOLECULES

The effect of the application of a magnetic field is to split each spin-rotational level into $(2J + 1)$ magnetic sub-levels, which are shown on the right-hand side of Figure I.4.1. In gas phase EPR, allowed transitions governed by the selection rules,

$$\Delta N = 0, \Delta J = 0, \pm 1, \Delta m_j = 0, \pm 1 \quad (\text{I.4.6})$$

are observed. Since many rotational levels in O_2 are occupied, this molecule has an extremely rich EPR spectrum, as is illustrated in the system in which the I atom is generated (Figure II.4.1). A transition which is described in Chapter VII is also illustrated in Figure I.4.1: this is the $N = 1, J = 1, m_j = 0 \leftarrow N = 1, J = 0, m_j = -1$ transition. At zero magnetic field, this occurs at 118.75 GHz (Ref. 8, Chapter VII), but can be tuned into resonance in the millimeter wave magnetic resonance spectrometer operating at a frequency of 131.8 GHz by applying a magnetic field of 0.667 T. Other examples of molecules which can be described in this manner include SO and SeO, whose EPR spectra are illustrated in Chapter V.

The NO molecule provides a suitable example of Hund's coupling case (a). Here, the ground state electron configuration is $(\pi^*)^1$, so that the ground state in this case has a $^2\Pi$ symmetry. In this case the spin-orbit coupling is strong: the effect of this is to tie the electron spin closely to the nuclear axis (the orbital angular momentum is forced to lie along this axis). The total electronic angular momentum has a component along the axis of,

$$\Omega = \Lambda + \Sigma \quad (\text{I.4.7})$$

Since Λ can take values of ± 1 , and Σ can take values of $\pm 1/2$, the possible values of Ω are $\pm 3/2$ and $\pm 1/2$. In the non-rotating molecule, states of the same $|\Omega|$ are degenerate, and states of different $|\Omega|$ are split by the spin-orbit coupling. In the case of NO, with its less than half-filled shell, the $|\Omega| = 1/2$ (i.e. the ${}^2\Pi_{1/2}$) level lies below the $|\Omega| = 3/2$ (i.e. the ${}^2\Pi_{3/2}$) level as is shown in Figure I.4.2.

When the molecule is allowed to rotate, its motion is described by the total (spin + orbital + rotational) quantum number J . Since $|\Omega|$ must represent the minimum value of J (as it is its component along the molecular axis), the possible values of J are,

$$J = |\Omega|, |\Omega| + 1, |\Omega| + 2, \dots \quad (\text{I.4.8})$$

so that in the example of NO, the ${}^2\Pi_{1/2}$ electronic level has $J = 1/2, 3/2, 5/2, \dots$ whereas the ${}^2\Pi_{3/2}$ electronic level has $J = 3/2, 5/2, 7/2, \dots$. These rotational levels are shown in Figure I.4.2. When the molecule is allowed to rotate, states of opposite Ω are no longer degenerate, and split into two - the phenomenon of Λ -doubling. Since this effect can be regarded as a coupling of the rotational angular momentum and the electron orbital angular momentum, its effect will be largest for molecules with large rotational constants (i.e. those which rotate fastest). In the case of the very light SiH the Λ -doubling is easily resolved even in infrared spectroscopy (Chapter VI): in the very heavy PO (Chapter V), it is not resolved even, by the very high resolution technique of gas

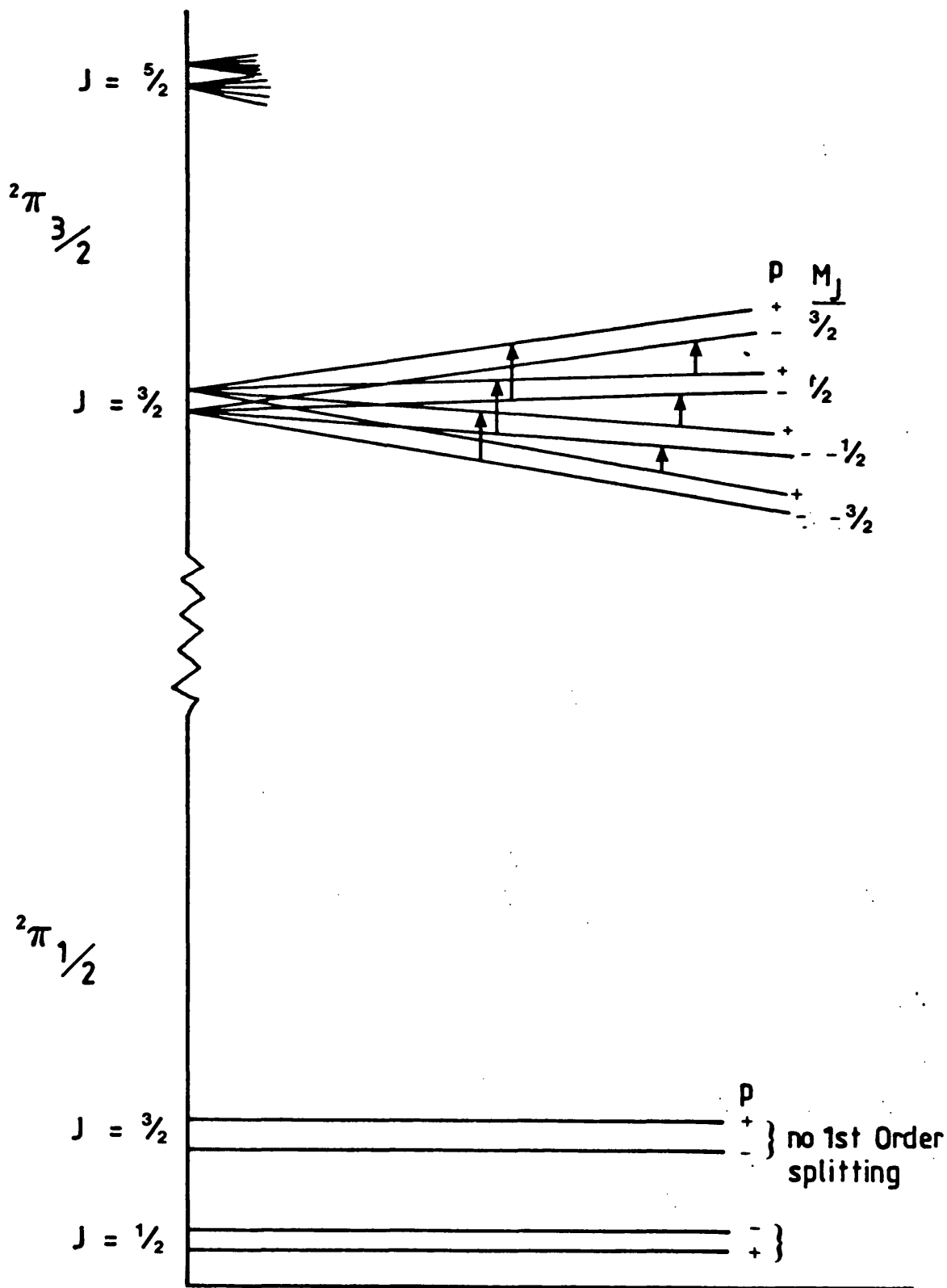


Figure I.4.2. The energy levels of a $^2\Pi$ molecule as a function of magnetic field. For details of the transitions indicated see text.

SECTION I.4 - MOLECULES

phase EPR. In NO, it is resolved as is illustrated in Figure V.4.1.

In the presence of a magnetic field, each rotational level is split into $(2J + 1)$ components. To a first approximation the Zeeman effect can be expressed by,

$$\Delta E_z = g_J \mu_B \Delta m_J \quad (\text{I.4.9})$$

where g_J is now given by,

$$g_J = \frac{(\Lambda + 2\Sigma)\Omega}{J(J + 1)} \quad (\text{I.4.10})$$

For the ${}^2\Pi_{3/2}$, $J = 3/2$ level of NO this yields a value for g_J of 0.8: it is interesting to note that in the ${}^2\Pi_{1/2}$ electronic level, $g_J = 0$, essentially because of the cancellation of the magnetic moments due to spin and orbital contributions in the opposite directions. As in the case of atoms, second-order Zeeman effects can be important: since interactions can now occur between more closely spaced rotational levels, this effect can be quite large, particularly for heavy molecules like PO. The predicted pattern for NO and PO then is of three lines corresponding to the transitions $m_J = -3/2 \rightarrow -1/2$, $-1/2 \rightarrow +1/2$, and the $+1/2 \rightarrow +3/2$ for the lowest $J = 3/2$ level, as is shown in Figure I.4.2.

In NO, the ${}^{14}\text{N}$ nucleus ($I = 1$) will interact with the electronic magnetic moments and produce a three-fold splitting of each line. The overall observed spectrum of NO consists of eighteen lines as is shown in Figure V.4.1. The selection rules

governing this spectrum are,

$$\Delta J = 0, \Delta m_j = \pm 1, \Delta m_l = 0, \Delta P = + \leftrightarrow - \quad (\text{I.4.11})$$

where P is the parity (+ or -) associated with the two fold $|\Omega|$ levels for electric dipole transitions or $\Delta P = + \leftrightarrow +, - \leftrightarrow -$ for magnetic dipole transitions.

The spectrum tentatively assigned to PO in Figure V.4.4 is similar to NO but with some differences. Since PO is heavier than NO, the second-order Zeeman effect splitting is larger, but the Λ -doubling is smaller. Also, since in ^{31}P the nuclear spin is $I = 1/2$, each line is doubled rather than tripled. This predicts a six line spectrum.

I.5 REFERENCES

1. "Molecular Spectra and Molecular Structure I: Diatomic Molecules, by G.Herzberg, Published by Prentice-Hall (1939); "Molecular Spectra and Molecular Structure II: Infrared and Raman Spectra of Polatomic Molecules", by G.Herzberg, Published by Van Nostrand (1945); "Molecular Spectra and Molecular Structure III: Electronic Spectra and Electronic Structure", by G.Herzberg, Published by Van Nostrand (1966).
2. "High Resolution Spectroscopy of Transient Molecules", by E.Hirota, Published by Springer-Verlag Chemical Physics, 40 (1985).
3. "High Resolution Spectroscopy", by J.M.Hollas, Published by Butterworths (1982).
4. D.K.Russell, "Angular Momentum Theory", course notes, Univ. of Cambridge, unpublished (1984).
5. "The Theory of Atomic Spectra", by E.U.Condon & G.H.Shortley, Published by Cambridge University Press (1970).
6. C.E.Moore, Atomic Energy Levels, National Bureau of Standards, Washington (1949).
7. "Atomic Spectra and Atomic Structure", by G.Herzberg, Published by Dover (1944).
8. B.T.Howard & R.E.Moss, Mol. Phys., 19, 433 (1970).
9. "Molecular Vibrations", by E.B.Wilson, J.C.Decius & P.C.Cross, Published by McGraw-hill (1955).
10. "Chemical & Biochemical Aspects of Electron-Spin Resonance Spectroscopy", by M.C.R.Symons, Published by Van Nostrand Reinhold (1978).

SECTION II.1 - INTRODUCTION

CHAPTER II - GENERATION BY MICROWAVE DISCHARGE

II.1 INTRODUCTION

In this Chapter the microwave discharge is examined as a device for producing transient species for detection by high resolution spectroscopic techniques. The type of precursors passed through the discharge and the subsequent species generated for detection or reaction to form other previously undetected species is then reviewed. An account of two new reaction schemes then follows along with the results obtained from these experiments.

II.2 REVIEW OF SPECIES GENERATED BY MICROWAVE DISCHARGE

This section of this Chapter contains a summary of the species produced via a microwave discharge in tabulated form for clarity and brevity. The generated transient species and their precursors are identified by virtue of their chemical formulae and the nomenclature used within the table is defined at the end of the table. The transient species generated by a microwave discharge and detected by one of the four high resolution spectroscopic techniques discussed in this thesis are shown in Table II.2.1.

SECTION II.2 - REVIEW

Species	Generation Method	Detection Method	Reference
As	$(\text{H}_2 + \text{N}_2)_{\text{MW}} + \text{AsCl}_3 + \text{He}$	EPR	1
Br	$(\text{Br}_2)_{\text{MW}}$	EPR	2
C	$(\text{F}_2 + \text{He})_{\text{MW}} + \text{CH}_4$	LMR	3
Cl	$(\text{Cl}_2)_{\text{MW}}$	EPR	4
	$(\text{Cl}_2 + \text{Ar})_{\text{MW}}$	IDL	5
	$(\text{Cl}_2)_{\text{MW}}$	LMR	6
F	$(\text{F}_2 + \text{Ar})_{\text{MW}}$	IDL	7
	$(\text{F}_2)_{\text{MW}}$	EPR	8
Ge	$(\text{CF}_4)_{\text{MW}} + \text{GeH}_4$	LMR	9
H	$(\text{H}_2)_{\text{MW}}$	EPR	10
Hg	$(\text{N}_2 + \text{Hg})_{\text{MW}}$	LMR	11
I	$(\text{O}_2)_{\text{MW}} + \text{CH}_3\text{I}$	EPR	12
N	$(\text{N}_2)_{\text{MW}}$	EPR	13
O	$(\text{O}_2)_{\text{MW}}$	EPR	14
	$(\text{O}_2)_{\text{MW}}$	LMR	15
S	$(\text{H}_2)_{\text{MW}} + \text{H}_2\text{S}$	EPR	16
Sb	$(\text{H}_2 + \text{N}_2)_{\text{MW}} + \text{SbCl}_3$	LMR	17
Se	$(\text{H}_2)_{\text{MW}} + \text{Se}_2\text{Br}_2$	EPR	18
Si	$(\text{CF}_4)_{\text{MW}} + \text{SiH}_4$	LMR	19
AsO	$(\text{H}_2 + \text{O}_2)_{\text{MW}} + \text{As}_{\text{metal}}$	LMR	20
BrO	$(\text{O}_2) + \text{Br}_2$	EPR	21
	(i) $(\text{O}_2)_{\text{MW}} + \text{Br}_2$	LMR	22
	(ii) $(\text{O}_2 + \text{Br}_2)_{\text{MW}}$		
CF	$(\text{CF}_4 + \text{He/Ar})_{\text{MW}}$	LMR	23
	$(\text{CF}_4)_{\text{MW}} + \text{CH}_3\text{CHO, etc.}$	EPR	24
ClO	$(\text{Cl}_2 + \text{O}_2)_{\text{MW}}$	EPR	25

SECTION II.2 - REVIEW

		$(\text{Cl}_2 + \text{O}_2)_{\text{MW}}$	LMR	26
		$(\text{Cl}_2 + \text{He})_{\text{MW}} + \text{O}_3 + \text{O}_2$	IDL	27
		$(\text{Cl}_2 + \text{O}_2)_{\text{MW}}$	MW	28
FO		$(\text{CF}_4)_{\text{MW}} + \text{silica}(\text{SiO}_2)$	IDL	29
		$(\text{CF}_4)_{\text{MW}} + \text{silica}(\text{SiO}_2)$	LMR	30
GeH		$(\text{CF}_4)_{\text{MW}} + \text{GeH}_4$	LMR	31
IO	(i)	$(\text{O}_2)_{\text{MW}} + \text{CH}_3\text{I}$	EPR	32
	(ii)	$(\text{O}_2)_{\text{MW}} + \text{CF}_3\text{I}$		
NF		$(\text{H}_2)_{\text{MW}} + (\text{N}_2\text{F}_4)_{\text{therm}}$	LMR	33
NH/ND		$(\text{CF}_4)_{\text{MW}} + \text{NH}_3/\text{ND}_3$	LMR	34
NS		$(\text{N}_2)_{\text{MW}} + \text{H}_2\text{S}$	EPR	35
NS		$(\text{N}_2)_{\text{MW}} + \text{S}_2\text{Cl}_2$	MW	36
NSe		$(\text{N}_2)_{\text{MW}} + \text{Se}_2\text{Cl}_2$	LMR	37
OH/OD		$(\text{H}_2\text{O}/\text{D}_2\text{O})_{\text{MW}}$	MW	38
OH/OD	(i)	$(\text{H}_2\text{O}/\text{D}_2\text{O})_{\text{MW}}$	EPR	39
	(ii)	$(\text{CF}_4)_{\text{MW}} + \text{H}_2\text{O}$		
OH/OD		$(\text{H}_2)_{\text{MW}} + \text{NO}_2$	LMR	40
PH/PD		$(\text{H}_2\text{O}/\text{D}_2\text{O})_{\text{MW}} + \text{P}_{\text{red}}$	LMR	41
PO		$(\text{H}_2 + \text{O}_2)_{\text{MW}} + \text{P}_{\text{red}}$	LMR	42
PO		$(\text{H}_2 + \text{O}_2)_{\text{MW}} + \text{P}_{\text{red}}$	MW	43
S ₂		$(\text{H}_2)_{\text{MW}} + \text{SCL}_2$	EPR	44
SF		$(\text{CF}_4)_{\text{MW}} + \text{OCS}$	MW	45
SF		$(\text{CF}_4)_{\text{MW}} + \text{OCS}$	EPR	46
SH/SD		$(\text{H}_2\text{O}/\text{D}_2\text{O})_{\text{MW}} + \text{H}_2\text{S}$	EPR	47
SH/SD		$(\text{H}_2/\text{D}_2)_{\text{MW}} + \text{S}_{\text{elem}}$	LMR	48
SO		$(\text{H}_2\text{O})_{\text{MW}} + \text{H}_2\text{S}$	EPR	49
SO		$(\text{O}_2 + \text{CF}_4)_{\text{MW}} + \text{OCS}$	LMR	50
SO	(i)	$(\text{O}_2)_{\text{MW}} + \text{H}_2\text{S}$	MW	51
	(ii)	$(\text{O}_2)_{\text{MW}} + \text{OCS}$		
SeF		$(\text{CF}_4)_{\text{MW}} + \text{OCSe}$	EPR	52

SECTION II.2 - REVIEW

SeH/SeD	$(\text{H}_2\text{O}/\text{D}_2\text{O})+\text{Se}$	LMR	53
SeO	(i) $(\text{O}_2)_{\text{MW}}+\text{OCSe}$	EPR	54
	(ii) $(\text{O}_2)_{\text{MW}}+\text{Se}_2\text{Cl}_2$		
SeO	$(\text{O}_2)_{\text{MW}}+\text{Se}_2\text{Cl}_2$	LMR	55
SeO	$(\text{O}_2)_{\text{MW}}+\text{Se}_2\text{Cl}_2$	MW	56
SiH	(i) $(\text{CF}_4)_{\text{MW}}+\text{SiH}_4$	LMR	57
	(ii) $(\text{F}_2+\text{He})_{\text{MW}}+\text{SiH}_4$		
BO ₂	$(\text{O}_2)_{\text{MW}}+\text{BCl}_3$	IDL	58
CF ₂	(i) $(\text{CF}_4+\text{Ar})_{\text{MW}}$	IDL	59
	(ii) $(\text{CF}_2\text{CFCl}+\text{Ar})_{\text{MW}}$		
CF ₂	$(\text{CF}_4+\text{Ar})_{\text{MW}}$	MW	60
CH ₂	$(\text{F}_2+\text{He})_{\text{MW}}+\text{CH}_4$	LMR	61
ClBO	$(\text{O}_2+\text{BCl}_3)_{\text{MW}}$	IDL	62
FCO	(i) $(\text{CF}_4)_{\text{MW}}+\text{HFCO}$	LMR	63
	(ii) $(\text{CF}_4+\text{CO})_{\text{MW}}$		
	(iii) $(\text{SF}_6+\text{CO})_{\text{MW}}$		
	(iv) $(\text{SF}_6+\text{CO}+\text{O}_2)_{\text{MW}}$		
FO ₂	$(\text{CF}_4)_{\text{MW}}+\text{O}_3$	LMR	64
FSO	$(\text{O}_2+\text{CF}_4)_{\text{MW}}+\text{OCS}$	MW	65
HCO/DCO	$(\text{CF}_4+\text{He})_{\text{MW}}+\text{H}_2\text{CO}/\text{D}_2\text{CO}$	LMR	66
HCO/DCO	$(\text{CF}_4)_{\text{MW}}+\text{H}_2\text{CO}/\text{D}_2\text{CO}$	MW	67
HCO	$(\text{CF}_4)_{\text{MW}}+\text{H}_2\text{CO}$	EPR	68
HO ₂ /DO ₂	(i) $(\text{O}_2)_{\text{MW}}+\text{hydrocarbons}/$ deuterated hydrocarbons	LMR	69
	(ii) $(\text{H}_2\text{O})_{\text{MW}}$		
	(iii) $(\text{H}_2)_{\text{MW}}+\text{O}_2$		
	(iv) $(\text{CF}_4)_{\text{MW}}+\text{H}_2\text{CO}+\text{O}_2$		
	(v) $(\text{CF}_4)_{\text{MW}}+\text{H}_2\text{O}_2$		
	(vi) $(\text{air}+\text{CF}_4)_{\text{MW}}+\text{H}_2\text{O}_2/\text{D}_2\text{O}_2$		
	(vii) $(\text{O}_2)_{\text{MW}}+\text{O}_2+\text{C}_2\text{H}_4$		

SECTION II.2 - REVIEW

HO ₂ /DO ₂	(i) (O ₂) _{MW} +CH ₂ CHCH ₂ OH	EPR	70
	(ii) (CF ₄) _{MW} +H ₂ O ₂ /D ₂ O ₂		
HO ₂ /DO ₂	(CF ₄) _{MW} +H ₂ O ₂ /D ₂ O ₂	MW	71
NCO	(CF ₄) _{MW} +HNCO	EPR	72
NCO	(CF ₄) _{MW} +HNCO	LMR	73
NCO	(CF ₄) _{MW} +HNCO	MW	74
NCS	(CF ₄) _{MW} +HNCS	EPR	75
NH ₂ /ND ₂	(i) (CF ₄) _{MW} +NH ₃ /ND ₃	LMR	76
	(ii) (CF ₄) _{MW} +N ₂ H ₄		
PH ₂	(H ₂ +O ₂) _{MW} +P _{red}	LMR	77
PH ₂	(i) (H ₂) _{MW} +P _{red}	MW	78
	(ii) (CF ₄) _{MW} +PH ₃		
PO ₂	(H ₂ +O ₂) _{MW} +P _{red}	LMR	79
PO ₂	(i) (H ₂ +O ₂) _{MW} +P _{red}	MW	80
	(ii) (H ₂ +O ₂) _{MW} +PH ₃		
SF ₂	(CF ₄) _{MW} +OCS	MW	81
CH ₂ Cl	(CF ₄) _{MW} +CH ₃ Cl	MW	82
CH ₂ F	(CF ₄) _{MW} +CH ₃ F	MW	83
CH ₂ OH	(Cl ₂ +He) _{MW} +CH ₃ OH	LMR	84
CH ₃ O	(CF ₄) _{MW} +CH ₃ OH	MW	85
CH ₃ O	(CF ₄) _{MW} +CH ₃ OH	LMR	86
CH ₃ S	(CF ₄) _{MW} +CH ₃ SH	MW	87
CH ₂ CHO	(CF ₄) _{MW} +CH ₃ CHO	MW	88

Table Definitions:

EPR : Electron Paramagnetic Resonance Spectroscopy.

IDL : Infrared Diode Laser Spectroscopy.

LMR : Laser Magnetic Resonance Spectroscopy.

MW : Microwave Spectroscopy.

(X₂)_{MW} : Precursor(s) passed through the Microwave discharge.

- H_2/D_2 : Substituted isotopic Species.
(ii) : Alternative Precursor Species.

Table II.2.1. Table showing the transient species generated by a microwave discharge and detected by one of the above mentioned spectroscopic techniques.

II.3 EXPERIMENTAL

(i) THE IODINE ATOM (I) SYSTEM:

The modified EPR Zeeman cavity was assembled with the two port end piece (Section V.3) and its resonant frequency in the TE₀₁₂ mode was measured to be 8710 MHz. The products of a 2450 MHz discharge of oxygen, O₂, were mixed inside the cavity with methyl iodide, CH₃I, in an attempt to generate signals arising from iodine atoms, I. Sufficient CH₃I was added to "titrate" away the the intense O atom signal (which was being monitored on the oscilloscope) until the optimum pressures were 0.5 :2.0 mBar respectively. After scanning the magnetic field from 0.300 to 0.675 T many signals were observed. This procedure was repeated with the exception that the 2450 MHz discharge was switched off to identify non-transient signals arising from molecular oxygen. A total of twelve signals did not appear on this second run. One of these signals was assigned to O atoms at 0.409 T¹⁴, a particularly strong one at 0.332 T to H atoms¹⁰, which was checked by setting the magnetic field to a value 0.05 T less (the approximate hyperfine splitting in the H atom) and a second signal of similar intensity was observed. The remaining ten signals were of similar intensity (S/N 20 : 1)

SECTION II.3 - EXPERIMENTAL

and varied in position between 0.353 and 0.507 T and were assigned to the ^{127}I atom⁸⁹.

(ii) THE FLUORINE ATOM (F) SYSTEM:

During the course of the experiments in the attempt to observe signals arising from the methoxy radical, CH_3O (Section V.4) a real piece of "serendipity" occurred. The modified Zeeman cavity was assembled with the two port end piece and its resonant frequency in the TE_{012} mode measured to be 8710 MHz. This system utilised the PTFE connectors (Section V.3). The products of a 2450 MHz discharge of CF_4 were being mixed inside the cavity with methanol, CH_3OH , and the F atom signals were being monitored on the oscilloscope. As the conditions employed were varied the position of the 2450 MHz discharge cavity was moved closer to the EPR cavity to increase the strength of the F atom signal until it was located such that the visible discharge plasma was actually in contact with the lower port PTFE connector. This caused the F atom signal to increase dramatically. It was later noticed that the regulator on the cylinder containing the CF_4 was in fact registering empty and yet the F atom signals were still as intense on the oscilloscope. Once the CH_3OH was shut off they further increased until they were optimised by passing O_2 through the 2450 MHz discharge at a measured pressure of 0.5 mBar. After scanning the magnetic field from 0.05 to 0.80 T many signals were observed. This procedure was repeated with the exception that the 2450 MHz discharge was switched off to identify non-transient signals arising from molecular oxygen. A total of nine signals did not appear on this second run. One of these signals was assigned to O atoms

SECTION II.3 - EXPERIMENTAL

at 0.409 T^{14} , six signals between 0.382 to 0.518 T were assigned to the high field F atom transitions⁸, leaving two unassigned signals of very narrow line width at 0.168 and 0.209 T . The cavity was then re-tuned to a higher frequency TE₀₁₃ mode measured at 9409 MHz and the magnetic field scanned from $0.19 \pm 0.05 \text{ T}$ and three signals of very narrow line width were observed. The outer two at 0.188 and 0.238 T appeared to have the same spacing between them as the two observed at 8710 MHz are were identified as these two signals. The nature of these three signals is discussed in the Section II.4.

II.4 RESULTS AND DISCUSSION

(i) THE IODINE ATOM (I) SYSTEM:

Figure II.4.1 shows the I atom signals observed from the products of a 2450 MHz discharge of O_2 discharge mixed in side the cavity with CH_3I . Aditya and Willard⁸⁹ reported eighteen lines due to the ^{127}I nucleus and of these ten were observed under this new method of generation. Table II.4.1 shows the measured field positions of the I atom signals compared to those reported. It should be noted that the microwave frequencies of the two data sets differ, consequently so do the magnetic field positions of the observed resonances, by approximately the expected amount, confirming the carrier of these signals as ^{127}I .

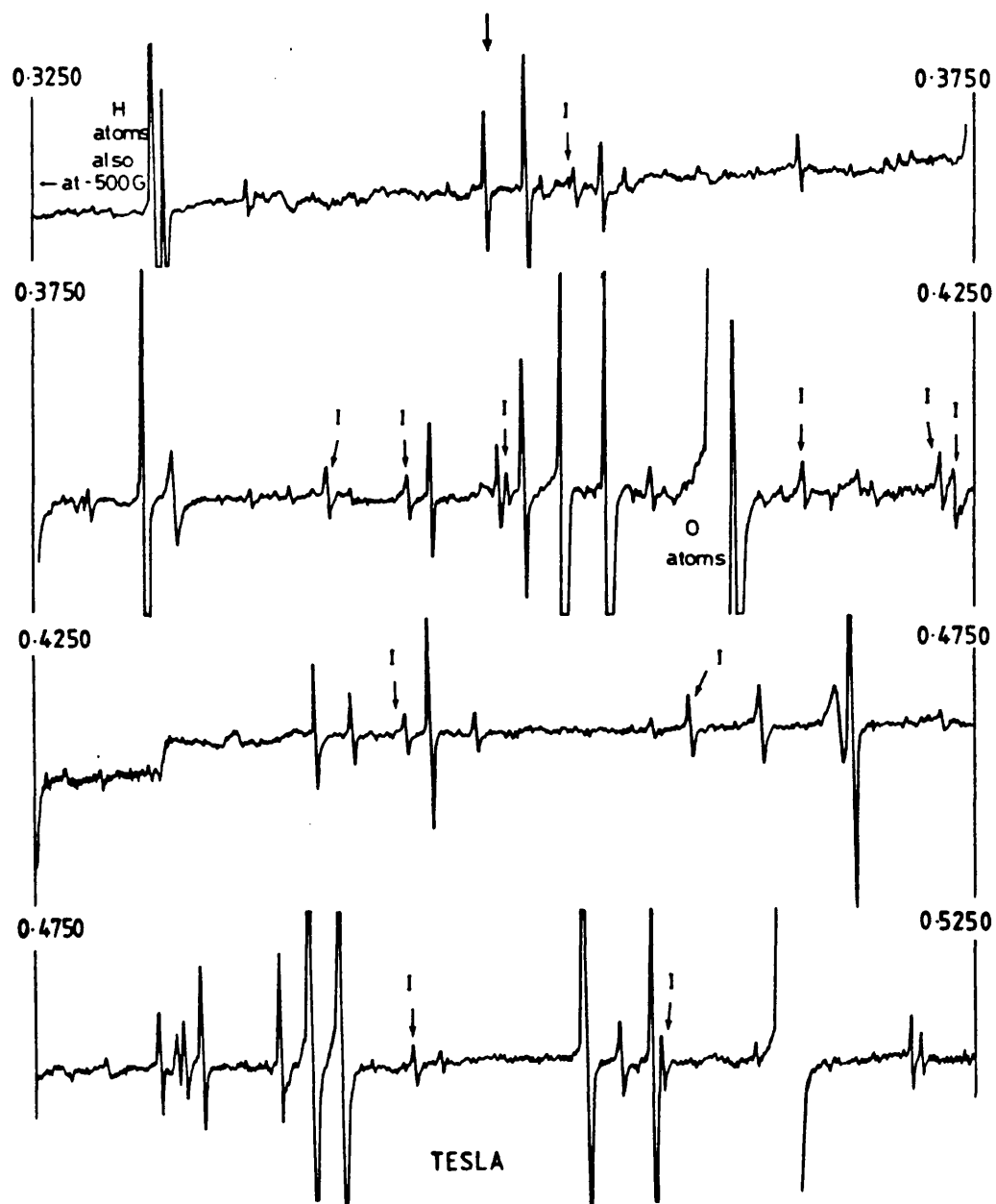


Figure II.4.1. Part of the EPR spectrum of iodine atoms from the products of a 2450 MHz discharge of O_2 mixed with CH_3I . O_2 pressure 2.0 mBar, CH_3I pressure 0.5 mBar, magnetic field 0.0500 - 0.6250 T, scan range ± 0.0250 T, time constant 0.3 s, microwave frequency 8710 MHz, modulation frequency 100 kHz.

SECTION II.4 - RESULTS AND DISCUSSION

Aditya & Willard ($\nu = 9.275$ GHz)	This work ($\nu = 8.710$ GHz)	Δ
T	T	T
0.3300	-	-
0.3954	-	-
0.3962	0.3546	0.0416
0.4284	0.3912	0.0372
0.4303	-	-
0.4365	0.4005	0.0360
0.4526	0.4164	0.0362
0.4610	0.4237	0.0373
0.4654	0.4244	0.0410
0.4827	0.4450	0.0377
0.4995	0.4602	0.0393
0.5287	-	-
0.5345	0.4950	0.0397
0.5383	0.5086	0.0397
0.5930	-	-
0.6130	-	-
0.6223	-	-

Table II.4.1. Table showing the I atom transitions of Aditya & Willard, this work and the difference between them due to the microwave frequency.

(ii) THE FLUORINE ATOM (F) SYSTEM:

Figure II.4.2 shows the F atom spectrum at 8710 and 9409 MHz

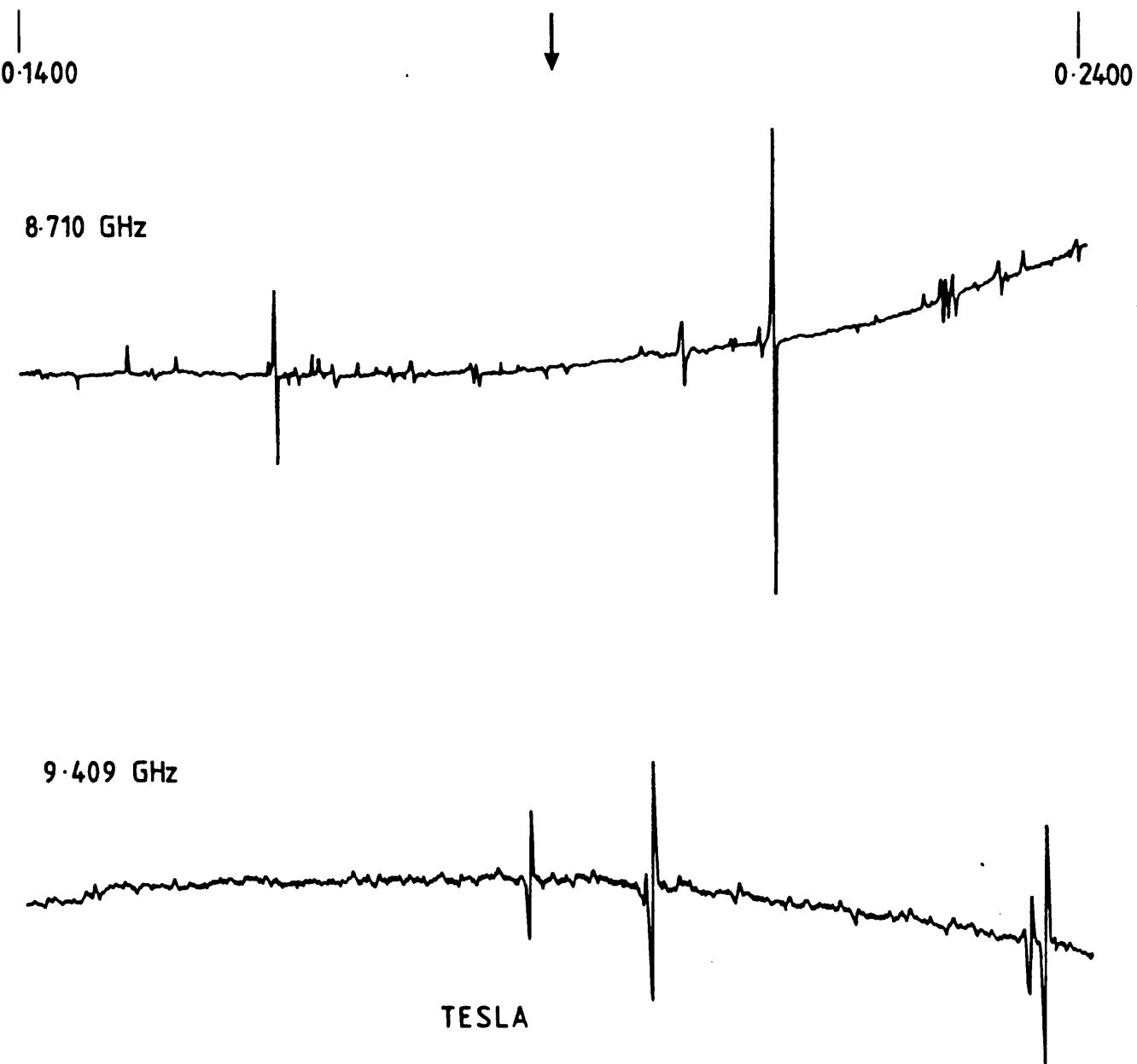


Figure II.4.2. Part of the EPR spectrum of fluorine atoms at 8710 and 9409 MHz. O_2 pressure 0.5 mBar, magnetic field 0.05 - 0.80 T, scan range ± 0.05 T, time constant 0.3 s, modulation frequency 100 kHz.

SECTION II.4 - RESULTS AND DISCUSSION

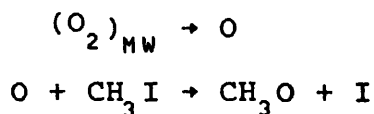
observed from the products of a 2450 MHz discharge of PTFE and oxygen. The origin of these transitions is shown in Chapter I, Figure I.2.3. The top spectrum shows the two low field transitions arising from transitions between the $F = 1$ and $F = 2$ levels in the low field limit ($^2P_{3/2}$ level at in the high field coupling scheme). These transitions actually occur between the $M_F = -1$ and $M_F = 0$ magnetic sub-levels with respect to increasing magnetic field viz. $F = 2, M_F = 0 \leftarrow F = 1, M_F = -1$ at approximately 0.1680 T and $F = 2, M_F = 0 \leftarrow F = 1, M_F = 1$ at approximately 0.2090 T⁹⁰. The bottom spectrum shows these same two outer transitions with a third one between arising from transitions between the $F = 0$ and $F = 1$ levels, in the low field description of the coupling scheme ($^2P_{1/2}$ in the high field description of the coupling scheme). This transition actually occurs between the $M_F = 0$ and the $M_F = -1$ magnetic sub-levels levels viz. $F = 1, M_F = -1 \leftarrow F = 0, M_F = 0$ at approximately 0.1990 T. This transition was not observed in the top spectrum because it tunes in the opposite direction and at about half the rate that the other two do and so would occur at a magnetic field beyond the range of that particular scan.

These two new ways of generating atomic F and I are interesting because in the first case a microwave discharge was used to generate I atoms whereas previously a UV photolysis mechanism was employed. The microwave discharge scheme used is known to produce the IO radical³², but no observation of the I atom utilising this production scheme has been reported.

Presumably this method of generating I atoms goes via a SN_2 displacement type reaction shown in Scheme I:

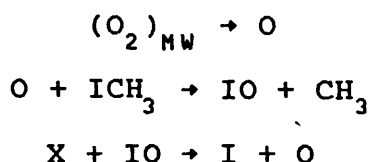
SECTION II.4 - RESULTS AND DISCUSSION

Scheme I



Another possibility however since the IO radical has been observed in this system is an O atom abstraction and subsequent decomposition (on collision of a third body X) of the IO radical shown in Scheme II:

Scheme II

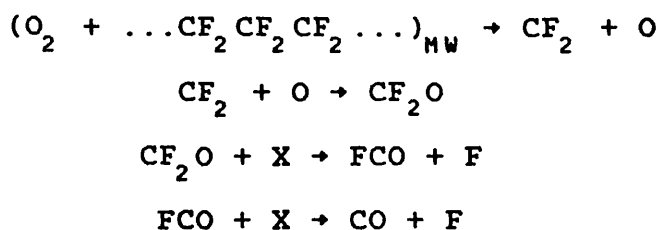


A perusal of Table II.2.1 reveals that over half of the radicals cited in it were produced by either employing the expensive CF_4 or F_2 with an an inert gas along with the handling difficulties associated with that system. The F atom signals generated from this much cheaper and vastly easier to handle solid are as intense (if not stronger) than those produced from either of the above production systems, suggesting this method as a useful alternative to the above mentioned methods. The mechanism is unclear except that O_2 is required for the production of F atoms, as has been observed in several systems that were using CF_4 to generate F atoms which subsequently undergo an abstraction reaction to generate the desired transient. The addition of a small amount of O_2 in these systems causes enhanced transient signals^{29,30,50,65,86}. Kawagachuchi et al.⁹¹ in their IDL

SECTION II.4 - RESULTS AND DISCUSSION

study of CF observed that CF_2CF_2 as a precursor instead of CF produced a signal enhancement of a factor of five in the observed CF signals. PTFE ($\dots CF_2CF_2CF_2 \dots$) is the polymerised solid of this gas and so a mechanism for the generation of F atoms from PTFE may be along the lines of that proposed in Scheme III:

Scheme III



II.5 CONCLUSIONS

Microwave discharges are the most prolifically used devices in the production schemes of transient free radicals and atoms for detection by high resolution spectroscopic techniques. The F atom and its subsequent H atom abstraction reaction with a hydrogen containing precursor is the most frequently employed mechanism in the production of these species. Allowing PTFE solid to come into contact with the microwave discharge products of O_2 , such that the solid itself is within the discharge, produces comparable F atom signals in an EPR spectrometer to any other known source without the expense of CF_4 or the hazards of handling F_2 . Alternatively, if the microwave discharge products of O_2 are allowed to react with CH_3I then this scheme provides a source of either I atoms or IO radicals, the particular species being dependent upon the actual conditions employed, although both could be generated simultaneously.

II.6 REFERENCES

1. W.G.Zijlstra, J.M.Henrichs, J.H.M Moog & J.D.W. Van Voorst, Chem. Phys. Letts., 7, 553 (1970).
2. J.S.M Harvey, R.A.Kamper & K.R.Lea, Proc. Phys. Soc. B76, 976 (1960).
3. J.M.Brown & K.M.Evenson, The British Radiofrequency Group Spring Meeting (1984).
4. V.Beltran-Lopez & H.G.Robinson, Phys. Rev., 123, 161 (1961).
5. P.B.Davies & D.K.Russell, Chem. Phys. Letts., 67, 440 (1979).
6. M.Dagenais, J.W.C.Johns & A.R.W.McKellar, Can. J. Phys., 54, 1438 (1976).
7. A.C.Stanton & C.E.Kolbe, J. Chem. Phys., 72, 6637 (1980).
8. V.Beltran-Lopez, V.W.Hughes & H.E.Radford, Phys. Rev., 123, 153 (1961).
9. J.M.Brown & K.M.Evenson, The British Radiofrequency Group Spring Meeting (1984).
10. Chapter IV, Section IV.4.
11. J.W.Johns, A.R.W.McKellar & M.Riggin, J. Chem. Phys., 66, 3962 (1977).
12. Chapter II, Section II.3.
13. Chapter IV, Section IV.4.
14. Chapter IV, Section IV.4.
15. P.B.Davies, B.J.Handy, E.K.Murray Lloyd & D.R.Smith, J. Chem. Phys., 68, (1978).
16. R.L.Brown, J. Chem. Phys., 44, 2827 (1966).
17. W.G.Zijlstra, J.M.Henrichs, J.H.M.Moog & J.D.W. Van Voorst, Chem. Phys. Letts., 7, 553 (1970).
18. W.G.Zijlstra, J.M.Henrichs, J,H.M.Moog &

SECTION II.6 - REFERENCES

- J.D.W. Van Voorst, Chem. Phys. Letts., 7, 553 (1970).
19. J.M.Brown & K.M.Evenson, The British Radiofrequency Group Spring Meeting (1984).
20. H.Uehara, Chem. Phys. Letts., 84, 539 (1981).
21. A.Carrington & D.H.Levy, J. Chem. Phys., 44, 1298 (1966).
22. A.R.W.McKellar, J. Mol. Spec., 86, 43 (1981).
23. M.A.Gondal, W.Rohrbeck, W.Urban, R.Blankart & J.M.Brown, J. Mol. Spec., 100, 290 (1983).
24. A.Carrington & B.J.Howard, Mol. Phys., 18, 225 (1970).
25. A.Carrington & D.H.Levy, J. Chem. Phys., 44, 1298 (1966).
26. R.S.Lowe & A.R.W.McKellar, J. Mol. Spec., 79, 424 (1980).
27. R.T.Menzies, J.S.Margolis, E.D.Hinkley & R.A.Toth, Appl. Opt., 16, 523 (1977).
28. T.Amano, S.Saito, E.Hirota, Y.Morino, D.R.Johnson & F.X.Powell, J. Mol. Spec., 30, 275 (1969).
29. A.R.W.McKellar, C.Yamada & E.Hirota, J. Mol. Spec., 97, 425 (1983).
30. A.R.W.McKellar, Can. J. Phys., 57, 2106 (1979).
31. J.M.Brown & D.Robinson, Mol. Phys., 51, 883 (1984).
32. A.Carrington, G.N.Currie, P.N.Dyer, D.H.Levy & T.A.Miller, Chem. Commun., 13, 641 (1967).
33. P.B.Davies & F.Temps, J. Chem. Phys., 74, 6556 (1981).
34. F.D.Wayne & H.E.Radford, Mol. Phys., 32, 1407 (1976).
35. A.Carrington & D.H.Levy, J. Chem. Phys., 44, 1298 (1965).
36. T.Amano, S.Saito, E.Hirota & Y. Morino, J. Mol. Spec., 32, 97 (1969).
37. H.Uehara & K.Hakuta, Proceedings of the 14th International Symposium on Free Radicals, Sanda, Japan (1979).
38. G.C.Dousmanis, T.M.Sanders & C.H.Townes,

SECTION II.6 - REFERENCES

- Phys. Rev., 100, 1735 (1955).
39. J.M.Brown, M.Kaise, C.M.L.Kerr & D.L.Milton,
Mol. Phys., 36, 553 (1978).
40. K.M.Evenson, J.S.Wells & H.E.Radford,
Phys. Rev. Letts., 25, 199 (1970).
41. P.B.Davies, D.K.Russell & B.A.Thrush,
Chem. Phys. Letts., 36, 280 (1975).
42. K.Kawaguchi, S.Saito & E.Hirota, To be Published.
43. K.Kawaguchi, S.Saito & E.Hirota, To be Published.
44. F.D.Wayne, P.B.Davies & B.A.Thrush,
Mol. Phys., 28, 989 (1974).
45. Y.Endo, S.Saito & E.Hirota,
J. Mol. Spec., 92, 443 (1982).
46. A.Carrington, G.N.Currie, P.N.Dyer, D.H.Levy &
T.A.Miller, Chem. Commun., 13, 641 (1967).
47. C.C.MacDonald, J. Chem. Phys., 39, 2587 (1963).
48. P.B.Davies, B.J.Handy, E.K.Murray Lloyd & D.K.Russell,
Mol. Phys., 36, 1005 (1978);
R.S.Lowe, Mol. Phys., 41, 929 (1980).
49. C.C.MacDonald, J. Chem. Phys., 39, 2587 (1963).
50. C.Yamada, K.Kawaguchi & E.Hirota,
J. Chem. Phys., 71, 3338 (1979).
51. W.W.Clark & F.C.De Lucia, J. Mol. Spec., 60, 332 (1976).
52. A.Carrington, G.N.Currie, P.N.Dyer, D.H.Levy &
T.A.Miller, Chem. Commun. 13, 641 (1967).
53. P.B.Davies, E.K.Murray Lloyd & D.K.Russell,
J. Chem. Phys., 3377 (1978).
54. A.Carrington, G.N.Currie, D.H.Levy & T.A.Miller,
Mol. Phys., 17, 535 (1969).
55. K.Hakuta & H.Uehara, J. Mol. Spec., 85, 97 (1981).

SECTION II.6 - REFERENCES

56. C.R.Parent & P.J.M.Kuijpers, *Chem. Phys.*, 40, 425 (1979).
57. J.M.Brown & D.Robinson, *Mol. Phys.*, 51, 883 (1984);
J.M.Brown, R.F.Curl & K.M.Evenson,
J. Chem. Phys., 81, 2884 (1984).
58. K.Kawaguchi, C.Yamada & E.Hirota,
Mol. Phys., 44, 509 (1981).
59. P.B.Davies & D.K.Russell, *J. Mol. Spec.*, 60, 201 (1980).
60. W.H.Kirchhoff, D.R.Lide & F.X.Powell,
J. Mol. Spec., 491 (1973).
61. T.J.Sears, P.R.Bunker, A.R.W.McKellar, K.M.Evenson,
P.A.Jennings & J.M.Brown,
J. Chem. Phys. 77, 5363 (1979).
62. K.Kawuguchi, Y.Endo & E.Hirota,
J. Mol. Spec., 93, 381 (1982).
63. J.Buttenshaw, PhD Thesis, Southampton University,
England (1979).
64. K.O.Christie, P.B.Davies, D.P.Stern, F.Temps, H.G.Wagner,
J. Phys. Chem., 87, 5086 (1983).
65. Y.Endo, S.Saito & E.Hirota,
J. Chem. Phys., 74, 1568 (1981).
66. H.E.Radford, K.M.Evenson & C.J.Howard,
J.Chem. Phys., 60, 3178 (1979); R.S.Lowe &
A.R.W.McKellar, *J. Chem. Phys.*, 74, 2686 (1981).
67. S.Saito, *Astrophys. J.*, 178, L95 (1972).
68. I.C.Bowater, J.M.Brown & A.Carrington,
J. Chem. Phys., 54, 4957 (1971).
69. H.E.Radford, K.M.Evenson & C.J.Howard,
J. Chem. Phys., 60, 3178 (1974); A.R.W.McKellar,
J.Chem. Phys., 71, 81 (1979).
70. C.E.Barnes, J.M.Brown, A.Carrington, J.Pinkstone,

SECTION II.6 - REFERENCES

- T.J.Sears & P.J.Thistlethwaite,
J. Mol. Spec., 72, 86 (1978); C.E.Barnes, J.M.Brown &
H.E.Radford, J. Mol. Spec., 84, 179 (1980).
71. Y.Beers & C.J.Howard, J. Chem. Phys., 63, 4212 (1975);
Y.Beers & C.J.Howard, J. Chem. Phys., 64, 1541 (1976).
72. A.Carrington, A.R.Fabris, B.J.Howard & N.J.D.Lucas,
J. Chem. Phys., 49, 5545 (1968).
73. C.E.Barnes, PhD Thesis, Southampton University,
England (1982).
74. K.Kawaguchi, S.Saito & E.Hirota,
Mol. Phys., 55, 341 (1985).
75. A.Carrington, A.R.Fabris & N.J.D.Lucas,
Mol. Phys., 16, 195 (1969).
76. P.B.Davies, D.K.Russell, B.A.Thrush & F.D.Wayne,
J. Chem. Phys., 62, 3739 (1975); G.W.Hills &
A.R.W.McKellar, J. Chem. Phys., 71, 3330 (1979).
77. P.B.Davies, D.K.Russell, B.A.Thrush & H.E.Radford,
Chem. Phys., 44, 421 (1979).
78. Y.Endo, S.Saito & E.Hirota,
J. Mol. Spec., 97, 204 (1983).
79. K.Kawaguchi, S.Saito & E.Hirota,
J. Chem. Phys., 82, 4893 (1985).
80. K.Kawaguchi, S.Saito & E.Hirota,
J. Chem. Phys., 82, 4893 (1985).
81. Y.Endo, S.Saito, E.Hirota & T.Chikaraishi,
J. Mol. Spec., 77, 222 (1971).
82. Y.Endo, C.Yamada, S.Saito & E.Hirota,
IMS Ann. Rev., 30 (1984).
83. Y.Endo, C.Yamada, S.Saito & E.Hirota,
J. Chem. Phys., 79, 1605 (1983).

SECTION II.6 - REFERENCES

84. H.E.Radford, K.M.Evenson & D.A.Jennings,
Chem. Phys. Letts., 78, 589 (1981).
 85. Y.Endo, S.Saito & E.Hirota,
J. Chem. Phys., 81, 122 (1984).
 86. H.E.Radford & D.K.Russell,
J. Chem. Phys., 66, 2222 (1977).
 87. Y.Endo, S.Saito & E.Hirota,
IMS Ann. Rev., 34 (1984).
 88. Y.Endo, S.Saito & E.Hirota,
IMS Ann. Rev., 30 (1984).
 89. S.Aditya & J.E.Willard, J. Chem. Phys., 44, 833 (1966).
 90. A.Carrington, D.H.levy & T.A.Miller,
J. Chem. Phys., 45, 4093 (1966).
 91. K.Kawaguchi, K.Nagai, C.Yamada, Y.Hamada & E.Hirota,
J. Mol. Spec., 86, 136 (1981).
-

SECTION III.1 - INTRODUCTION

CHAPTER III - GENERATION BY ELECTRICAL GLOW DISCHARGE

III.1 INTRODUCTION

In this Chapter the DC glow discharge is examined as a method of producing transient species for detection by high resolution spectroscopic techniques. The type of precursors passed through the discharge and the subsequent species generated for detection or reaction to form other previously undetected species is then reviewed. An account of the general characteristics of a DC discharge followed by the development of such a DC discharge in three different spectrometers operating in three different wavelength regions of the electromagnetic spectrum is given along with the experiments performed with the discharges. Finally the results obtained from these experiments are presented.

III.2 REVIEW OF SPECIES GENERATED BY ELECTRICAL DISCHARGE

This section of this Chapter contains a summary of the radicals and atoms produced via either a 50/60 Hz alternating or a direct current electrical glow discharge in tabulated form for clarity and brevity. The generated transient species and their precursors are identified by virtue of their chemical formulae and the nomenclature used within the table is defined at the end of the table. The transient species generated by an electrical glow discharge and detected by one of the high resolution spectroscopic techniques discussed in this thesis are shown in Table III.2.1.

SECTION III.2 - REVIEW

Species	Generation Method	Detection Method	Reference
H	$(\text{H}_2)_{\text{DC}}$	EPR	1
He(meta)	$(\text{He})_{\text{DC}}$	IDL	2
Kr(meta)	$(\text{Kr}+\text{He})_{\text{DC}}$	LMR	3
N(grd,exc)	$(\text{N}_2)_{\text{DC}}$	EPR	4
O	$(\text{O}_2)_{\text{DC}}$	EPR	5
P	$(\text{P}_{\text{white}}+\text{He}/\text{Ar})_{\text{DC}}$	EPR	6
Xe(meta)	$(\text{Xe}+\text{He})_{\text{DC}}$	LMR	7
CCl	$(\text{CCl}_4+\text{Ar})_{\text{AC}}$	IDL	8
CCl	$(\text{CCl}_4)_{\text{AC}}$	MW	9
CF	(i) $(\text{CF}_4)_{\text{AC}}$	IDL	10
	(ii) $(\text{C}_2\text{F}_4)_{\text{AC}}$		
CS	$(\text{CS}_2)_{\text{AC}}$	IDL	11
CS	$(\text{CS}_2)_{\text{AC}}$	MW	12
ClO	$(\text{FCLO}_3)_{\text{AC}}$	MW	13
HCO	(i) $(\text{CF}_4+\text{He})_{\text{DC}}+\text{H}_2\text{CO}$	LMR	14
	(ii) $(\text{O}_2)_{\text{DC}}+\text{H}_2\text{CO}$		
HSO/DSO	$(\text{O}_2+\text{H}_2\text{S}/\text{D}_2\text{O})_{\text{DC}}$	MW	15
NCl	$(\text{N}_2+\text{Cl}_2)_{\text{AC}}$	MW	16
PCl	$(\text{PCl}_3)_{\text{AC}}$	MW	17
PCl	$(\text{PCl}_3+\text{H}_2)_{\text{AC}}$	IDL	18
PF	(i) $(\text{PH}_3+\text{CF}_4)_{\text{AC}}$	MW	19
	(ii) $(\text{PH}_3+\text{CF}_4)_{\text{DC}}$		
SF	$(\text{OCS}+\text{CF}_4)_{\text{DC}}$	MW	20
SH	$(\text{H}_2)_{\text{DC}}+\text{S}_{\text{elem}}$	LMR	21
SeH	$(\text{H}_2)_{\text{DC}}+\text{S}_{\text{elem}}$	EPR	22

SECTION III.2 - REVIEW

SiF	$(\text{SiF}_4 + \text{SiH}_4)_{\text{DC}}$	MW	23
SiH	(i) $(\text{SiH}_4 + \text{H}_2)_{\text{DC}}$	IDL	24
	(ii) $(\text{SiH}_4 + \text{He})_{\text{DC}}$		
	(iii) $(\text{SiH}_4 + \text{Ar})_{\text{DC}}$		
SiN	$(\text{SiH}_4 + \text{N}_2)_{\text{AC}}$	IDL	25
SiN	$(\text{SiCl}_4 + \text{N}_2)_{\text{DC}}$	MW	26
TeH	$(\text{H}_2)_{\text{DC}} + \text{Te}_{\text{elem}}$	EPR	27
BO ₂	$(\text{BCl}_3 + \text{O}_2)_{\text{AC}}$	IDL	28
C ₂ O	$(\text{C}_3\text{O}_2)_{\text{DC}}$	MW	29
ClBO	$(\text{O}_2 + \text{BCl}_3)_{\text{AC}}$	IDL	30
FCO	(i) $(\text{C}_2\text{F}_4 + \text{He} + \text{O}_2)_{\text{AC}}$	IDL	31
	(ii) $(\text{SF}_6 + \text{CO})_{\text{AC}}$		
	(iii) $(\text{C}_2\text{F}_4 + \text{CO})_{\text{AC}}$		
PF ₂	$(\text{PH}_3 + \text{CF}_4)_{\text{AC}}$	MW	32
PH ₂	$(\text{PH}_3 + \text{CF}_4)_{\text{DC}}$	MW	33
CF ₃	$(\text{CF}_3\text{I})_{\text{AC}}$	MW	34
CH ₃	(i) $(\text{CH}_3\text{I})_{\text{AC}}$	IDL	35
	(ii) $((\text{CH}_3)_2\text{CO})_{\text{AC}}$		
	(iii) $(\text{CH}_3\text{OH})_{\text{AC}}$		
	(iv) $(\text{CH}_3\text{SH})_{\text{AC}}$		

Table Definitions:

EPR : Electron Paramagnetic Resonance Spectroscopy.

IDL : Infrared Diode Laser Spectroscopy.

LMR : Laser Magnetic Resonance Spectroscopy.

MW : Microwave Spectroscopy.

$(\text{X}_2)_{\text{AC}}$: Precursor(s) passed through a 50/60 Hz
alternating current electrical discharge.

$(\text{X}_2)_{\text{DC}}$: Precursor(s) passed through a direct current
discharge.

H_2/D_2 : Substituted isotopic Species.

(iii) : Alternative Precursor Species.

Table III.2.1. Table showing the transient species generated by either a 50/60 Hz alternating current or a direct current discharge and detected by one of the above mentioned spectroscopic techniques.

III.3 DEVELOPMENTAL

Electrical discharges in breaking apart gases have certain general characteristics in the production of the gas plasma. A glow discharge consists of four general regions. The region nearest the cathode is cathode dark space or Crooke's space after its discoverer. The next is the region of negative glow in which the electron concentration is at its maximum. The next region is the Faraday dark space also named after its discoverer and the remainder of the discharge is taken up by the region of positive column all the way back to the anode. The extent of these regions is pressure dependant but the above description serves for the pressures under consideration in this Chapter. Unstable discharges tend to flicker to the eye whereas stable ones are steady. If a discharge is unstable it will tend to propagate noise "spikes" whereas stable ones do not. Discharge stability tends to increase with decreasing pressure down to about 1.0 mBar (or the lowest pressure which will sustain a glow) whilst it is usually difficult to sustain a glow discharge above about 40 mBar. The current also tends to interact with the modulation current if one is being employed. The

SECTION III.3 - DEVELOPMENTAL

performance of the discharge tends to degrade after hours or days of running, as sputtered material (copper, iron, chromium, nickel and plasma generated materials) becomes deposited on the electrodes. The minimum pressure required to sustain a glow discharge can be reduced by a factor of two if the discharge tube diameter is reduced by a factor of two. The important parameters describing the plasma as it interacts with the microwave radiation (frequency $\omega/2\pi$) are the plasma frequency,

$$\omega_p = [\eta e^2 / (m \epsilon_0)]^{1/2} \quad (\text{III.3.1})$$

where η is the electron concentration, e is the charge on the electron, m is the mass of the electron ϵ_0 is the electric field strength. The electron collision frequency, ν is the other important parameter³⁶. These have been estimated to be $\omega_p = 300$ to 1000 MHz and $\nu = 50$ MHz while the electron cyclotron frequency $\omega_b < 20$ MHz is small enough to be ignored in the absence of a magnetic field.

The primary difference between this type of glow discharge and conventional noise sources is a difference of several orders of magnitude in pressure, and therefore the collision frequency ν . Discharges of this type are not blackbody radiators, but almost transparent greybodies. They belong to that class of plasmas for which the noise emission is best treated, not as blackbody but as Bremsstrahlung radiation in a transparent medium³⁶. The noise emission is very strongly linked to the attenuation coefficient α of the plasma in the same sense as the Einstein coefficient, A , is related to the B coefficient. Roughly speaking, the noise radiation from a plasma slab of thickness, l , would increase with l until a

SECTION III.3 - DEVELOPMENTAL

point was reached where radiation emitted from the distant part slab was largely attenuated on its way to the observer (namely, where the optical path $2\alpha l$ was near unity), and this point would correspond to the blackbody limit. Since,

$$2\alpha \cong v\omega_p^2 / \omega^2 c \cong 10^{-7} \text{ to } 10^{-6} \text{ (cm}^{-1}\text{)} \text{ and } l \cong 30 \text{ cm (III.3.2)}$$

the optical depth is only 3×10^{-4} to 3×10^{-5} , and so the radiation is correspondingly weaker than blackbody. This means that noise radiation should be too weak to observe. At pressure of mBar and tens of mBar v (and thus α) is very much larger, and the noise begins to become significant. For the pressure range typical for high resolution spectroscopy there should be no noticeable noise due to the random thermal motions of the electrons. Since the plasma phase shift varies as ω^{-1} , more noise is expected at lower microwave frequencies (X-band) than at higher (millimeter wave) frequencies³⁶.

The upper limit of the plasma densities which are suitable for use in the microwave region depends on the microwave frequency under consideration, the magnetic field, the amount of noise, baseline or shift that can be tolerated and the practical questions of heat dissipation and arcing tendency and the success of maintaining the discharge. The most fundamental limitation is embodied in following condition,

$$\omega \gg \omega_p \quad \text{(III.3.3)}$$

that the detection frequency ω should be greater than the frequency of the plasma ω_p .

a) WITHIN THE EPR SPECTROMETER CAVITY

Figure V.3.1 in Section V.3 is a schematic diagram of the

SECTION III.3 - DEVELOPMENTAL

experimental arrangement of a quartz pill-box inside a Varian V-4535 large access cavity operating in a TE₀₁₂ mode. The quartz pill-box is connected to the vacuum system by two quartz to Pyrex graded seals and the appropriate QF connectors. A pair of tungsten electrodes were sealed into the Pyrex portions of the cavity and whole assembly evacuated. A DC power supply capable of supplying 0 - 500 V and 0 - 100 mA was connected to the tungsten electrodes and a discharge struck perpendicular to the applied magnetic field when helium at 1.0 mBar was flowed through the cavity. The discharge running at 300 V and 50 mA severely disturbed the cavity mode pattern to the extent that no cavity dip was visible (Figure V.3.2) and consequently the automatic frequency control, AFC, on the EPR would not lock in. On applying the magnetic field the discharge visibly "moved" until a field in excess of 0.15 T was applied at which point the discharge went out.

The discharge power supply was modified to deliver smaller currents between 0 and 10 mA to minimise the disruption that the discharge was causing to the cavity mode pattern and the AFC. The quartz pill-box was also modified so that a pair of detachable brass electrodes could be fitted on to the existing tungsten bars such that they adhered as closely as possible to the quartz pill-box walls to prevent them from disturbing the cavity Q. The whole was assembled and evacuated. A DC discharge was struck parallel to the magnetic field when helium at 1.0 mBar was flowed through the cavity. The discharge running at 10 mA and 500 V allowed both the cavity dip to be displayed upon the oscilloscope and the AFC to lock on to the cavity frequency, however the very bottom of the dip appeared to be flattened or cut off by the discharge.

b) WITHIN THE MILLIMETER WAVE MAGNETIC RESONANCE SPECTROMETER CAVITY

Figure VII.2.4 shows a scale drawing of the Fabry-Perot cavity employed in the millimeter wave magnetic resonance spectrometer. Also shown are the rectangular plate electrodes which were sealed in to the cavity's Pyrex wall. Not shown in the Figure VI.2.4 are the inlet and outlet ports which connect the millimeter wave cavity to the vacuum system. After evacuation, the DC power supply was connected to the electrodes and a discharge struck parallel to the applied magnetic field when helium at 1.0 mBar was flowing through the cavity. A range of discharge conditions were employed and the noise level on the millimeter wave detector was monitored on the oscilloscope. There appeared to be no visible increase in the detector noise output whilst the DC discharge was running even at 500 V and 100 mA.

c) WITHIN THE INFRARED DIODE LASER ABSORPTION TUBE

A DC discharge of silane, SiH_4 , with either He, H_2 or Ar was struck inside this tube³⁹, the details of which can be found in Section VI.3.

III.4 EXPERIMENTAL

a) WITHIN THE EPR SPECTROMETER CAVITY³⁷

(i) THE OXYGEN ATOM (O) SYSTEM:

The quartz pill-box EPR cavity was assembled with the detachable brass electrodes aligned such that they were inside the pill-box parallel to the applied magnetic field. They were positioned as closely to the walls as possible to

SECTION III.4 - EXPERIMENTAL

minimise the disruption they cause to the cavity Q. It was noted that this position was half way up the side of the quartz cylinder in a region the standing microwave pattern where the electric field was essentially zero for the TE₀₁₂ mode pattern employed within the cavity³⁸. The whole was then evacuated and the cavity frequency in the TE₀₁₂ mode was measured to be 8576 MHz. The products of a 2450 MHz discharge were passed through the cavity to establish the magnetic field position of the O atom signal at the cavity's resonant frequency.

The 2450 MHz discharge was then switched off and a DC glow discharge of 500 V and between 1 to 10 mA struck. The noise on the detector increased by a factor of about twenty and when the region of the magnetic field was scanned which previously produced the O atom signal generated by the 2450 MHz discharge no similar signal arising from the DC glow discharge was observed. It was also noted that as the field approached the electron free spin value (approx. 0.33 T) the noise reached a maximum then decreased beyond this value.

(ii) THE FLUORINE ATOM (F) SYSTEM:

Due to the observation on the previous system that the noise decreased away from the 0.33 T the higher field F atom signals at approximately 0.5 T were selected as possible candidates for generation by the DC discharge. The products of a 2450 MHz of CF₄ were passed through the discharge and into the cavity. Three strong F atom signals were observed at approximately 0.5 T. The DC discharge was then switched on (whilst the 2450 MHz discharge was still producing the F atom signals) and the relative increase in the noise on the

SECTION III.4 - EXPERIMENTAL

detector was estimated at a factor ten. The 2450 MHz discharge was then switched off (whilst the DC discharge was still running) and the noise on the detector increased by a further factor of ten presumably due to the removal of a large concentration of conducting species produced by the 2450 MHz discharge. The F atom signals were subsequently obscured by this increased level of noise, so it was not possible to observe whether F atom signals of comparable strength were being generated.

In attempt to reduce the level of noise on the detector He was added to the DC discharge, but this did not reduce the noise on the detector to a sufficient level for the F atom signals to be observed by the DC discharge alone. It did however enhance the F atom signals with just the 2450 MHz discharge running. As a consequence of this the F atom signals were sufficiently intense to make them observable with both of the discharges running, however it was clear that they arose from the 2450 MHz discharge and not from the DC discharge. Helium, He, was replaced by argon, Ar, in the manner described above but this inert gas only served to enhance the noise by a factor of about five on the detector presumably because Ar has a lower ionisation potential than He and so is likely to produce more electrons and hence more cyclotron-related noise which was occurring at $g=2$ due to the application of the magnetic field, for the same power applied across the electrodes.

SECTION III.4 - EXPERIMENTAL

b) WITHIN THE MILLIMETER WAVE MAGNETIC RESONANCE SPECTROMETER CAVITY

THE SULPHUR MONOXIDE RADICAL (SO) SYSTEM:

The millimeter wave magnetic resonance spectrometer cavity was tuned into resonance as described in Section VII.2. The products of a DC discharge of sulphur dioxide, SO_2 in helium, He, were discharged inside the cavity and the spectrometer was set to spectrum acquisition mode. A wide range of discharge conditions were utilised and there was no increase in the noise on the detector even at the maximum ratings that the DC power supply could deliver. A deep SO blue(!) was observed in the cavity and solid elemental sulphur began to deposit on the cavity walls. Extensive searches for transitions arising from the SO radical were curtailed by the untimely demise of the IMPATT oscillator for reasons outlined in Section VII.2.

c) WITHIN THE INFRARED DIODE LASER ABSORPTION TUBE

THE SILICON HYDRIDE (SiH) AND SILYLENE RADICAL (SiH_2) SYSTEM:

The infrared diode spectrometer was set into spectrum acquisition mode as described in Section VI.2. The products of a DC glow discharge of silane, SiH_4 in either hydrogen, H_2 , helium, He, or argon, Ar were discharged inside the absorption tube. Pure SiH_4 discharges were found to be unstable and they caused noise "spikes" on the infrared diode laser detector signal. On the addition of either of the above mentioned buffer gases the discharge became "quiet" and stable. Amorphous silicon deposits began to coat the tube as the discharge was run for prolonged periods, necessary to observe the transient signals. As was observed in the above

SECTION III.4 - EXPERIMENTAL

experiment, the DC glow discharge did not generate any noise provided it was kept stable with the addition of a buffer gas.

III.5 RESULTS AND DISCUSSION

In both the EPR and MMR cavities it was found that DC glow discharge could be maintained provided the discharge was parallel to the applied magnetic field. This is presumably due to the field enhancing the cycling of the charged species when it is parallel but inhibiting this motion when it is perpendicular until such a time as the magnetic field prevents the acceleration of electrons towards the anode resulting in the glow discharge being put out as was observed in the EPR cavity.

a) WITHIN THE EPR SPECTROMETER CAVITY

The condition outlined in Equation III.3.3 that the frequency of the radiation used should be much greater than the frequency of the plasma proved in the case of X-band frequencies to be the overriding factor in the signal to noise ratio observed. The DC glow discharge inside the EPR cavity was at worst disastrous and at best impractical. It was thought that the detection frequency may be too close to that of plasma frequency, but that the enhanced concentration of the transient species derived from producing the species inside the EPR cavity would outweigh the unfavourable closeness of the detection and plasma generation frequencies. The reverse of this proved to be the case.

SECTION III.5 - RESULTS AND DISCUSSION

b) WITHIN THE MILLIMETER WAVE MAGNETIC RESONANCE SPECTROMETER CAVITY

The condition outlined in Equation III.3.3 proved to be much more favourable in the case of the millimeter wave magnetic resonance spectrometer. It was found that this increase by a factor of more than ten in frequency over the EPR detection frequency was sufficient to prevent any noise from the DC discharge disturbing the millimeter wave detector.

c) WITHIN THE INFRARED DIODE LASER ABSORPTION TUBE

The condition outlined in Equation III.2.3 proved to be also favourable in the case of the IDL absorption tube DC glow discharge. No increase in noise on the IDL detector when the glow discharge was struck under a variety of conditions was observed. An increase in noise was however observed once the discharge had been running for a long period of time (hours), but this was found to be due to the "dendritic" growths of amorphous silicon which were reflecting the diode laser beam from its prescribed path and could be eliminated on their removal. The DC glow discharge was an excellent method of generating transients in relatively high concentrations to the extent that both the fundamental and the first vibrational levels of SiH were clearly visible on the oscilloscope and some other transient signals tentatively assigned to the SiH₂ radical were observed on the chart recorder (Chapter VI, Section VI.2 and Section VI.3).

III.6 CONCLUSIONS

A DC glow discharge as a method of generating transient species has been employed in three different regions of the

SECTION III.6 - CONCLUSIONS

electromagnetic spectrum viz. X-band microwave wave (8.5 - 12.4 GHz), millimeter wave and infrared frequencies. In the first of these regions it was found that the plasma frequency was too close to the detection frequency to make it a practical method of producing transient species inside the EPR spectrometer cavity. In the second case it was found that the DC glow discharge did not impair the detection system even under vigorous discharge conditions, however due to the failure of the IMPATT oscillator no signals arising from the SO radical were observed. In the third case the DC glow discharge was again found not to interfere with the IDL detector and proved to be an excellent method of generating transient species with the added bonus of producing them in excited states.

SECTION III.7 - REFERENCES

III.7 REFERENCES

1. R. Beringer & E.B.Rawson, Phys. Rev., 87, 228 (1952).
2. K.Nagai, K.Tanaka & E.Hirota, (To be Published).
3. R.Panock, M.Rosenbluh, B.Lax & T.A.Miller,
Phys. Rev., 22A, 1050 (1980).
4. M.A.Heald & R.Beringer, Phys. Rev., 96, 645 (1954).
5. E.B.Rawson & R. Beringer, Phys. Rev., 88, 677 (1952).
6. H.G.Dehmelt, Phys. Rev., 99, 527 (1955).
7. T.J.Sears & A.R.W.McKellar,
Can. J. Phys., 60, 345 (1982).
8. C.Yamada, K.Nagai & E.Hirota,
J. Mol. Spec., 85, 416 (1981).
9. Y.Endo, S.Saito & E.Hirota,
J. Mol. Spec., 94, 199 (1982).
10. K.Kawaguchi, K.Nagai, C.Yamada, Y.Hamada & E.Hirota,
J. Mol. Spec., 86, 136 (1981).
11. C.Yamada & E.Hirota, J. Mol. Spec., 74, 203 (1979).
12. T.R.Todd & W.B.Olson, J. Mol. Spec., 205 (1979).
13. T.Amano, S.Saito, Y.Morino, D.R.Johnson & F.X. Powell,
J. Mol. Spec., 30, 275 (1969).
14. H.E.Radford, K.M.Evenson & C.J.Howard,
J. Chem. Phys., 60, 3178 (1974).
15. Y.Endo, S.Saito & E.Hirota,
J. Chem. Phys., 75, 4379 (1981).
16. C.Yamada, Y.Endo & E.Hirota,
J. Chem. Phys., 74, 4159 (1983).
17. T.Minowa, S.Saito & E.Hirota, IMS Ann. Rev., 31 (1984).
18. H.Kanamori, C.Yamada, K.Kawaguchi, J.E.Butler & E.Hirota,
IMS Ann. Rev., 32 (1984).
19. S.Saito, Y.Endo & E.Hirota,

SECTION III.7 - REFERENCES

- J. Chem. Phys., 82, 2947 (1985).
20. Y.Endo, S.Saito, & E.Hirota,
J. Mol. Spec., 92, 443 (1982).
21. P.B.Davies, B.J.Handy, E.K.Murray Lloyd & D.K.Russell,
Mol. Phys., 36, 1005 (1978).
22. H.E.Radford, J. Chem. Phys., 40, 2732 (1964).
23. M.Tanimoto, S.Saito, Y.Endo & E.Hirota,
J. Mol. Spec., 100, 205 (1983).
24. P.B.Davies, N.A.Isaacs, S.A.Johnson and D.K.Russell,
J. Chem. Phys., 83, 2060 (1985).
25. C.Yamada & E.Hirota, J. Chem. Phys., 82 (1985).
26. S.Saito, Y.Endo & E.Hirota,
J. Chem. Phys., 78, 6447 (1983).
27. H.E.Radford , J. Chem. Phys., 40, 2732 (1964).
28. K.Kawaguchi, E.Hirota & C.Yamada,
Mol. Phys., 44, 509 (1981).
29. C.Yamada, H.Kanamori, S.Saito & E.Hirota,
IMS Ann. Rev., 38 (1984).
30. K.Kawaguchi, Y.Endo & E.Hirota,
J. Mol. Spec., 93, 381 (1982).
31. K.Nagai, C.Yamada, Y.Endo, & E.Hirota,
J. Mol. Spec., 89, 520 (1981).
32. S.Saito, Y.Endo & E.Hirota, IMS Ann. Rev., 36 (1983).
33. Y.Endo, S.Saito & E.Hirota,
J. Mol. Spec., 97, 204 (1983).
34. Y.Endo, C.Yamada, S.Saito & E. Hirota,
J. Chem. Phys., 75, 4379 (1981).
35. C.Yamada, K.Nagai & E.Hirota,
J. Chem. Phys., 75, 5256 (1981).
36. R.C.Woods, Rev. Sci. Inst., 44, 282 (1973).

SECTION III.7 - REFERENCES

37. N.A.Isaacs,* B.J.Kelly,* R.M.Lindsay & D.K.Russell,
*3rd Undergraduate Year Project, (unpublished results).
 38. C.P.Poole, "Electron Spin Resonance: a Comprehensive
Treatise on Experimental Techniques", Interscience
Publishers, a Division of John Wiley & Sons,
New York, London, Sydney (1967).
 39. S.A.Johnson, Ph.D. Thesis (1986), Cambridge, England.
-

SECTION IV.1 - INTRODUCTION

CHAPTER IV - GENERATION BY CARBON DIOXIDE LASER AND SULPHUR HEXAFLUORIDE PHOTSENSITISATION

IV.1 INTRODUCTION

In this Chapter the carbon dioxide laser and sulphur hexafluoride photosensitisation method is examined as a method for producing transient species for detection by high resolution spectroscopic techniques. Transient species produced by carbon dioxide lasers are first reviewed and this is followed by a series of experiments which may be considered as feasibility studies for the generation of such species. An account of some experiments in which information pertaining to the effective temperatures involved in this generation method was obtained is also reported, and this is followed by a series of experiments in which both indirect and direct generation schemes were utilised to produce free radicals for high resolution spectroscopic detection.

IV.2 REVIEW

Much of the literature on the development of the application of carbon dioxide lasers to the breaking apart of stable precursors has been in the field of isotopic selectivity and enrichment, particularly by groups interested in nuclear physics (atomic energy generating agencies). The carbon dioxide laser in these systems was used alone without a photosensitiser and as a consequence of this relied upon the fact that the precursor under consideration must have an infrared absorption coincidental or close to the carbon dioxide laser output. Since this method is not sufficiently general in its applicability to transient generation this work has been omitted.

SECTION IV.2 - REVIEW

The literature concerned with the more general application of a photosensitiser in conjunction with a carbon dioxide laser is sparse in comparison, as is quantitative data on such systems. Photosensitisers which have been utilised in this manner are sulphur hexafluoride (SF_6), tetrafluorosilane (SiF_4), ammonia (NH_3), boron trichloride (BCl_3), ethene (C_2H_4) and tetrafluorohydrazine, (N_2F_4)¹.

Simple hydrocarbons such as methane, (CH_4)², ethane, (C_2H_6) and propane, (C_3H_8)², have been photosensitised with SF_6 . In the study on CH_4 a pulsed laser generating peak powers of the order of 350 Watts irradiated samples of SF_6 and CH_4 , causing the SF_6 to fragment forming fluorine atoms which subsequently reacted with the CH_4 in a free radical mechanistic manner. It was noted that the addition of oxygen, O_2 , increased the concentration of the fragments detected and that the slowest step in the process was the vibration-translation energy transfer within the SF_6 , and it was estimated to be of the order of 150 μs . This value is much longer than the time scale for ionisation within this system which was estimated as being of the order of $< 10 \mu\text{s}$. It should also be noted that the SF_6 was not acting as a true photosensitisation agent in this system since it was actually participating in the reaction and not acting purely as an energy transfer agent.

A continuous wave carbon dioxide laser in association with SF_6 as a photosensitiser was used to break apart C_2H_6 and C_3H_8 ³. The observed products from ethane were ethene, C_2H_4 and methane, CH_4 . Infrared spectroscopy and mass spectrometry were utilised for product identification.

The carbon dioxide laser and SF_6 photosensitisation of

SECTION IV.2 - REVIEW

ferrocene ($\text{Fe}(\text{C}_5\text{H}_5)_2$), molybdenum hexacarbonyl ($\text{Mo}(\text{CO})_6$) and carbonyl sulphide (OCS) all resulted in the observed deposition of solid matter⁴. The $\text{Fe}(\text{C}_5\text{H}_5)_2$ deposited metallic iron, the $\text{Mo}(\text{CO})_6$ produced metallic molybdenum and gaseous carbon monoxide, and OCS deposited elemental sulphur and carbon monoxide. The gaseous products were identified by infrared spectroscopy and mass spectrometry. Mixtures of 1,2-dichloroethene (CHClCHCl) and SF_6 were irradiated with a pulsed carbon dioxide laser to induce photoisomerisation of the *cis*- CHClCHCl to the *trans*- CHClCHCl ⁵. A bright emission was noticed from the *cis*- CHClCHCl when the laser was focussed down on to the cell. Other observed products which were identified by infrared spectroscopy were chloroethyne, ClCCH , and ethyne, C_2H_2 .

The most significant paper in terms of its relevance to this Chapter was the recent 'Detection of Transient Laser Magnetic Resonance Signals in Pulsed CO_2 Laser Irradiation of $\text{SF}_6/\text{H}_2\text{O}$ and SF_6/NO Mixtures', by Smith *et al.*⁶. This paper describes the first observation of the transient hydroxyl radical, OH, by LMR spectroscopy, generated by a pulsed carbon dioxide laser and its associated SF_6 photosensitiser. These experiments are very similar in nature to the nitrogen difluoride radical system described in Section IV.3(c)(ii), with the exceptions that in the latter case EPR spectroscopy was used as the radical detection system and the carbon dioxide laser operated in a chopped continuous wave mode as opposed to pulsed. The latter part of the paper by Smith *et al.* describes the observation of an LMR signal from the stable paramagnetic nitric oxide molecule (NO) which is also very similar to the oxygen atom system described in

SECTION IV.2 - REVIEW

Section IV.3(c)(i), with the exceptions that the carbon dioxide laser was in continuous wave mode and the EPR signal decreased (as opposed to increased), and the transient O atom was generated from a 2450 MHz discharge.

Tetrafluorosilane (SiF_4) has also been used as photosensitisation agent in conjunction with a carbon dioxide laser since this molecule also possesses an infrared coincidence and is relatively inert to chemical attack. Mixtures of allene, CH_2CCH_2 , and SiF_4 were irradiated with a carbon dioxide laser and the observed products (identified by infrared spectroscopy and flame ionisation gas chromatography) were ethyne (C_2H_2) and methylethyne (CH_3CCH)⁷. SF_6 was also used as a photosensitisation agent but it was found to be not as effective in producing the observed products. Mixtures of 1,2-dichloropropane, $\text{CH}_3\text{CHClCH}_2\text{Cl}$ and SiF_4 were irradiated with either a focussed or unfocussed pulsed carbon dioxide laser and the products and mechanisms proposed compared to those under thermal and unsensitised systems⁸. The products from the photosensitisation experiments, which were identified by flame ionisation gas chromatography, were the four main isomeric chloropropenes.

SiF_4 , like SF_6 , has also been used with a carbon dioxide laser to generate a transient species for spectroscopic detection. Mixtures of silane, SiH_4 , and SiF_4 , were irradiated with an unfocussed pulsed carbon dioxide laser to break apart the SiH_4 and the fragments monitored by their emission spectra⁹. The silylene radical, SiH_2 , was unambiguously proved to present from the emission spectrum of its $^1\text{B}_1$ excited electronic state, which had been previously recorded.

SECTION IV.2 - REVIEW

Finally, ammonia, (NH_3), has been used as a photosensitisation agent for a carbon dioxide laser¹⁰. Mixtures of cyclobutanone ($\text{C}_4\text{H}_6\text{O}$), and NH_3 were irradiated with a pulsed carbon dioxide laser. The observed products, analysed by flame ionisation gas chromatography, were found to be ethene (C_2H_4), propene (C_3H_6), cyclopropane (C_3H_6) (which isomerised to propene), carbon monoxide (CO), and ketene (CH_2CO).

IV.3 EXPERIMENTAL

The experiments described within this Section utilised a carbon dioxide, CO_2 , laser, unfocussed unless specified (the Edinburgh Instruments PL-4 at Leicester (without a tuning grating or the Apollo 550 at Cambridge with a tuning grating tuned to the $^{10}\text{P}_{20}$ line) and a photosensitiser, SF_6 , and they can be divided into three. The first sub-section may be classed as feasibility studies on the generation of silicon containing intermediates and radicals which were also of interest to another group within this department¹¹. The second sub-section can be classed as feasibility studies for the generation of atoms and radicals for direct detection by one of the three high resolution spectroscopic techniques discussed within this thesis. The final sub-section contains experiments which were partly of an informative nature on this species generation system itself, and partly experiments studying both indirect and direct generation of the species and subsequent detection.

A gas phase cell, the body of which consisted of two greaseless, 'O'-ring cones (B19) and a greaseless tap was constructed. Two greaseless, 'O'-ring, sockets were truncated

SECTION IV.3 - EXPERIMENTAL

and the ends of which were ground down to provide a smooth surface on to each of which a zinc selenide, ZnSe, window was sealed with an epoxy resin. This provided a gas phase cell with a system for removing the windows for cleaning, an internal diameter of 10 mm and a path length of 120 mm, which was sufficiently small in length to fit inside the sample beams of a variety of available infrared spectrometers. In an attempt to establish whether the specified precursors could generate the specified transient for possible detection by the specified spectroscopic technique, the precursor below and SF₆ were admitted in to the cell and an infrared spectrum (low resolution) taken to identify those absorptions arising from the specified precursor and SF₆ in each case. The cell was then placed in front of a carbon dioxide laser (Apollo model 550 tuned to the ¹⁰P₂₀ line or the Edinburgh Instruments PL4) to deliver 30 Watts and irradiated for 30 s. An infrared spectrum of the contents of the cell was then taken in each case which revealed a number of the precursor bands had decreased substantially in intensity whilst a number of new bands appeared. An approximate ratio of 4:1 SF₆ to precursor was kept throughout as this was found to be the most effective pressure composition for product generation

a) SILICON CONTAINING INTERMEDIATES FOR DETECTION BY INFRARED DIODE LASER (IDL) SPECTROSCOPY

(i) THE 1,1-DIMETHYLSILYACYCLOBUTANE (DMSCB) SYSTEM:

2.0 mBar of DMSCB and 8.0 mBar of SF₆ were irradiated with 30 Watts for 30 s to establish whether DMSCB could generate the 1,1-dimethylsilaethene intermediate, (CH₃)₂SiCH₂, (DMSE) for possible detection by IDL spectroscopy. The positions of the

SECTION IV.3 - EXPERIMENTAL

new infrared bands from the products of the irradiation are summarised in Table IV.4.1.

(ii) THE VINYLDIMETHYLCARBINOXYDIMETHYLSILANE (VCS) SYSTEM:

1.0 mBar VCS and 3.0 mBar of SF_6 were irradiated with 30 Watts for 30 s to establish whether VCS could generate the 1,1-dimethyl silanone intermediate, $(CH_3)_2SiO$, (DMSO) for possible detection by IDL spectroscopy. A solid white deposit was formed on the inside of the cell walls during irradiation. An infrared spectrum of the contents of the cell was then taken which revealed a number of the precursor bands had decreased substantially in intensity whilst a number of new bands appeared.

(iii) THE DIHYDRIDOSILACYCLOBUTANE SYSTEM (DHSCB):

5.0 mBar of DHSCB and 15.0 mBar of SF_6 were irradiated with 30 Watts for 30 s to establish whether DHSCB be a source of the silylene radical, SiH_2 , for possible detection by IDL spectroscopy. The positions of the new infrared bands from the products of the irradiation are summarised in Table IV.4.2.

b) POTENTIAL ATOM AND RADICAL SOURCES FOR HIGH RESOLUTION SPECTROSCOPIC DETECTION

(i) THE METHYL IODIDE (CH_3I) SYSTEM:

1.0 mBar of methyl iodide, CH_3I and 3.0 mBar of SF_6 were irradiated for 30 Watts for 30 s to establish whether CH_3I could generate iodine atoms, I , and methyl radicals, CH_3 , for possible detection by EPR spectroscopy in the former case and millimeter wave resonance magnetic (MMR) spectroscopy in the

SECTION IV.3 - EXPERIMENTAL

latter. A thin purple coating of molecular iodine was clearly visible on the inside of the cell walls after irradiation. The positions of the new infrared bands from the products of the irradiation are summarised in Table IV.4.3.

(ii) THE ACETONE ((CH₃)₂CO) SYSTEM:

3.0 mBar of (CH₃)₂CO and 12.0 mBar of SF₆ were irradiated with 30 Watts for 30 s in an attempt to establish whether (CH₃)₂CO could generate CH₃ radicals, for possible detection by MMR spectroscopy. The positions of the new infrared bands are shown in Figure IV.4.1(b).

(iii) THE ACETALDEHYDE (CH₃CHO) SYSTEM:

3.0 mBar of CH₃CHO and 12.0 mBar of SF₆ were irradiated with 30 Watts for 30 s to establish whether CH₃CHO could generate CH₃ HCO radicals, for possible detection by MMR spectroscopy. The positions of the new infrared bands from the products of the irradiation are summarised in Figure IV.4.2(b).

(iv) THE IRON PENTA-CARBONYL (Fe(CO)₅) SYSTEM:

In an attempt to establish whether Fe(CO)₅ could generate Fe atoms, for possible detection by EPR spectroscopy, 2.0 mBar of Fe(CO)₅ and 8.0 mBar of SF₆ were irradiated with 30 Watts for 30 s and a clearly visible iron mirror was deposited on the inside of the cell walls during irradiation. The positions of the new infrared bands from the products of the irradiation are summarised in Figure IV.4.3(b).

SECTION IV.3 - EXPERIMENTAL

(v) THE SULPHUR HEXAFLUORIDE (SF_6) SYSTEM:

3.0 mBar of SF_6 was irradiated with 50 Watts for 30 s and a clearly visible red glow proceeded down the cell. The reason for the irradiation was to establish the maximum power the SF_6 could absorb as a photosensitisation agent and establish whether it could be used as a possible source of F atoms for detection by EPR spectroscopy. The positions of the new infrared bands from the products of the irradiation are summarised in Figure IV.4.4(b).

c) INFORMATIVE, INDIRECT AND DIRECT GENERATION SYSTEMS

(i) THE OXYGEN ATOM EFFECTIVE TEMPERATURE SYSTEM:

The modified EPR Zeeman cavity (Section V.3) was assembled with the two port end piece and its resonant frequency in the TE₀₁₂ was measured to be 8626 MHz. The products of a 2450 MHz discharge in O_2 were passed through the cavity and the O atom signal monitored on the oscilloscope. The pressure of the O_2 was then reduced to 0.15 mBar to resolve the four $^3\text{P}_2$ signals and the outer $^3\text{P}_1$ signals and the spectrum was recorded on the chart recorder. SF_6 was then mixed inside the cavity via the top port at a pressure of 0.15 mBar. The CO_2 laser was then aligned so as to pass through the zinc selenide port hole (Figure V.3.3(a)) at a measured power of 10 Watts. The O atom spectrum was then re-recorded with SF_6 photosensitiser mixing with the products of the 2450 MHz discharge and the CO_2 laser emitting 10 Watts, and it was noticed that the intensities of the O atom signals decreased dramatically. On increasing the power of the CO_2 laser to 20, 30, 40 Watts further decreases in the intensity of the O atom signal were observed. A constant pressure of SF_6 to an incremented

SECTION IV.3 - EXPERIMENTAL

pressure of O_2 against increasing laser powers were then recorded and these results are tabulated in Table IV.4.4.

(ii) THE SULPHUR MONOXIDE RADICAL (SO) SYSTEM:

The modified EPR Zeeman cavity (Section V.3) was assembled with the two port end piece and its resonant frequency in the TE₀₁₂ was measured to be 8541 MHz. Elemental sulphur was then placed in a porcelain cup ground down to fit inside the top vacuum line tube on to which had been blown a greaseless 'O'-ring cone (B19) to allow a zinc selenide window to be fitted to the end of the tube allowing the CO₂ laser beam passage up the tube to hit the sample in the cup just outside the EPR cavity. The products of a 2450 MHz discharge in O₂ were passed through the cavity and the O atom signal monitored on the oscilloscope. The CO₂ laser at a power of between 30 - 40 watts was aligned on to the elemental sulphur whilst a background pressure of argon, Ar, at 0.1 mBar acted as carrier gas over the top of the sulphur which was now being vaporised. When the magnetic field was scanned through 0.25 to 0.35 T an intense signal arising from the SO radical was detected and is shown in Figure IV.3.1. This signal did not disappear when the laser was turned off, but it did when the 2450 MHz discharge was switched off indicating that it arose from deposited sulphur on the inside of the EPR cavity walls reacting with atomic oxygen.

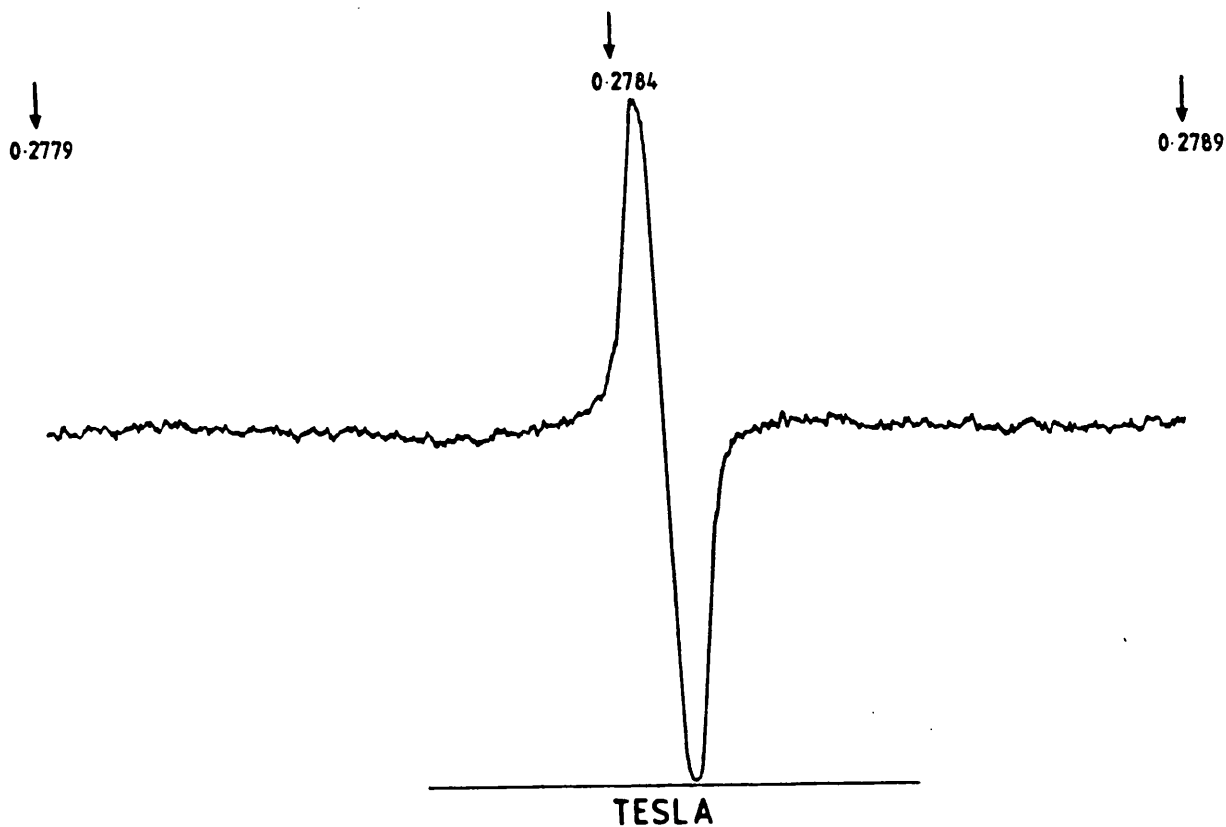


Figure IV.3.1. The SO radical EPR signal arising from CO₂ laser deposited sulphur and the products of a 2450 MHz discharge in O₂. O₂ pressure 0.3 mBar, magnetic field, 0.2784 ± 0.0005 T, time constant 0.3 s, modulation frequency 100 kHz.

SECTION IV.3 - EXPERIMENTAL

(iii) THE NITROGEN DIFLUORIDE RADICAL (NF_2) SYSTEM:

2.0 mBar of N_2F_4 and 8.0 mBar of SF_6 were admitted in to the gas phase cell described above and the IDL spectrometer beam aligned through it with the aid of helium-neon laser such that the CO_2 laser beam (Apollo 550), tuned to the $^{10}\text{P}_{20}$ line, and the diode beam were coincident on the front window of the cell. The IDL spectrometer was set up such that a mode pattern (at 1005 cm^{-1}) was being swept on the oscilloscope and numerous absorptions arising from N_2F_4 were clearly visible. When the CO_2 laser at a measured power of 20 Watts was switched on these absorption disappeared, but they were immediately replaced by a second set, identified as arising from the NF_2 radical¹².

The modified EPR Zeeman cavity (Section V.3) was assembled with the two port end piece and its resonant frequency in the TE_{012} was measured to be 8511 MHz. 2.0 mBar of N_2F_4 and 8.0 mBar of SF_6 were flowed into the cavity and the CO_2 laser beam (Edinburgh Instruments PL-4) aligned through the zinc selenide port hole. A chopper at 1.0 Hz was then placed in front of the CO_2 laser beam and the magnetic field set to scan from 0.25 to 0.35 T whilst the CO_2 laser beam, measured at 30 Watts, irradiated the gases in the cavity. Figure IV.3.2 shows the signal observed due to the NF_2 radical. It should be noted that this figure does not show any rotational fine structure, but it does show the effect on the signal intensity of effectively switching the CO_2 laser beam on and off at regular 1.0 Hz intervals.

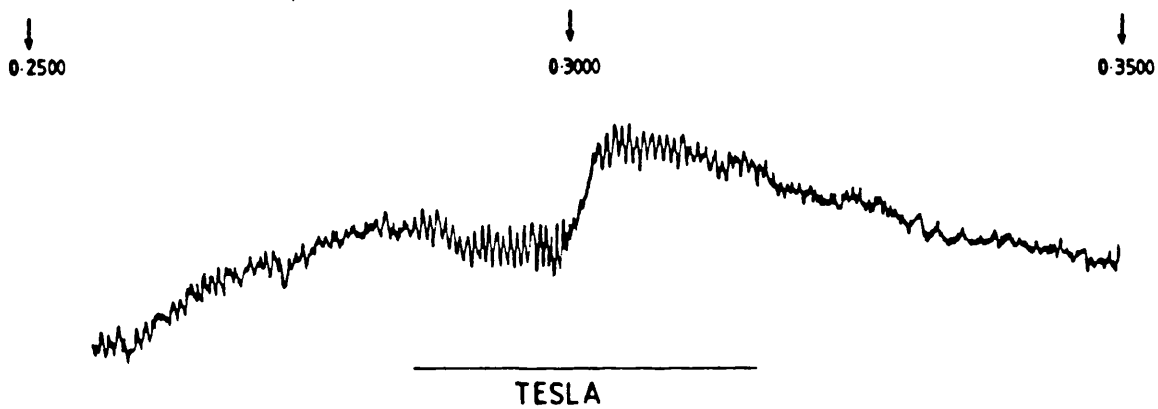


Figure IV.3.2. The NF_2 radical EPR signal from N_2F_4 and a 1.0 Hz chopped laser beam. N_2F_4 pressure 2.0 mBar, SF_6 pressure 8.0 mBar, magnetic field 0.30 ± 0.050 T, time constant 1.0 s, modulation frequency 100 kHz.

SECTION IV.3 - EXPERIMENTAL

(iv) THE IODINE ATOM (I) SYSTEM:

In an attempt to detect signals arising from iodine atoms, I, the modified EPR Zeeman cavity (Section V.3) was assembled with the two port end piece and its resonant frequency in the TE₀₁₂ was measured to be 8710 MHz. CH₃I and SF₆ were flowed through the cavity at a variety of pressure conditions and the CO₂ laser beam (Edinburgh Instruments PL-4) irradiated the gases in the cavity. Although a wide range of conditions were employed no I atom signals could be detected. It was thought that this may be due to the small photolysis region of the CO₂ laser beam generating too small a concentration of I atoms in a small volume of the EPR cavity for them to be detected: consequently a de-focusing convex lens of focal length 25 mm was purchased and fitted in place of the zinc selenide window and the experiment repeated. Even though a wide range of conditions were employed using the lens no I atom signals could be detected.

(v) THE SELENIUM CHLORIDE RADICAL (SeCl) SYSTEM:

In an attempt to detect signals arising from the selenium chloride radical (SeCl) the modified EPR Zeeman cavity (Section V.3) was assembled with the two port end piece and its resonant frequency in the TE₀₁₂ was measured to be 8710 MHz. Se₂Cl₂ and SF₆ were flowed through the cavity (Se₂Cl₂ as described in Section V.4 (xiii)) at a variety of pressure conditions and the CO₂ laser beam (Edinburgh Instruments PL-4) irradiated the gases in the cavity. Although a wide range of conditions were employed no signals arising from the SeCl radical could be detected. It was thought that this may be due to the small photolysis region

SECTION IV.3 - EXPERIMENTAL

of the CO₂ laser beam generating too small a concentration of SeCl radicals in a small area of the EPR cavity for them to be detected, consequently a de-focusing convex lens was fitted in place of the zinc selenide window and the experiment repeated. Even though a wide range of conditions were employed using the lens no signals arising from the SeCl radical could be detected.

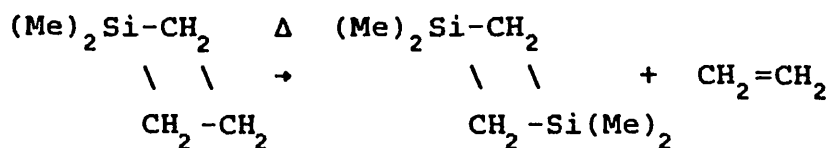
IV.4 RESULTS AND DISCUSSION

a) THE SILICON CONTAINING INTERMEDIATES FOR DETECTION BY INFRARED DIODE LASER (IDL) SPECTROSCOPY

(i) THE 1,1-DIMETHYLSILACYCLOBUTANE (DMSCB) SYSTEM:

An analysis of the post laser pyrolysis infrared spectrum revealed that extensive changes had taken place. The observed products under normal pyrolysis from this reaction are the head-to-tail dimer (1,1,3,3-tetramethyldisilacyclobutane) and ethene¹³, as can be seen from Scheme I:

Scheme I



The post laser pyrolysis infrared spectrum revealed that both of these products were present in the cell characterised by the absorptions shown in Table IV.4.1.

SECTION IV.4 - RESULTS AND DISCUSSION

New bands :	3100	1440	940
Products :	C ₂ H ₄	C ₂ H ₄	Dimer

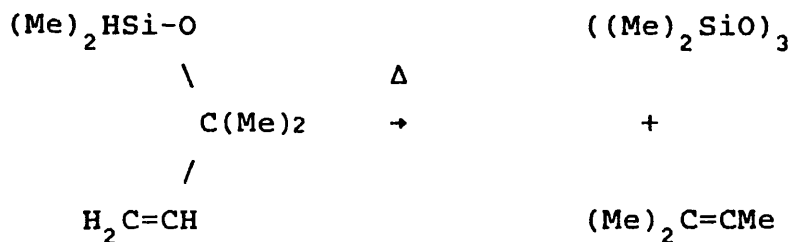
Table IV.4.1. Table showing the wavenumbers of the characteristic product bands from the photolysis products of DMSCB.

On the basis of the study it appears that DMSCB can act as a precursor for the 1,1-dimethylsilaethene (DMSE) intermediate utilising this SF₆ photosensitisation of the CO₂ laser generation scheme.

(ii) THE VINYL DIMETHYL CARBINOXY DIMETHYL SILANE (VCS) SYSTEM:

An analysis of the post laser pyrolysis infrared spectrum revealed that extensive change had taken place. The observed products under normal pyrolysis are the trimer and 2-methylbut-2-ene¹⁴, as can be seen from Scheme II:

Scheme II



SECTION IV.4 - RESULTS AND DISCUSSION

An analysis of the post laser pyrolysis infrared spectrum revealed that no bands from the 2-methylbut-2-ene were present, however methane (from its characteristic absorptions at 3002 and 1302 cm^{-1}) was, and the white solid deposit was thought to be a polymer of the 1,1-dimethyl silanone. On the basis of the study it appears that VCS can act as a precursor for the 1,1-dimethyl silanone intermediate utilising this SF_6 photosensitisation of the CO_2 laser generation scheme.

(iii) THE DIHYDRIDOSILACYCLOBUTANE SYSTEM (DHSCB):

An analysis of the post laser pyrolysis infrared spectrum revealed that extensive change had taken place. The observed products under normal pyrolysis are hydrogen, propene and other cyclic silicon-hydrogen containing compounds, but the initial step is believed to be the formation of propene and silylene¹⁵, as is shown in Scheme III:

Scheme III



An analysis of the post laser pyrolysis infrared spectrum revealed that both bands from silane (SiH_4), methane (CH_4), and ethyne (C_2H_2) were present, and the position of their characteristic absorptions are shown in Table IV.4.2.

SECTION IV.4 - RESULTS AND DISCUSSION

New Bands :	3010	2190	1710	1305	730
Products :	CH ₄	SiH ₄	C ₂ H ₂	CH ₄	CH ₄

Table IV.4.2. Table showing the wavenumbers of the characteristic product bands from the photolysis of DHSCB

In the previous study on the pyrolysis of DHSCB¹⁵, mass spectrometry was employed in the analysis of the products, but this spectroscopic technique is insensitive to SiH₄, due to the relative instability of the SiH₄⁺ cation¹⁶. The infrared spectrum clearly showed that SiH₄ was a major product after irradiation with the carbon dioxide laser and this information is now throwing new light on the mechanism of the pyrolysis of DHSCB. On the basis of the study it appears that DHSCB can act as a precursor for the SiH₂ radical utilising this SF₆ photosensitisation of the CO₂ laser generation scheme.

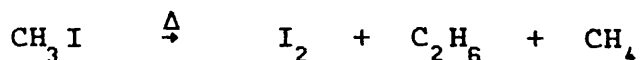
b) POTENTIAL ATOM AND RADICAL SOURCES FOR HIGH RESOLUTION SPECTROSCOPIC DETECTION

(i) THE METHYL IODIDE (CH₃I) SYSTEM:

An analysis of the post laser pyrolysis infrared spectrum revealed that extensive change had taken place. The observed products under normal pyrolysis are CH₄, C₂H₆ and I₂ as is shown in Scheme IV:

SECTION IV.4 - RESULTS AND DISCUSSION

Scheme IV



An analysis of the post laser pyrolysis infrared spectrum revealed that bands from ethane (C_2H_6), methane (CH_4), were present, and the positions of their characteristic absorptions are shown in Table IV.4.3.

New Bands :	3200	3010	1305	830	730
Products :	C_2H_6	CH_4	CH_4	C_2H_6	CH_4

Table IV.4.3. Table showing the wavenumbers of the characteristic product bands from the photolysis of CH_3I

On the basis of the study it appears that CH_3I can act as a precursor for both I atoms and CH_3 radicals utilising this SF_6 photosensitisation of the CO_2 laser generation scheme.

(ii) THE ACETONE ($(\text{CH}_3)_2\text{CO}$) SYSTEM:

An analysis of the pre and post laser pyrolysis infrared spectra revealed that extensive change had taken place (Figure IV.4.1(a),(b)). The observed products under normal pyrolysis are CH_4 and H_2CCO , but at higher temperatures CH_4 and CO as is shown in Scheme V:

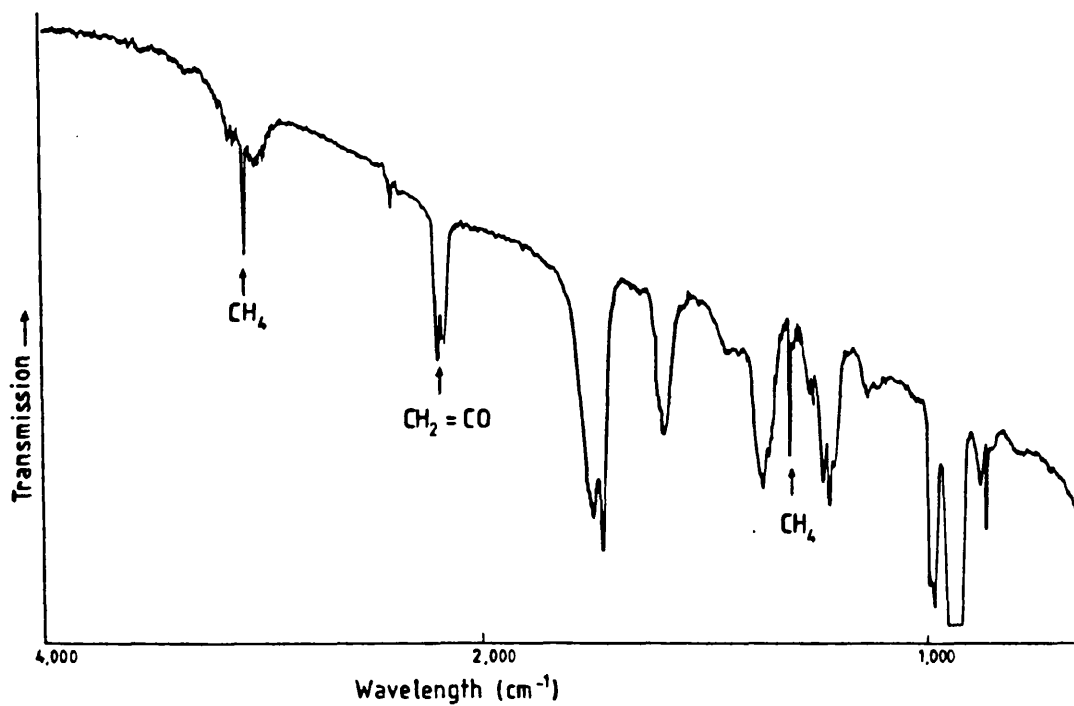
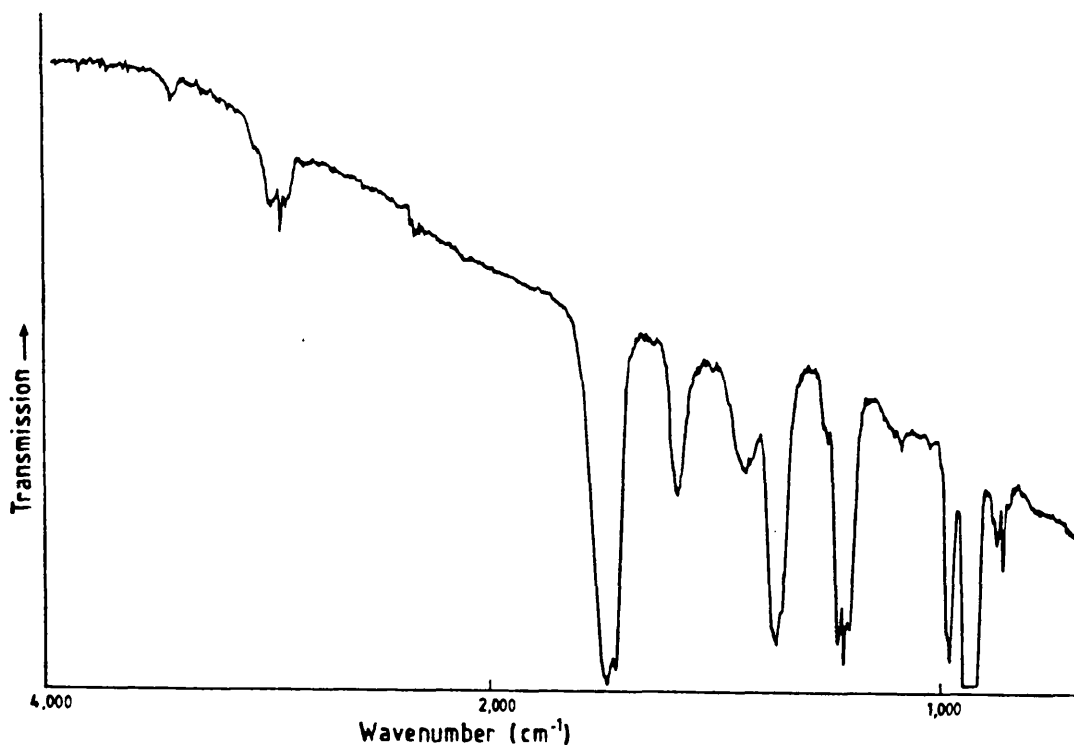
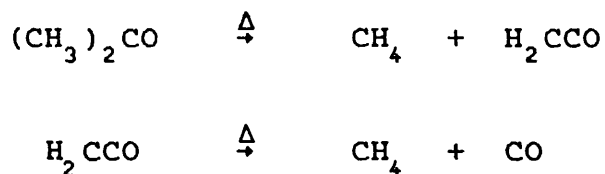


Figure IV.4.1(a)(b). The pre and post laser pyrolysis infrared spectra of $(\text{CH}_3)_2\text{CO}$ after irradiation of 30 Watts for 30 s. $(\text{CH}_3)_2\text{CO}$ pressure 3.0 mBar, SF_6 pressure 12.0 mBar.

SECTION IV.4 - RESULTS AND DISCUSSION

Scheme V



An analysis of the post laser pyrolysis infrared spectrum revealed that bands from methane (CH_4) and ketene (H_2CCO) were present, and the position of their characteristic absorptions are shown in Figures IV.4.1(b). On the basis of the study it appears that $(\text{CH}_3)_2\text{CO}$ can act as a precursor for CH_3 radicals utilising this SF_6 photosensitisation of the CO_2 laser generation method.

(iv) THE ACETALDEHYDE (CH_3CHO) SYSTEM:

An analysis of the pre and post laser pyrolysis infrared spectra revealed that extensive change had taken place (Figure IV.4.2(a),(b)). The observed products under normal pyrolysis are CH_4 and CO as is shown in Scheme VI:

Scheme VI



An analysis of the post laser pyrolysis infrared spectrum revealed that bands from methane (CH_4) and carbon monoxide (CO) were present, and the position of their characteristic absorptions are shown in Figures IV.4.2(b). On the basis of the study it appears that $(\text{CH}_3)_2\text{CO}$ can act as a precursor for CH_3 and HCO radicals utilising this SF_6 photosensitisation of the CO_2 laser generation method.

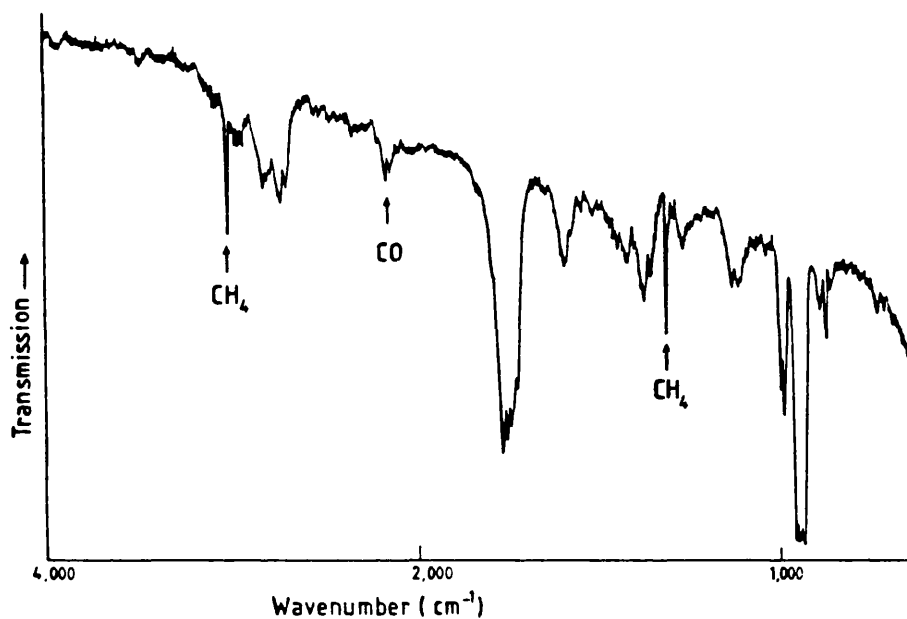
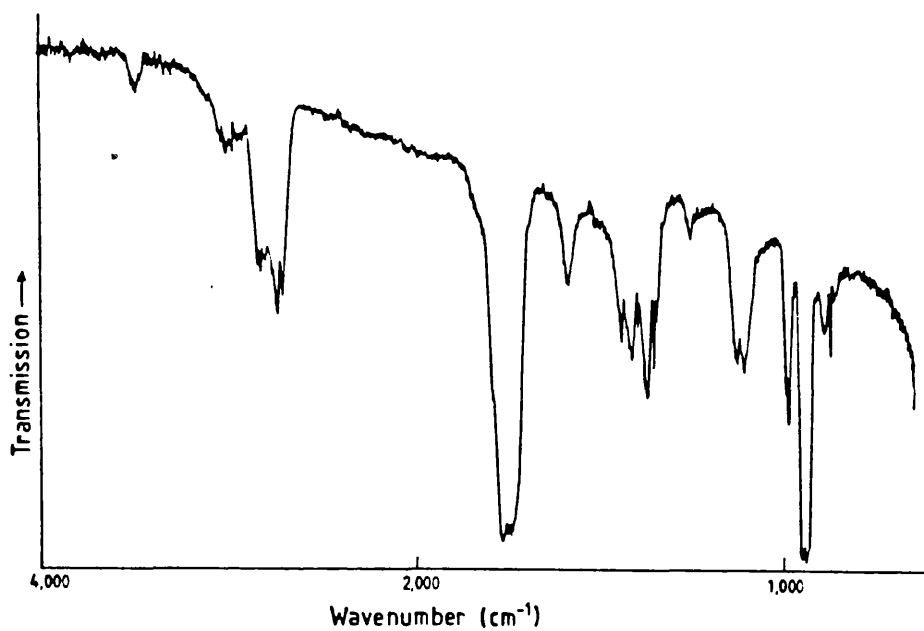


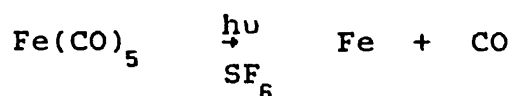
Figure IV.4.2(a)(b). The pre and post laser pyrolysis infrared spectra of CH_3CHO after irradiation of 30 Watts for 30 s. CH_3CHO pressure 3.0 mBar, SF_6 pressure 12.0 mBar.

SECTION IV.4 - RESULTS AND DISCUSSION

(v) THE IRON PENTACARBONYL ($\text{Fe}(\text{CO})_5$) SYSTEM:

An analysis of the pre- and post laser pyrolysis infrared spectra revealed that extensive change had taken place (Figure IV.4.3(a),(b)), and the reaction probably proceeds as is shown in Scheme VII:

Scheme VII



Inspection of the cell revealed a metallic iron mirror had formed during laser pyrolysis and an analysis of the post laser pyrolysis infrared spectrum revealed that bands from carbon monoxide (CO) were present, and the position of their characteristic absorptions are shown in Figures IV.4.3(b). On the basis of the study it appears that $\text{Fe}(\text{CO})_5$ can act as a precursor for Fe atoms utilising this SF_6 photosensitisation of the CO_2 laser generation method.

(vi) THE SULPHUR HEXAFLUORIDE (SF_6) SYSTEM:

An analysis of the pre and post photolysis infrared spectra revealed that extensive change had taken place (Figure IV.4.4(a),(b)), and the reaction probably initially proceeds as is shown in Scheme VIII:

Scheme VIII



An analysis of the post photolysis infrared spectrum

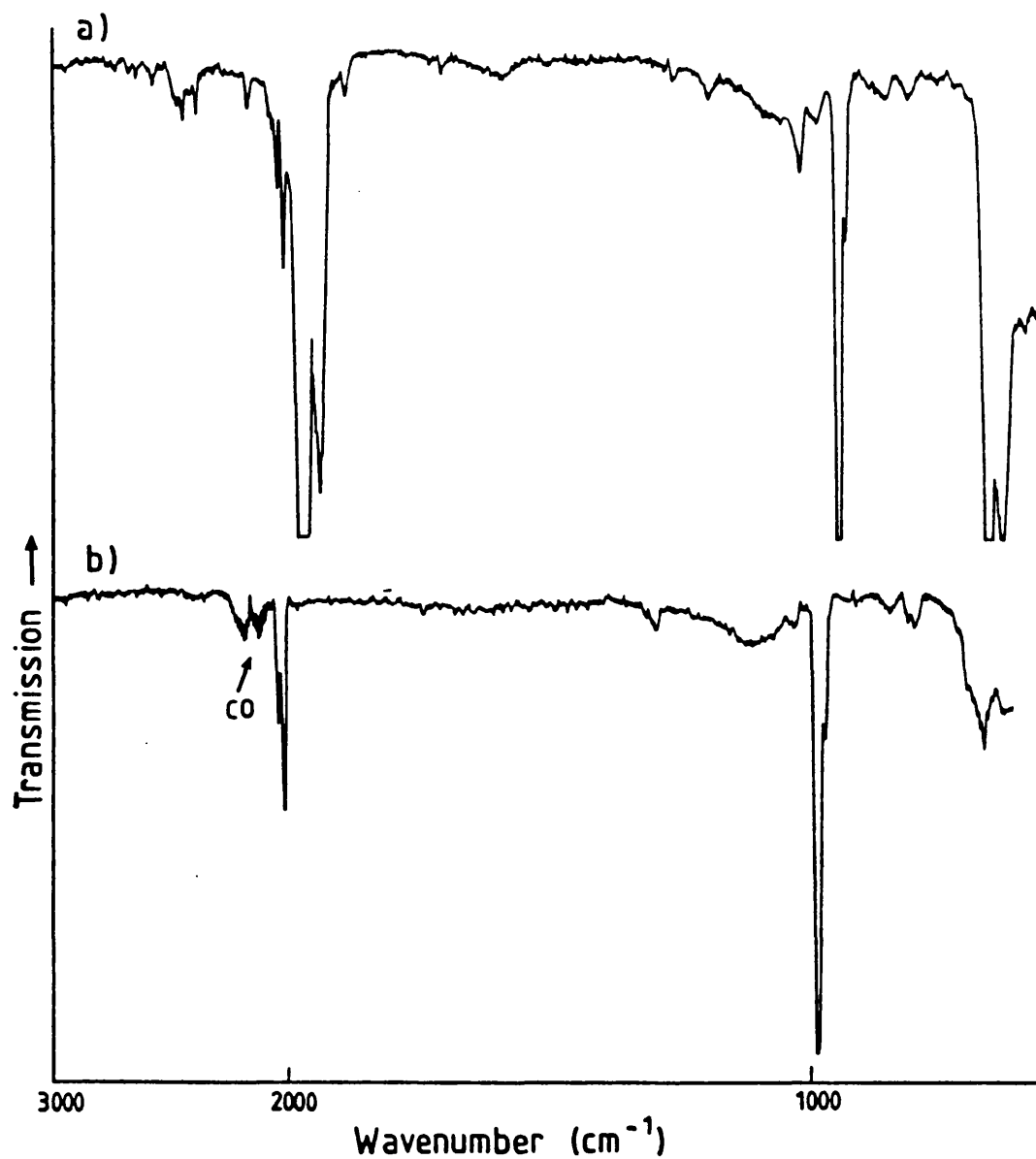


Figure IV.4.3(a)(b). The pre and post laser pyrolysis infrared spectra of $\text{Fe}(\text{CO})_5$ after irradiation of 30 Watts for 30 s. $\text{Fe}(\text{CO})_5$ pressure 2.0 mBar, SF_6 pressure 8.0 mBar.

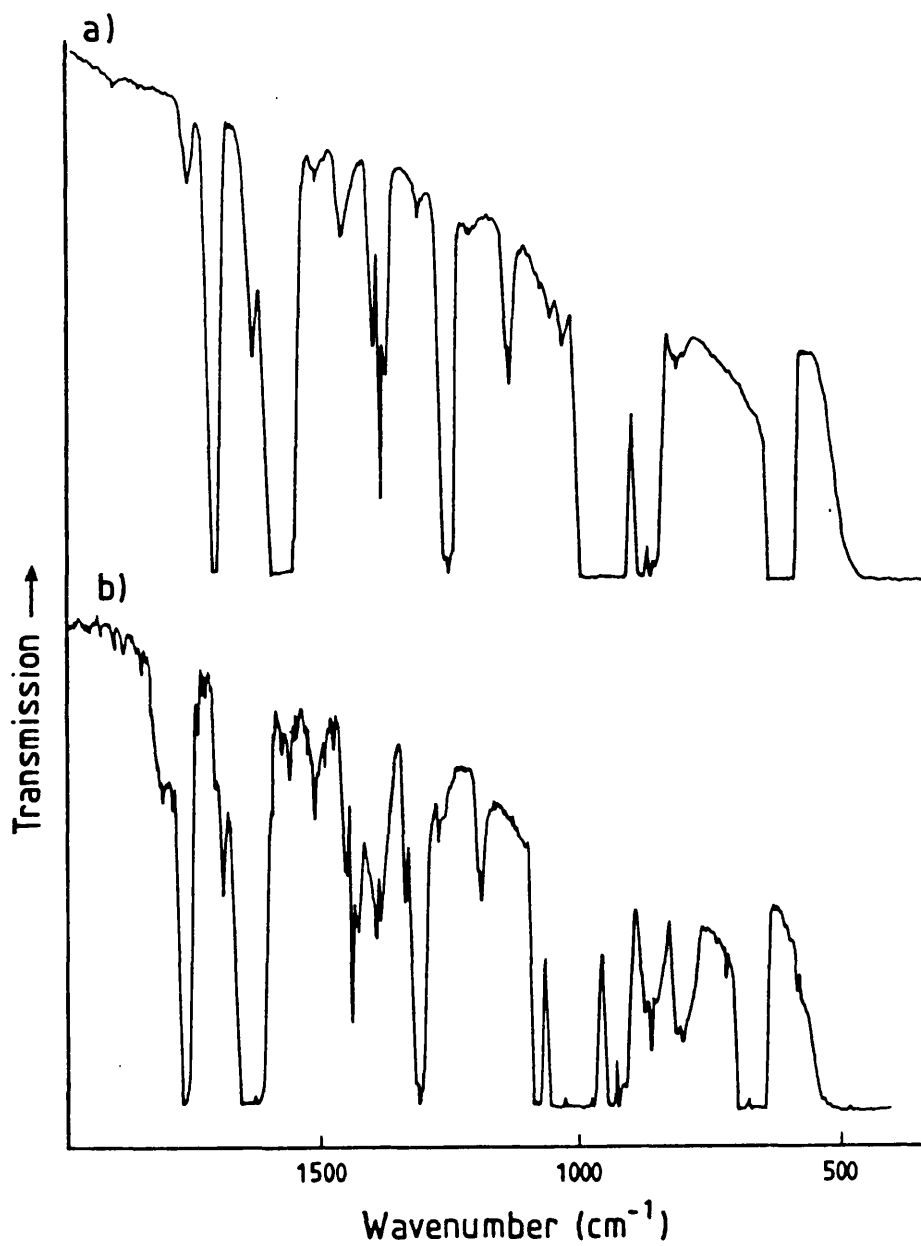


Figure IV.4.4(a)(b). The pre and post laser pyrolysis infrared spectra of SF₆ after irradiation of 50 Watts for 30 s. SF₆ pressure 3.0 mBar.

SECTION IV.4 - RESULTS AND DISCUSSION

revealed that many new bands were present, probably from various sulphur and fluorine compounds, but the spectrum was complex and no further product analysis was attempted since the point of the experiment was to break apart the SF₆ and a perusal of Figures IV.4.4(a),(b) shows that this was clearly achieved. On the basis of this study it appears that SF₆ can act as a precursor for both F atoms and possibly other sulphur and fluorine containing radicals utilising the CO₂ laser generation scheme, under more severe conditions than are normally used when employing SF₆ as a photosensitisation agent.

c) THE INFORMATIVE, INDIRECT AND DIRECT GENERATION SYSTEMS

(i) THE OXYGEN ATOM EFFECTIVE TEMPERATURE SYSTEM:

The EPR O atom signal was observed to decrease in intensity with increased applied CO₂ laser power. This behaviour can be understood in terms of the ground state O atoms being excited to higher levels by collisions with the "hot" SF₆ molecules, consequently depleting the ground state population and causing a decrease in the signals' intensities. It was noted that this decrease would be temperature related and could be used to calculate an "effective" temperature for the CO₂ laser and SF₆ photosensitisation system at various power outputs.

A computer program, OASPEC (Appendix II), was written firstly to simulate the O atom EPR spectrum, secondly to calculate the intensities of the individual signals when the observed signal was a broad overlapping envelope as the signal width (pressure) was increased, and then to calculate a calibration graph so that any envelope signal height could be used to determine an individual component height. Finally, the program used this calibration graph to calculate from a given

SECTION IV.4 - RESULTS AND DISCUSSION

experimental envelope the actual height of the component underneath it, and this 3P_2 signal height together with a measured 3P_1 height was used in a rearranged Boltzman distribution calculation to obtain an "effective" temperature. Table IV.4.4 shows the calculated "effective" temperature at a constant SF_6 pressure with varying O_2 pressure and CO_2 laser power.

SECTION IV.4 - RESULTS AND DISCUSSION

Power (W)	Width (mm)	3P_1 Height (mm)	3P_2 Height (mm)	Temp. (K)
0	11	27	158	313
10	12	26	145	346
20	12	18	97	365
30	11	13	65	403

SF_6 at 0.15 mBar and O_2 at 0.50 mBar

20	16	21	128	458
30	16	18	112	461
40	15	22	125	490

SF_6 at 0.15 mBar and O_2 at 0.75 mBar

0	20	18	180	313
10	20	17	171	472
20	20	18	135	529
30	20	10	76	513

SF_6 at 0.15 mBar and O_2 at 1.00 mBar

Table IV.4.4. Table showing the variation of laser power output with O atom signals' intensities and the resultant calculated "effective" temperature.

The trend in this system is shown in Figure IV.4.5 which is

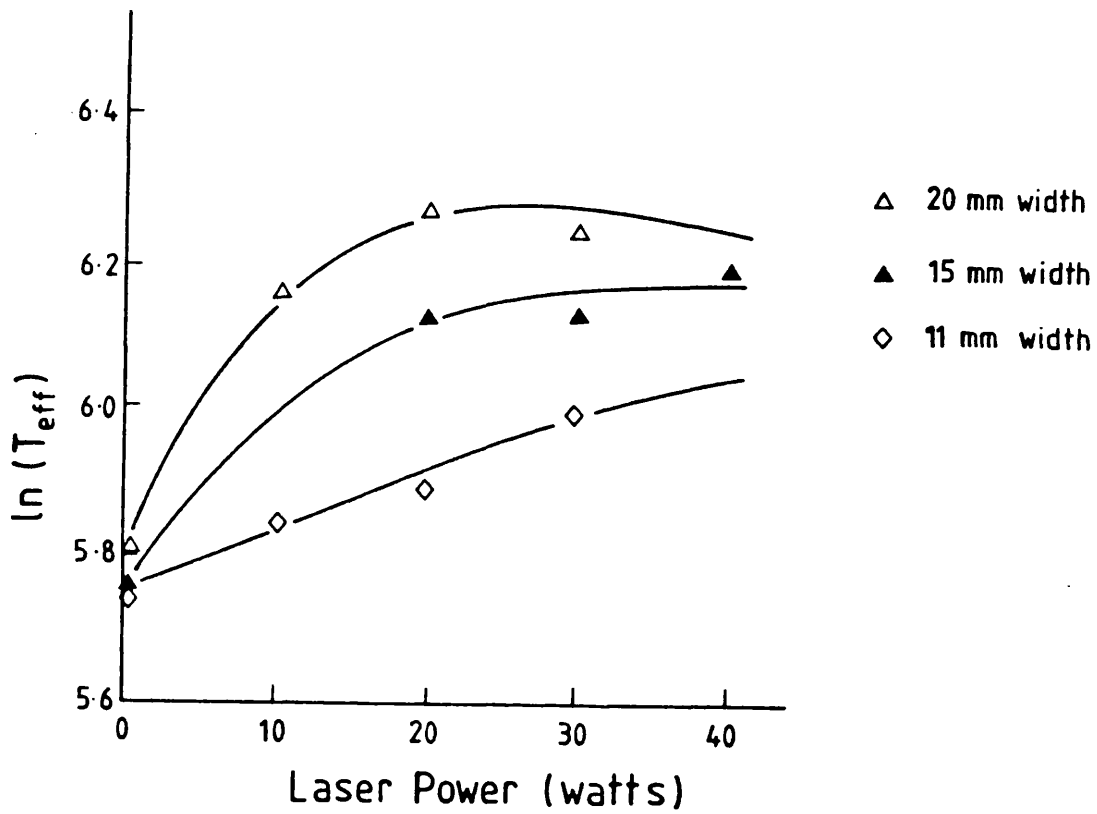


Figure IV.4.5. A plot of CO₂ laser power output versus ln (calculated effective temperature) at incremented O₂ pressures.

SECTION IV.4 - RESULTS AND DISCUSSION

a plot of the power output from the CO₂ laser against the natural logarithm of this calculated temperature at incremented O₂ pressures. Although the data presented in Figure IV.4.1 is sparse, the general nature of the trend in the system is evident and "effective" temperatures of the order of 500 K appear to be accessible at higher CO₂ laser powers employing this photosensitisation scheme, sufficient for the pyrolysis of a number of relevant compounds.

(ii) THE SULPHUR MONOXIDE RADICAL (SO) SYSTEM:

The intense SO signal observed from the laser vaporised sulphur which condensed in the cavity and subsequently reacted with atomic oxygen is probably due to the active nature of the surface of the deposited sulphur. A similar observation in the phosphorus system which generated the PO radical has also been reported¹⁷. One advantage noted in this system was the ability of the CO₂ laser to deposit the sulphur very thinly inside the cavity providing a good coating, and because of the layer's thinness it did not degrade the cavity Q (Section V.3). Another advantage noted was the relative low pressure (0.2 mBar) of the O₂ required to generate a signal of this intensity, since alternative generation methods require an increase in the total pressure by a factor of ten for a signal of comparable intensity (Section V.4) and pressure broadening effects then become evident.

(iii) THE NITROGEN DIFLUORIDE RADICAL (NF₂) SYSTEM:

Both of the experiments described in Section IV.3 on the N₂F₄ system on the IDL and EPR spectrometers are neat examples of

SECTION IV.4 - RESULTS AND DISCUSSION

how this generation method can be used to produce radicals for high resolution spectroscopic detection. The latter to the author's knowledge is the first observation of the EPR spectrum of the NF_2 radical, even though it is a rather broad, unresolved and uninformative signal. The technique of chopping the CO_2 laser beam, and the effect this has on the observed signal (Figure IV.3.2), demonstrates the possibility of using molecular modulation of the signal for detection purposes with the chopper supplying the reference frequency to the phase sensitive detector, provided the chopping period is greater than the lifetime of the radical being studied.

(iv) THE IODINE ATOM (I) SYSTEM:

On the basis of the feasibility study done on the CH_3I system (in which reaction was clearly occurring), and the success encountered with the NF_2 radical the failure to detect I atoms by EPR spectroscopy using this generation method was disappointing. Even the expanding of the photolysis region with the convex lens did not generate a detectable concentration. One major difference between this system and the N_2F_4 system is that the photolysis products (I and CH_3) do not regenerate CH_3I whereas the NF_2 radicals do regenerate N_2F_4 . This difference may give an insight into why a detectable concentration of I atoms did not build up, in that the rate constants for the radicals to form products may be faster than the photolysis rate constants, consequently the steady state concentration of I atoms is too low to be detected.

SECTION IV.4 - RESULTS AND DISCUSSION

(v) THE SELENIUM CHLORIDE RADICAL (SeCl) SYSTEM:

The failure to detect any signals arising from the SeCl radical from this CO_2 laser and SF_6 photosensitisation generation method is consistent with the fact that the radical is as yet undetected by a high resolution spectroscopic technique. Even though two SeCl radicals should have been produced initially, this may again be due to the rate constants in operation for the production of the products as has been outlined above. An inspection of the inside of the cavity after the experiment revealed that solid selenium had been deposited proving that reaction was indeed occurring, but presumably not at a sufficiently fast rate to build up a detectable steady state concentration for detection by EPR spectroscopy under these conditions.

IV.5 CONCLUSIONS

The CO_2 laser and SF_6 photosensitisation generation method on the basis of the feasibility studies undertaken appears to be a viable method of producing transient species. The experiments in which direct detection was employed revealed that further work into the kinetics of the system is required. The initial process of absorption of the CO_2 radiation may be assumed to be relatively fast, and the system seems capable of producing "effective" temperatures of a sufficiently high magnitude to break even carbon-carbon bonds in favourable cases, although a limit of approximately 50 Watts is the power input limitation because at this power level SF_6 , the photosensitisation agent, breaks apart. The collisional excitation rate of a precursor by the "hot" SF_6 is the the unknown parameter in the system, and its magnitude

SECTION IV.5 - CONCLUSIONS

needs to be established so that it can be compared to the rate constants in operation for the production of the products, for the particular system being employed, to establish whether a detectable steady state concentration can be achieved through the application of this generation method. In simpler systems such as the $N_2F_4/2NF_2$ equilibrium a detectable steady state concentration can probably be established relatively easily.

IV.6 REFERENCES

1. W.M.Shaub & S.H.Bauer,
Int. J. Chem. Kinet., 7, 509 (1975).
2. F.F. Cruin, G.H.Kwei & J.L.Kinsey,
Chem. Phys. Letts., 49, 529 (1977).
3. H.Pazendah, C.Marsal, F.Lempereur
& J.Tardieu de Maleissye,
Int. J. Chem. Kinet., 11 595 (1977).
4. B.J.Orr & M.V.Keentok, Chem. Phys. Letts., 42 202 (1976).
5. K.Naga & H.Katayama, Chem. Phys. Letts., 51, 329 (1978).
6. G.S.Geiger, D.R.Smith & J.D.Bennett,
Chem Phys. Letts., 74, 239 (1983).
7. C.Chang & P.Keelin, J. Am. Chem. Soc., 99, 5808 (1977).
8. W.Tsang, J.A.Walker & W.Braun,
J. Phys. Chem., 86, 719 (1982).
9. J.F.O'Keefe & F.W.Lampe,
Appl. Phys. Letts., 42, 217 (1983).
10. C.Steel, V.Starav, L.Rinaldo, P.John & R.G.Harrison,
Chem. Phys. Letts., 62, 121 (1979).
11. I.M.T.Davidson and co-workers,
Leicester University, England (Private Communication).
12. P.B.Davies, B.J.Handy & D.K.Russell,
Chem. Phys. Letts., 68, 395 (1979).
13. T.H.Lane & C.L.Frye,
J. Organomet. Chem., 172, 213 (1979).
14. M.C.Flowers & L.E.Gusel'nikov,
J. Chem. Soc. B, 428, 1396 (1968).
15. I.M.T.Davidson, A.Fenton, S.Ijad-Maghsoodi, R.J.Scampton,
N.Auner, J.Grobe, N.Tillman & T.J.Barton,
Organometalics, 3, 1593 (1984).

SECTION IV.6 - REFERENCES

16. P.Haaland & A.Rahbee,
Chem. Phys. Letts., 114, 571 (1985).
 17. K.Kawaguchi, S.Saito & E.Hirota, (To be Published).
-

CHAPTER V - DETECTION BY ELECTRON PARAMAGNETIC RESONANCESPECTROSCOPYV.1 INTRODUCTION

In this Chapter EPR spectroscopy as a detection system for free radicals and atoms in the gas phase is examined. The technique is firstly historically reviewed, indicating significant observations where relevant. A practical discussion on the sensitivity of an EPR Zeeman cavity is given, along with the subsequent improvements made to the existing system. An account of the experiments performed using this detection system then follows along with the results obtained from these experiments.

V.2 HISTORICAL REVIEW OF PREVIOUS WORK

The first EPR spectrum of an atom in the vapour phase was performed by Beers et al. on the caesium atom, ^{133}Cs , in its $^2\text{S}_{1/2}$ state¹. The spectrum was unusual because the microwave frequency used was very close to the hyperfine splitting ($I=7/2$) due to the ^{133}Cs nucleus and so only low magnetic fields were require to bring the transitions into resonance. The spectrum also revealed seven additional transitions due to the electron and nuclear spins being strongly coupled under the influence of the low and zero magnetic field. These normally "forbidden $\Delta m_I \neq 0$ " transitions arise due to the electron spin interacting with the nuclear spin and causing it to "flip". The eighth "forbidden" transition was not observed because the levels associated with it could not be tuned into resonance by the low magnetic field and the centre one of the seven was too weak to be modulated. Thus Beers et al. observed fourteen out

SECTION V.2 - HISTORICAL REVIEW

of the expected fifteen transitions for the ^{133}Cs atom.

The first gas to be studied by EPR was the oxygen molecule, O_2 , in its $^3\Sigma_g^-$ state by Beringer and Castle². This spectrum of magnetic dipole transitions was extremely rich and consisted of many lines due to the intermediate nature of the coupling between the electron and the nuclei. This resulted in the many K and J levels being split into their magnetic sub-levels giving rise to several hundred levels between which transitions occurred. Beringer and Castle continued their work in this field by studying nitric oxide, NO , in its $^2\Pi_{3/2}$ state³. The spectrum of magnetic dipole transitions arose from transitions between the magnetic sub-levels in the $J=3/2$ rotational level of the $^2\Pi_{3/2}$ spin component. The expected nine line pattern was observed (^{14}N , $I=1$), but their resolution was insufficient to resolve the Λ -doubling of each of these lines⁴.

The first triatomic species to be studied by EPR was nitrogen dioxide, NO_2 , in its 2A_1 state⁵. The observed spectrum contained three broad overlapping lines at high pressure, but on reduction of the pressure a partially resolved spectrum of a large number of lines was observed, but not assigned. The first short-lived species to be studied by EPR was the hydrogen atom, H , in its $^2S_{1/2}$ state⁶. A discharge-flow system was employed to generate H atoms and the expected two line spectrum due to the ^1H nucleus ($I=1/2$) centred at approximately $g=2$ was observed. This same method of production was also employed to produce the O atom in its 3P_J ($J=0,1,2$) state⁷. The observed spectrum consisted of the two 3P_1 transitions flanking the four 3P_2 transitions and an unassigned three line spectrum which interleaved the 3P_2

SECTION V.2 - HISTORICAL REVIEW

transitions. These latter three transitions were probably "forbidden" multi-quantum transitions caused by a high microwave power level. The third short-lived species to be observed was the nitrogen atom, N, in its $^4S_{3/2}$ state⁸. The observed spectrum consisted of three lines due to the ^{14}N nucleus ($I=1$) hyperfine interaction centred at approximately $g=2$. The equivalent atom in the second row of the periodic table, the phosphorus atom, P, in its $^4S_{3/2}$ state, was observed by Dehmelt⁹. In these experiments the N atom hyperfine lines were sufficiently intense to be observed on an oscilloscope and this spectrum was used to calibrate the observed two line pattern centred at approximately $g=2$. The ^{31}P nucleus ($I=1/2$) interacts with the electron to give the expected two line hyperfine doublet.

The next three atoms to be detected by EPR in the gas phase were the first three halogens of group VII¹⁰⁻¹². The fluorine atom, F, in its $^2P_{3/2}$ state produced a spectrum of six lines initially and revealed a large hyperfine splitting due to the ^{19}F nucleus ($I=3/2$), similar to the ^{133}Cs nucleus. This large hyperfine splitting allowed two "forbidden" low field transitions to come into resonance due to the ^{19}F nuclear spin "flipping". The chlorine atom, Cl, in its $^2P_{3/2}$ state and with its two naturally abundant isotopes which both possess a nuclear spin viz. ^{35}Cl ($I=3/2$) (75.5%), ^{37}Cl ($I=3/2$) (24.5%), produced twelve transitions for each isotope¹³. The bromine atom, Br, in its $^3P_{3/2}$ state also has two naturally abundant isotopes which both possess a nuclear spin viz. ^{79}Br ($I=3/2$) (50.5%), ^{81}Br ($I=3/2$) (49.5%). All twelve transitions for both of these isotopes were observed¹³. These three halogens' ground electronic states

SECTION V.2 - HISTORICAL REVIEW

are inverted 2P ; the $^2P_{1/2}$ lying above the $^2P_{3/2}$.

The first short-lived diatomic radical to be detected by EPR was the hydroxyl radical, OH, in its $^2\Pi_{3/2}$ state, along with its deuterium analogue, OD by Radford¹⁴. This spectrum was also significant because it revealed a new type of transition to be detected by EPR. The transitions observed were of electric dipole type between the two members of the Λ -type doublets. Λ -type doubling permits paramagnetic resonance transitions of electric dipole type as well as the magnetic dipole type. This spectrum was assigned to two groups of lines clustered at either side of where the magnetic dipole transitions would have occurred had they been of sufficient intensity to be observed. The separation of these low and high field groups of lines is a measure of the Λ -type doubling interval and they were assigned to the parity changed $^2\Pi_{3/2}$ in the $J=3/2$ transitions between the Λ -type doublets. The other groups of lines observed were similarly assigned to the low field groups of the $J=5/2$ and the $J=7/2$ rotational levels, the high field groups being beyond the tuning range of the magnetic field. The deuterium isotope was also shown to exhibit these transitions in the $J=3/2$ level although the Λ -type doubling was considerably smaller as would be expected for a heavier, more slowly rotating molecule.

Following the observation of OH the second row analogue, thiyl radical, SH, in its $^2\Pi_{3/2}$ and its deuterium analogue were observed by MacDonald¹⁵. The spectrum contained all of the twelve predicted lines for the $J=3/2$ rotational level, whilst the deuterium isotopic species, SD, contained six lines, its hyperfine being unresolved, 2D ($I=1$). The same

SECTION V.2 - HISTORICAL REVIEW

experiment also yielded the EPR spectrum of the sulphur monoxide radical, SO, in its $^3\Gamma^-$ ground electronic state. The observed signals arose from transitions between the Zeeman levels (magnetic sub-levels) of differing rotational levels in both the ^{32}SO (95.0%) and ^{34}SO (4.2%) isotopes. Partially analysed EPR spectra of the selenium hydride radical, SeH, and the tellurium hydride radical, TeH, in their $^2\Pi_{3/2}$ states were reported by Radford¹⁶. The first EPR spectrum of a radical in an excited electronic state was observed by Falick *et al.*¹⁷. O_2 in its $^1\Delta_g$ first electronic excited state produced four signals arising from transitions between the magnetic sub-levels of the $J=2$ rotational level.

The EPR spectra of the chlorine monoxide radical, ClO, and the bromine monoxide radical, BrO, both in their $^2\Pi_{3/2}$ states, both with their naturally abundant isotopes (in which $I=3/2$) were observed by Carrington and Levy¹⁸. All twelve lines for both the Cl nuclei were observed, but six of the lines arising from the Br isotopes were obscured by the intense O_2 spectrum. The sulphur nitride radical, NS, in its $^2\Pi_{3/2}$ upper spin-orbit state was also observed. The nine line pattern, arising from the $J=3/2$ rotational level, consisted of three widely spaced triplets due to the second order Zeeman splitting and a ^{14}N ($I=1$) hyperfine splitting.

The EPR spectrum of the remaining non-radioactive halogen, the iodine atom, I, in its $^2P_{3/2}$ state was observed by Aditya and Willard for both the ^{127}I ($I=5/2$) and ^{129}I ($I=7/2$) nuclei¹⁹. All eighteen lines for ^{127}I and twenty-three lines for ^{129}I (one line was an unresolved doublet) were observed. The sulphur atom, S, in its 2P_j state was observed by Brown²⁰ and resembled the O atom spectrum in

SECTION V.2 - HISTORICAL REVIEW

that it contained transitions arising from the 3P_1 and 3P_2 magnetic sub-levels. Elemental sulphur has a third naturally abundant isotope, ^{33}S (0.74%) ($I=3/2$), and a signal arising from its monoxide, ^{33}SO , was detected as a quartet by Carrington et al.²¹ along with ^{32}SO in its $^1\Delta$ first excited electronic state.

The diatomic radicals sulphur fluoride, SF, and selenium fluoride, SeF, both in their $^2\Pi_{3/2}$ states had not previously been detected by any spectroscopic method, but Carrington et al.²² obtained their EPR spectra arising from transitions between their magnetic sub-levels within their $J=3/2$ rotational levels. The signals obtained were quasi-second derivative in shape due to the application of a Stark cavity for detection and the superposition of parity differenced doublets. The spectra were used for the first time to determine the r_0 bond lengths of these diatomic radicals. The iodine monoxide radical, IO, in its $^2\Pi_{3/2}$ was also detected by this group; the spectrum observed contained eighteen lines arising from the second order Zeeman splitting and the ^{127}I ($I=5/2$) nucleus. N atoms in their first excited electronic state, $^2D_{5/2}$, were first detected by EPR in both the $J=5/2$ and $J=3/2$ spin-orbit levels (the latter being above the former) by Radford and Evenson²³. A quintet of triplets and a triplet of triplets were the spectra observed for the respective J levels. The selenium monoxide radical, SeO, in its $^3\Sigma^-$ ground electronic state and $^1\Delta$ first electronic state was observed by Carrington et al.²⁴; the $^1\Delta$ was a previously undetected electronic state for this radical. The ^{77}Se (7.5%) ($I=1/2$) was also observed as signals from the ^{77}SeO as satellite doublets to the main SeO lines.

SECTION V.2 - HISTORICAL REVIEW

The first short-lived, linear, triatomic to be observed by EPR was the cyano radical, NCO, in its ${}^2\Pi_{3/2}$ ($n=1$), ${}^2\Delta_{5/2}$ ($n=2$) and ${}^2\Phi$ ($n=3$) vibronic states²⁵. This was shortly followed by the equivalent sulphur radical viz. NCS in its ${}^2\Pi_{3/2}$ vibronic state²⁶. The EPR spectra of the alkali metals sodium, Na, potassium, K, rubidium, Rb and caesium, Cs, in their ${}^2S_{1/2}$ states, containing hyperfine split transitions were monitored as a measurement of their spin exchange cross-sections²⁷. The EPR spectrum of the carbon fluoride radical, CF,²⁸ in its ${}^2\Pi_{3/2}$, $J=3/2$, $J=5/2$ rotational levels, produced five quasi-second derivative and six resolved doublets (the two high field doublets being beyond the tuning range of the magnetic field) signals respectively.

The group V atoms arsenic, As and antimony, Sb, in their ${}^4S_{3/2}$ states were studied by EPR by Zijlstra et al.²⁹. Twelve lines arising from the ${}^{75}\text{As}$ ($I=3/2$), eighteen lines from the ${}^{121}\text{Sb}$ and twenty-four lines from the ${}^{123}\text{Sb}$ ($I=7/2$) nuclei were observed.

The first short-lived, non-linear, triatomic to be detected by EPR was the formyl radical, HCO³⁰. The four transitions detected arose between the K doublets of the $2_{12} \leftarrow 2_{11}$ rotational transition. The disulphide molecule, S_2 , in its ${}^3\Sigma_g^-$ state was observed by Wayne et al.³¹. The doublet spectrum of S_2 and the mixed isotope ${}^{32}\text{S}{}^{34}\text{S}$ (8.7%) was also observed, the latter by a signal averaging process.

The most recent radical to be reported in the literature is the hydroperoxy, HO_2 , along with its substituted deuterium analogue^{32,33}. Twenty-one lines were observed in HO_2 arising from the $J=5/2$ and the $J=3/2$ magnetic sub-levels and the ${}^1\text{H}$ ($I=1/2$) hyperfine interactions. DO_2 yielded twenty-three

SECTION V.2 - HISTORICAL REVIEW

lines all of which were similarly assigned. Most were of a-type, K doubling, but four low field transitions were of b-type ($5_{05} - 4_{14}$) and this was the first instance of this type of transitions being detected by EPR. Finally, the NF_2 radical has been observed (Section IV.3). The spectrum consisted of a broad unresolved signal centred at approximately $g=2$.

V.3 DEVELOPMENTAL

The early microwave cavities utilised for gas phase EPR were of cylindrical symmetry and when employed in a discharge-flow system they contained quartz tube inserts or pill-boxes. Absorptions of microwave radiation within these cavities were detected by the application of an oscillating magnetic field, produced by a pair of Helmholtz coils mounted parallel to the applied, scanning magnetic field. This type of cavity is referred to as a Zeeman cavity because of the absorption signal modulation technique it employs.

Microwave power storage in these cavities results in a cavity mode, at a specific resonant frequency, dependent upon the physical size of the cavity and the frequency of the microwave radiation being transmitted to it. Gas phase EPR cavities operate, generally, in TE_{mnp} or TM_{mnp} where the m , n , and p subscripts refer to the number of half-cycle variations in the angular (ϕ), radial (r) and longitudinal (z) directions respectively, in relation to the transverse electric (TE_{mnp}) and transverse magnetic (TM_{mnp}) fields within the resonant cavity³⁴.

The power storage within a cavity is described by its quality factor, the Q ³⁴. In a high Q resonator the electric

SECTION V.3 - DEVELOPMENTAL

and magnetic fields are at 90° out of time phase with each other. When the electric fields are at a maximum, the magnetic fields are at zero and *vica versa*. hence the stored energy in the electric fields U_E

$$U_E = \frac{\epsilon}{2} \int |E_m|^2 d\tau \quad (V.3.1)$$

equals the stored energy in the magnetic fields U_H

$$U_H = \frac{\mu}{2} \int |H_m|^2 d\tau. \quad (V.3.2)$$

when each is evaluated at the part of the cycle corresponding to the maximum value denoted by the subscript m. The losses in cavity arise from the dissipation of heat by the surface current density J in the skin effect resistance R_s , and this ohmic power loss P_L is given by

$$P_L = \frac{R_s}{2} \int |H_{tm}|^2 dS \quad (V.3.3)$$

where the maximum tangential field H_{tm} along the surface is integrated over all the cavity walls. H_t and J are parallel to the surface. There will also be losses from radiation coupling in and out of the cavity coupling hole.

When the Q of a resonant cavity arises only from ohmic losses in the walls it is called the unloaded Q , denoted by Q_u and is given by

$$Q_u = \frac{\omega \mu \int |H_m|^2 d\tau}{R_s \int |H_{tm}|^2 d\tau} \quad (V.3.4)$$

where ω is the frequency of the radiation. The overall Q

SECTION V.3 - DEVELOPMENTAL

(denoted by Q_L) may be computed by summing the reciprocals of Q_ϵ due to the dielectric losses, the Q_r due to the cavity coupling hole, and Q_u , and hence it has the form

$$\frac{1}{Q} = \frac{1}{Q_u} + \frac{1}{Q_\epsilon} + \frac{1}{Q_r} \quad (\text{V.3.5})$$

where the individual quality factors are defined by equation V.3.4 and

$$Q_r = \frac{2\pi(\text{stored energy})}{(\text{energy lost per cycle})} \quad (\text{V.3.6})$$

$$Q_\epsilon = \frac{2\pi(\text{stored energy})}{(\text{energy lost in dielectric per cycle})} = \frac{\mu \int |H_m|^2 d\tau}{\int \epsilon'' |E_m|^2 d\tau} \quad (\text{V.3.7})$$

where ϵ'' is the dielectric constant for the cavity walls. The Q of the cavity then, is degraded by, ohmic losses due to the walls, dielectric losses, losses due to the cavity coupling hole (through which the microwave radiation is coupled in and out of the cavity), losses due to the gas inlet and outlet ports and losses due to the quartz tube inserts or pill-boxes through microwave absorption. The sensitivity of a resonant cavity can be expressed as

$$\text{sensitivity} \propto \sqrt{Q} \quad (\text{V.3.8})$$

Figure V.3.1 is a schematic diagram of the experimental arrangement of a pill-box inside a Varian V-4535 large sample access cavity operating in the TE₀₁₂ mode. This system has three main disadvantages. The first disadvantage is that any short-lived species generated just outside this cavity will tend to recombine on the inner tube leading up to the quartz

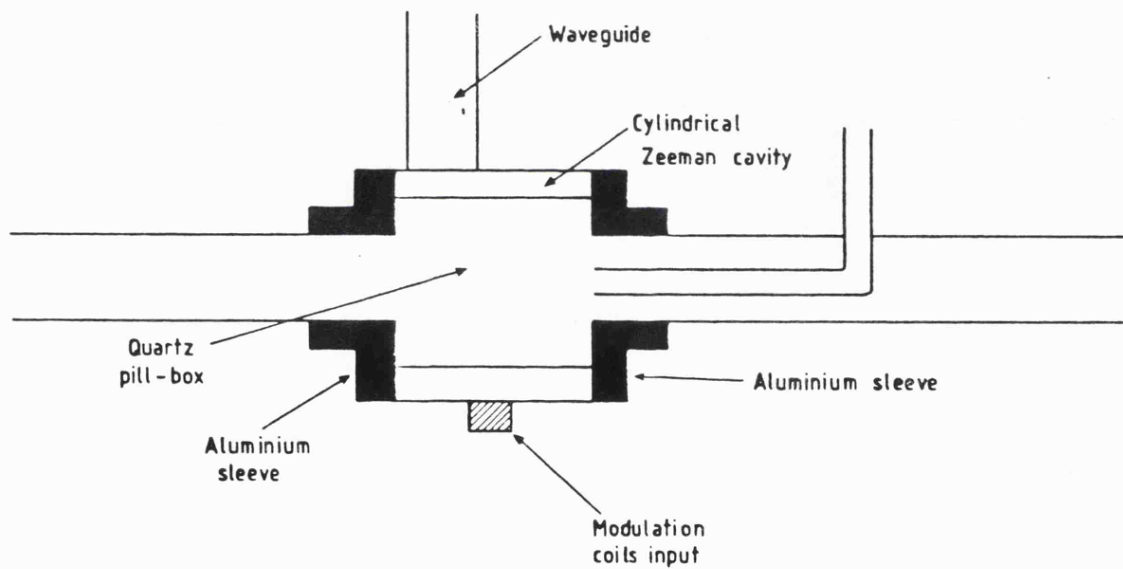


Figure V.3.1. Schematic diagram of a Varian V-4535 Zeeman cavity containing a quartz pill-box.

SECTION V.3 - DEVELOPMENTAL

pill-box. Secondly, the large amount of quartz inside the cavity seriously degrades the Q through microwave absorption. Thirdly, the large inlet and outlet ports give poor microwave reflection due to the large holes required the aluminium sleeves to fit over the quartz pill-box. Figure V.3.2 shows a typical mode pattern produced by this system and it yields a measured Q of 500.

In an attempt to minimise these disadvantages a second system was designed and built. This system is shown in Figure V.3.3(a) the central inner flow tube was completely removed and replaced by a pair of angled gas ports. The aluminium microwave sleeves (which are integral parts of the resonant structure) were replaced by a non-magnetic brass end piece and an aluminium end piece. The brass end piece acted as a part of the resonant structure, the gas inlet ports' housing and an 'O'-ring vacuum seal housing. This piece was also later adapted to accommodate for a central, circular, zinc selenide window to allow the carbon dioxide laser beam to enter the cavity (Chapter IV). The aluminium end piece acted as the other part of the resonant structure, a single gas outlet port housing, the other 'O'-ring vacuum seal housing and a poly-tetrafluoroethylene (PTFE) stub housing which matches (its impedance at a given frequency) the cavity into resonance. The quartz pill-box was replaced by a thin walled quartz cylinder whose ends were ground flat to ensure a good vacuum seal on the lightly greased 'O'-rings. The whole assembly was made vacuum tight by tightening the retaining screws. This modified Zeeman cavity resonating in its TE_{012} mode gave a measured Q of approximately 12 000 and a typical mode pattern is shown in Figure V.3.4

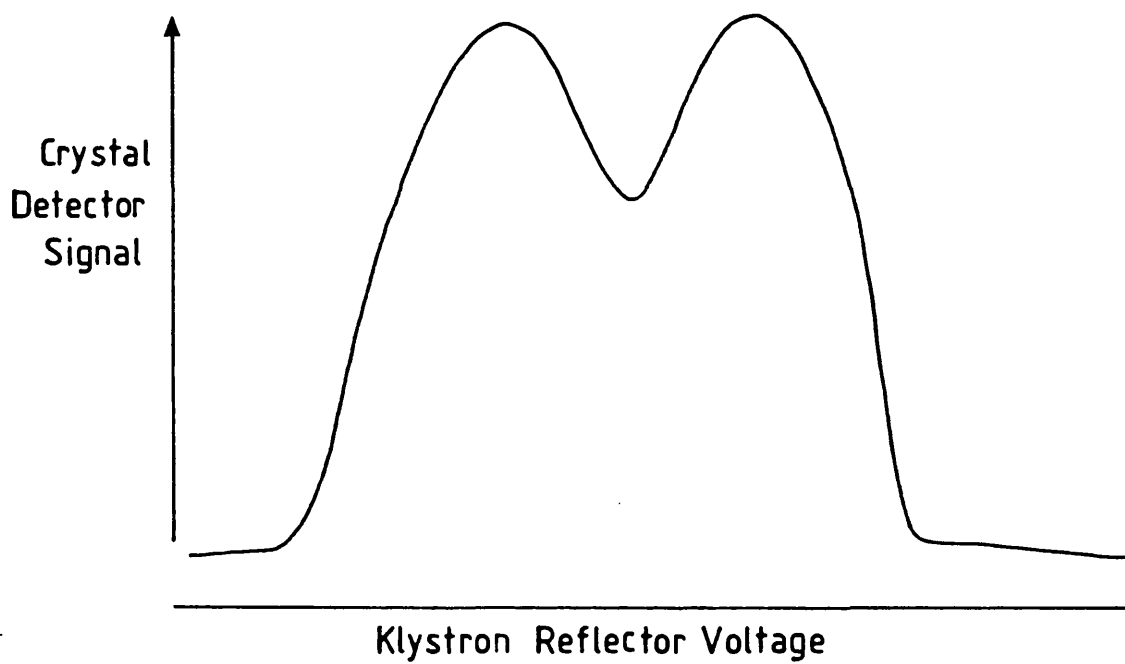


Figure V.3.2. The TE_{012} mode pattern produced by a quartz pill-box inside a Varian V-4535 Zeeman cavity.

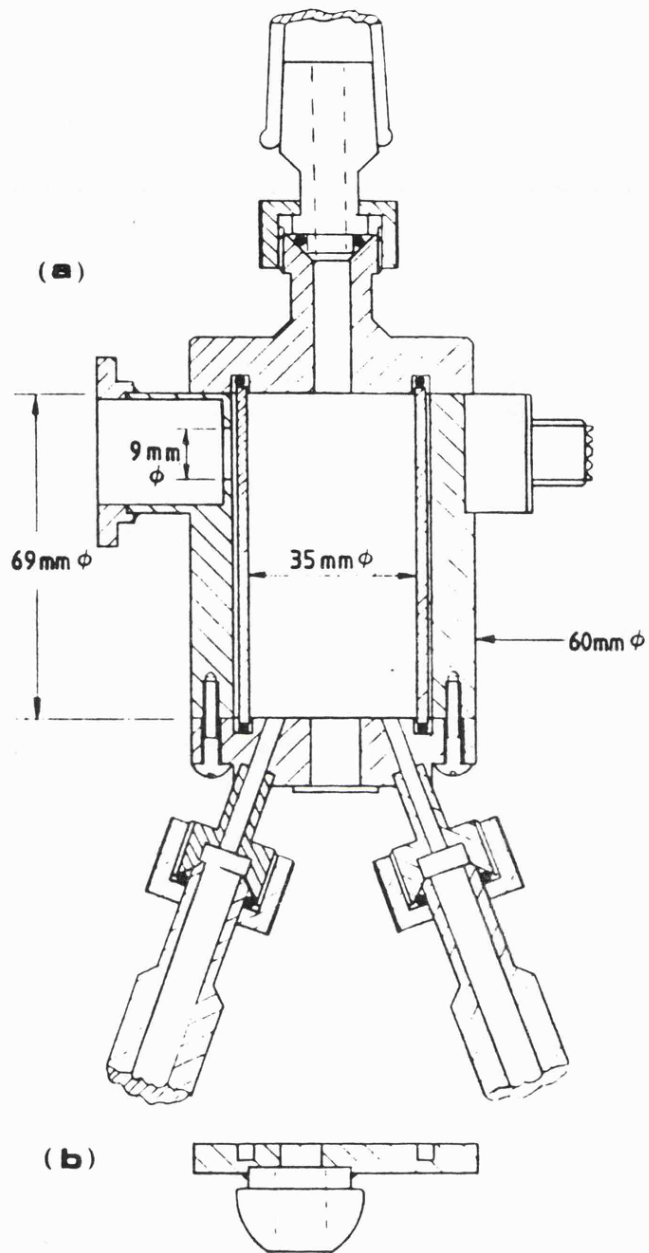


Figure V.3.3(a). A scale drawing of the modified Zeeman cavity with the two port end piece and laser port-hole.

Figure V.3.3(b). A scale drawing of the one port "discharge" end piece.

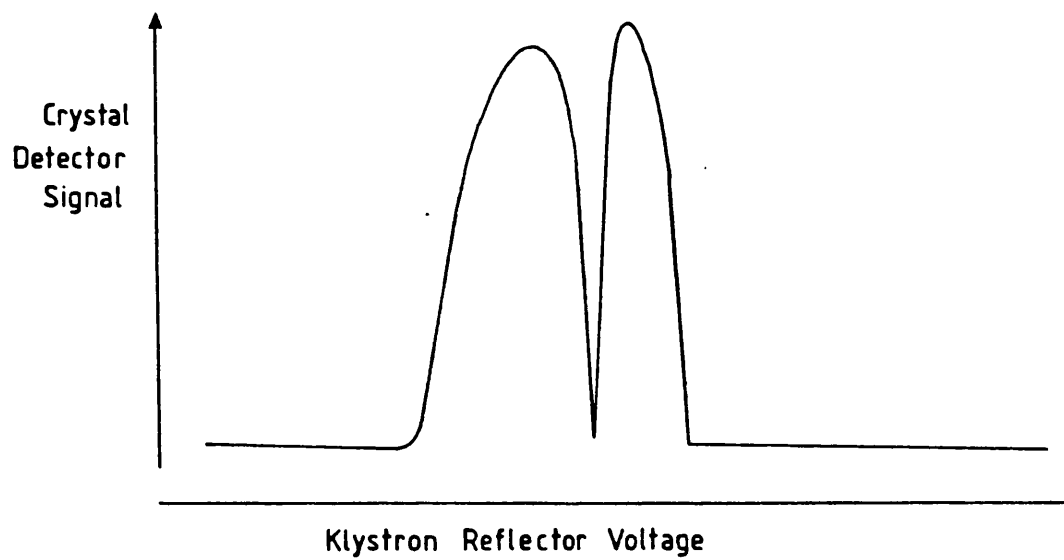


Figure V.3.4. The TE_{012} mode pattern produced by the modified Zeeman cavity fitted with the two port end piece.

SECTION V.3 - DEVELOPMENTAL

The gas inlet and outlet connectors were constructed out of PTFE and non-magnetic brass respectively and turned down to the appropriate quickfit (QF) connector. All three of these connectors were made vacuum-tight by 'O'-ring seals which were tightened by an outer threaded, compression sleeve which battened down on to a brass ring, which in turn battened down on to its 'O'-ring completing the vacuum seal. It was found that this vacuum system could support vacuums in excess of 10^{-3} mbar.

The PTFE connectors had three advantages. Firstly, they improved EPR signals from gaseous atoms due to reduced reaction with the inert PTFE surface, secondly, they were not prone to fracture as was the pyrex to quartz graded seal needed for the pill-box system and thirdly, they could be interchanged with the Stark cavity (Section V.4).

A second non-magnetic brass end piece was designed and constructed specifically for detecting signals arising from the reaction of gaseous atoms and small amounts of solids placed inside the cavity on the quartz cylindrical insert (Figure V.3.3(b)). This end piece acted as an off-centre inlet port in the region of maximum magnetic field in the microwave standing wave pattern³⁴ and an 'O'-ring housing. Connection of the gas handling system to the cavity via this end piece was achieved by sealing a ball joint (QF S29) with an epoxy resin to the appropriate glassware.

V.4 EXPERIMENTAL

(i) THE NITRIC OXIDE (NO) SYSTEM:

The modified Zeeman cavity was assembled with the two port end piece and its resonant frequency in the TE₀₁₂ mode was

SECTION V.4 - EXPERIMENTAL

measured to be 8817 MHz. It was tested initially on the "calibrant" gas NO. The spectrum (Figure V.4.1) which the gas produced in a static system and at a measured pressure of approximately 1.0 mBar showed the clearly resolved Λ -doublets characteristic of NO.

(ii) THE OXYGEN ATOM (O) SYSTEM:

The cavity was then assembled with the one port "discharge" end piece and its resonant frequency in the TE₀₁₂ mode was measured to be 8561 MHz. It was tested under discharge-flow conditions by passing the products of a 2450 MHz discharge in O₂ through it producing the O atom spectrum with the central four ³P₂ signals clearly resolved (Figure V.4.2) at a pressure of 0.1 mBar.

(iii) THE HYDROGEN ATOM (H) SYSTEM:

The products of a 2450 MHz discharge of H₂ at a pressure of 0.5 mBar produced the hyperfine doublet characteristic of H atoms at approximately g=2.

(iv) THE NITROGEN ATOM (N) SYSTEM:

The products of 2450 MHz discharge of N₂ also at a pressure of 0.5 mBar produced the hyperfine triplet spectrum characteristic of N atoms at approximately g=2.

(v) THE CHLORINE ATOM (Cl) SYSTEM:

The products of a 2450 MHz discharge of Cl₂ with air being employed as a carrier gas produced the Cl atom spectrum for both the ³⁵Cl and ³⁷Cl nuclei at measured pressures of 0.15 : 0.95 mBar respectively. The spectrum (Figure V.4.3) showed

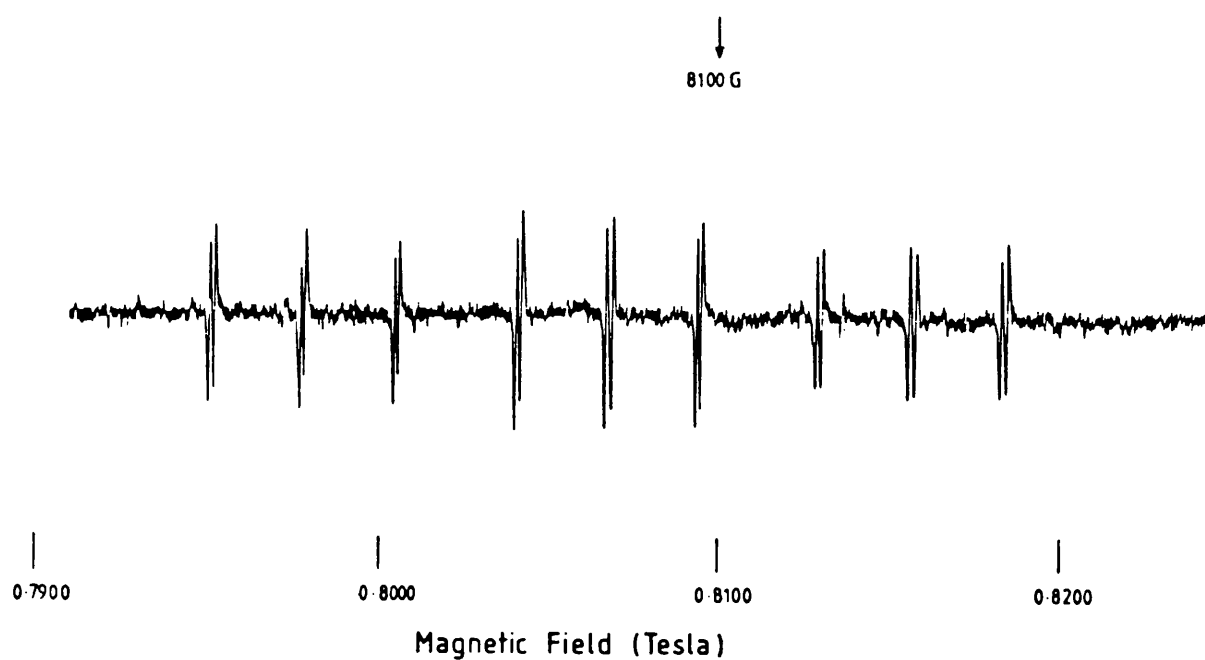


Figure V.4.1. The EPR spectrum of NO at a pressure of 1.0 mBar, magnetic field 0.8100 ± 0.250 T, frequency 8817 MHz, scan time 10.0 min, time constant 0.1 s, modulation frequency 100 kHz.

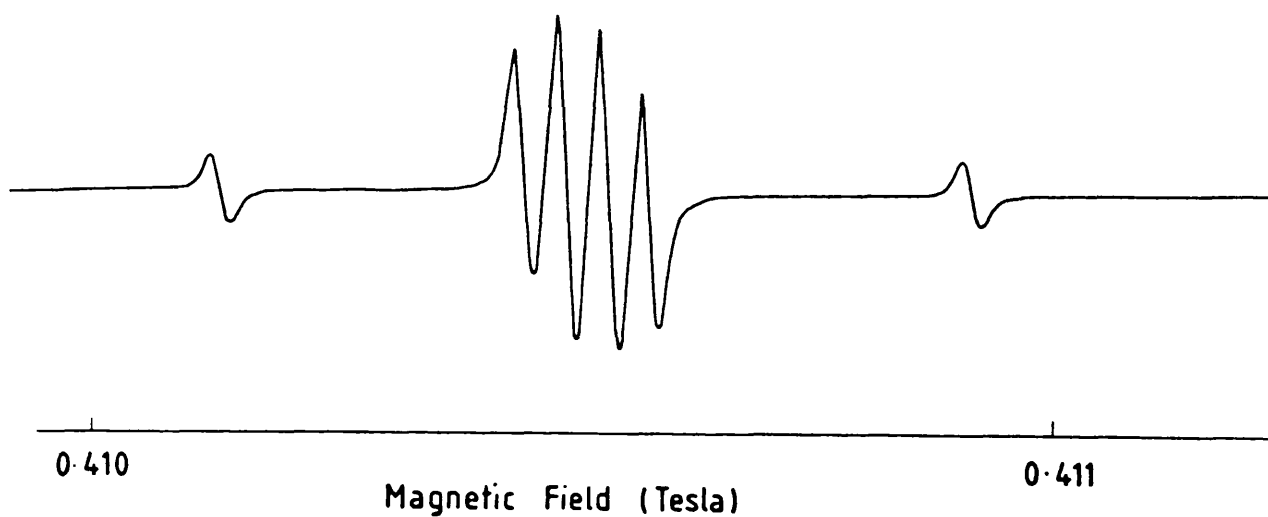


Figure V.4.2. The EPR spectrum of O atoms at a pressure of 0.1 mBar, magnetic field 0.4105 ± 0.00125 T, frequency 8561 MHz, scan time 5.0 min, time constant 1.0 s, modulation 100 kHz.

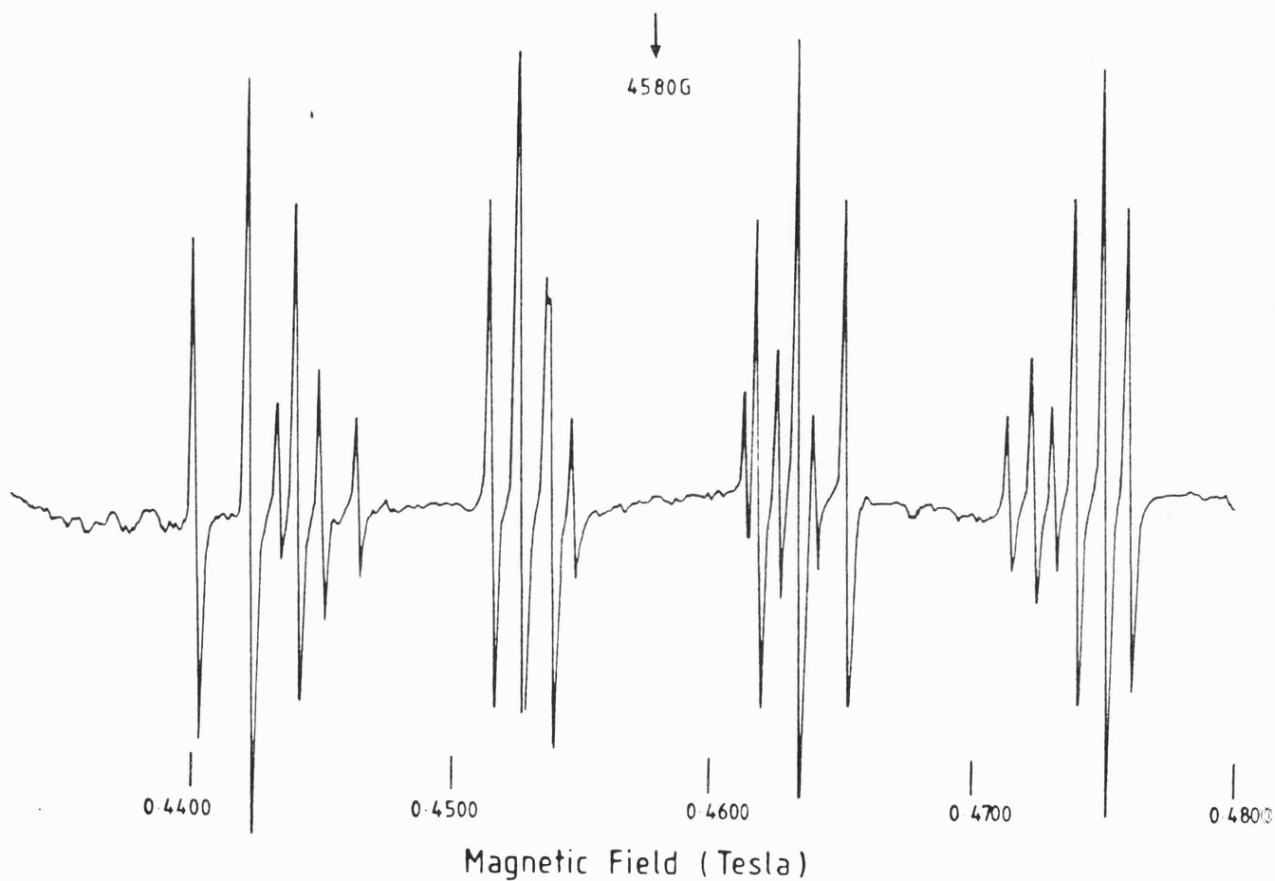


Figure V.4.3. The EPR spectrum of ^{35}Cl and ^{37}Cl atoms with air as a carrier gas (0.95 mBar) at a pressure of 0.15 mBar, magnetic field 0.4580 ± 0.0250 T, frequency 8561 MHz, scan time 10.0 min, time constant 1.0 s, modulation frequency 100 kHz.

SECTION V.4 - EXPERIMENTAL

clearly the resolved spectra of the two isotopic nuclei with the exception of the line coincidences which occurred at this microwave frequency and magnetic field.

(vi) THE FLUORINE ATOM (F) SYSTEM:

The products of a 2450 MHz discharge of CF_4 at a pressure of 0.5 mBar produced strong signals arising from F atoms.

(vii) THE HYDROXYL RADICAL (OH) SYSTEM:

The cavity was assembled with the two port end piece and its resonant frequency in the TE₀₁₂ mode was measured at 8710 MHz and the products of a 2450 MHz discharge of hydrogen peroxide, H_2O_2 , (degassed three times) at a pressure of 1.0 mBar were passed through it yielding weak signals arising from OH radicals.

(viii) THE SULPHUR MONOXIDE RADICAL (SO) SYSTEM:

The products of a 2450 MHz discharge of O_2 were mixed inside the cavity with sulphur(I) chloride, S_2Cl_2 , (degassed three times) and signals arising from $^3\Sigma^- \text{SO}$ were observed.

(ix) THE METHOXY RADICAL (CH_3O) SYSTEM:

The products of a 2450 MHz discharge of CF_4 were mixed inside the cavity with methanol, CH_3OH , in attempt to produce signals arising from CH_3O . Sufficient CH_3OH was added to "titrate" away the F atom signals (which were being monitored on the oscilloscope) until the optimum pressures were 0.1 : 0.5 mBar respectively. Although a wide range of conditions were employed this proved unsuccessful.

SECTION V.4 - EXPERIMENTAL

(x) THE FLUROSULPHITE RADICAL (FSO_3) SYSTEM:

The products of a 2450 MHz discharge of CF_4 were mixed inside the cavity with fluoro-sulphuronic acid, FHSO_3 , (degassed three times) in an attempt to produce signals arising from the fluorsulphite radical, FSO_3 . Sufficient FHSO_3 was added to "titrate" away the F atom signal (which was being monitored on the oscilloscope) until the optimum pressures were 0.5 : 0.5 mBar respectively. Although a wide range of conditions were employed this proved to be unsuccessful.

An EPR Stark cavity³⁵ in which absorption signals are detected by applying a small A.C. modulating electric field superimposed upon a D.C. bias was assembled with the PTFE connectors. The cavity's resonant frequency operating in a TE_{011} mode was measured to be 9585 MHz.

SECTION V.4 - EXPERIMENTAL

(xi) THE PHOSPHORUS OXIDE RADICAL (PO) SYSTEM:

The products of a 2450 MHz discharge (on the minimum power, 40 Watts, sufficient to maintain the discharge) of H_2 and O_2 were passed over red phosphorus, P, which had been compressed flat on the bottom of the cavity to avoid degrading the cavity Q. The O_2 pressure of 0.1 mBar and the H_2 pressure of 0.65 mBar maintained a pale green glow above a small sample of the red phosphorus located just outside the cavity in front of the discharge. When a D.C. bias of 300 V was applied five (possibly six) transient signals were observed (Figure V.4.4), but all attempts to increase the signal to noise ratio resulted in the signals being "pessimised".

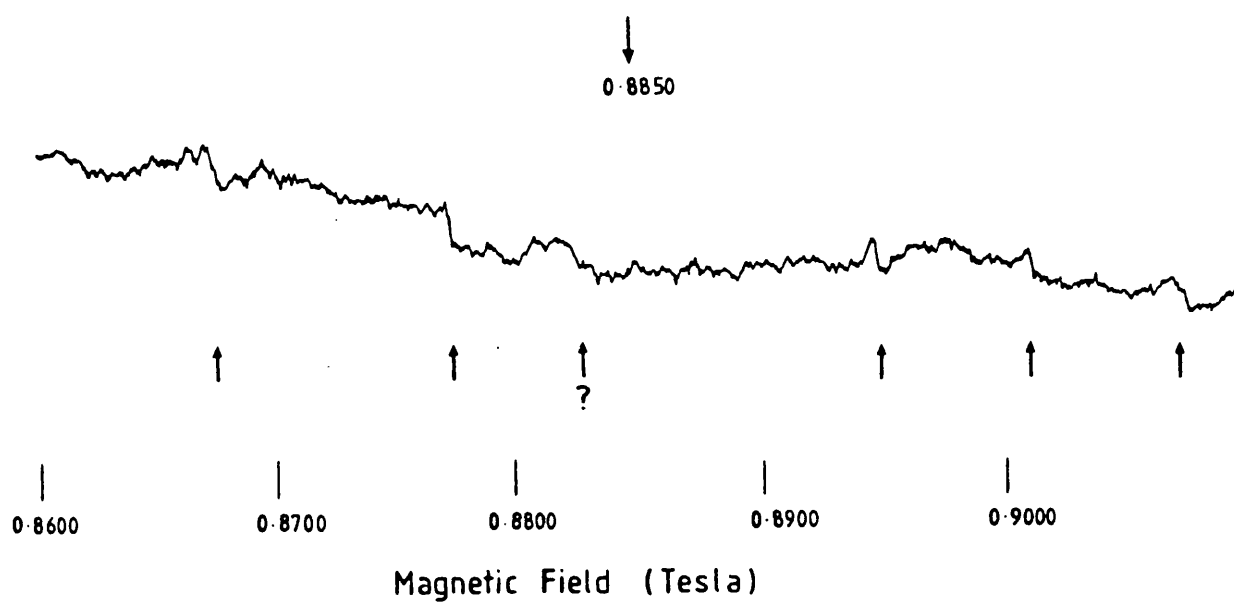


Figure V.4.4. An EPR spectrum tentatively assigned to the PO radical. O_2 pressure 0.1 mBar, H_2 pressure 0.65 mBar flowing over red phosphorus, magnetic field 0.8850 ± 0.0250 T, frequency 9585 MHz, scan time 5.0 min, time constant 1.0 s, modulation frequency 100 kHz.

SECTION V.4 - EXPERIMENTAL

(xii) THE ARSENIC OXIDE RADICAL (AsO) SYSTEM:

The products of a 2450 MHz discharge of O_2 and H_2 were passed over a few grains of metallic arsenic, As, in an attempt to observe signals arising from the AsO radical. A small sample of As metal placed just outside the cavity produced a pale violet glow when a range of H_2 and O_2 pressures were passed over the top of it. This proved unsuccessful even though a wide range of conditions were employed. Two PTFE insulating gaskets were constructed to lower the Stark cavity's resonant frequency whilst operating in the TE₀₁₁ mode to avoid the high field regulation problems encountered in the past. With these fitted the cavity's resonant frequency was measured to be 9162 MHz.

(xiii) THE SELENIUM OXIDE RADICAL (SeO) SYSTEM:

The products of a 2450 MHz discharge (on full power 200 Watts) of O_2 were mixed inside the cavity with selenium(I) chloride, Se_2Cl_2 . The Se_2Cl_2 was warmed into the vapour phase by electrically heating a high resistance wire, wound from the sample tube to the cavity, insulated with lagging with a VARIAC. The O_2 at a pressure of 3.2 mBar and the Se_2Cl_2 at a pressure of 0.8 mBar (65-70°C) maintained a deep blue glow in front of the discharge which was situated 70mm from the PTFE connector. When a D.C. bias of 200 V was applied two signals were observed each having a first derivative line shape, but they were of opposite phase due to the signals having differing parities (Figure V.4.5).

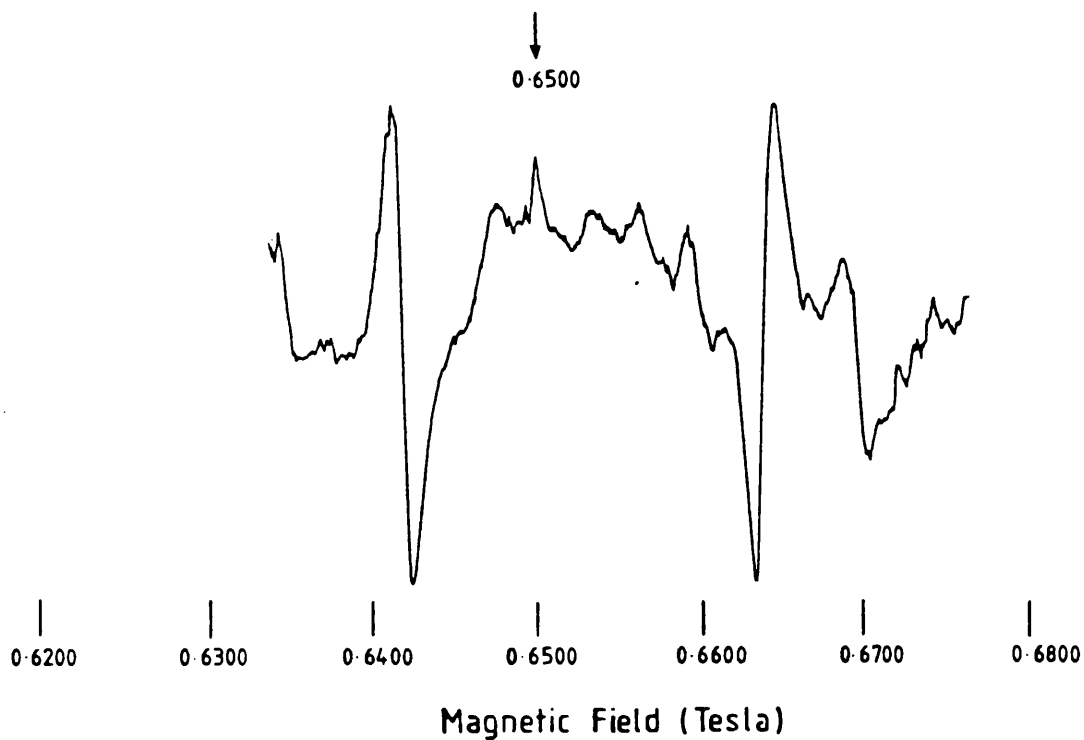


Figure V.4.5. Part of the EPR spectrum of the SeO radical showing two signals of opposite phase due to their different parities. O_2 pressure 3.2 mBar, Se_2Cl_2 pressure 0.8 mBar, magnetic field 0.6500 ± 0.0500 T, frequency 9162 MHz, scan time 5.0 min, time constant 1.0 s, modulation frequency 100 kHz.

SECTION V.4 - EXPERIMENTAL

(xiv) THE SELENIUM NITRIDE RADICAL (SeN) SYSTEM:

The products of a 2450 MHz discharge of N_2 were mixed inside the cavity with Se_2Cl_2 as described above in attempt to observe signals arising from the selenium nitride radical, SeN, under the same conditions which produced the SeO signals. This proved unsuccessful even after a wide range of conditions were employed.

(xv) THE SELENIUM CHLORIDE RADICAL (SeCl) SYSTEM:

The products of a 2450 MHz discharge (50 Watts) of O_2 and H_2 were mixed inside the cavity with Se_2Cl_2 as described above in an attempt to observe signals arising from the selenium chloride radical, SeCl, under the same conditions which produced the SeO signals. Even though the intense OH signals (Figure V.4.6) were "titrated" away on addition of the Se_2Cl_2 this proved unsuccessful over the wide range of conditions employed. The modified Zeeman cavity was assembled with the one port "discharge" end piece and its resonant frequency in the TE₀₁₂ mode was measured at 8561 MHz. A modified glass discharge tube containing a short (30mm), central, second, gas inlet port to mix the Se_2Cl_2 as close to the cavity as possible was constructed terminating in an QF S29 cup. The products of a 2450 MHz discharge of H_2 were passed into the cavity and mixed with Se_2Cl_2 as described above, in an attempt to observe signals arising from the SeCl radical. Sufficient Se_2Cl_2 was added to "titrate" away the H atom signals (which were being monitored on the oscilloscope) until the optimum pressures were 1.0 : 0.8 mBar respectively.

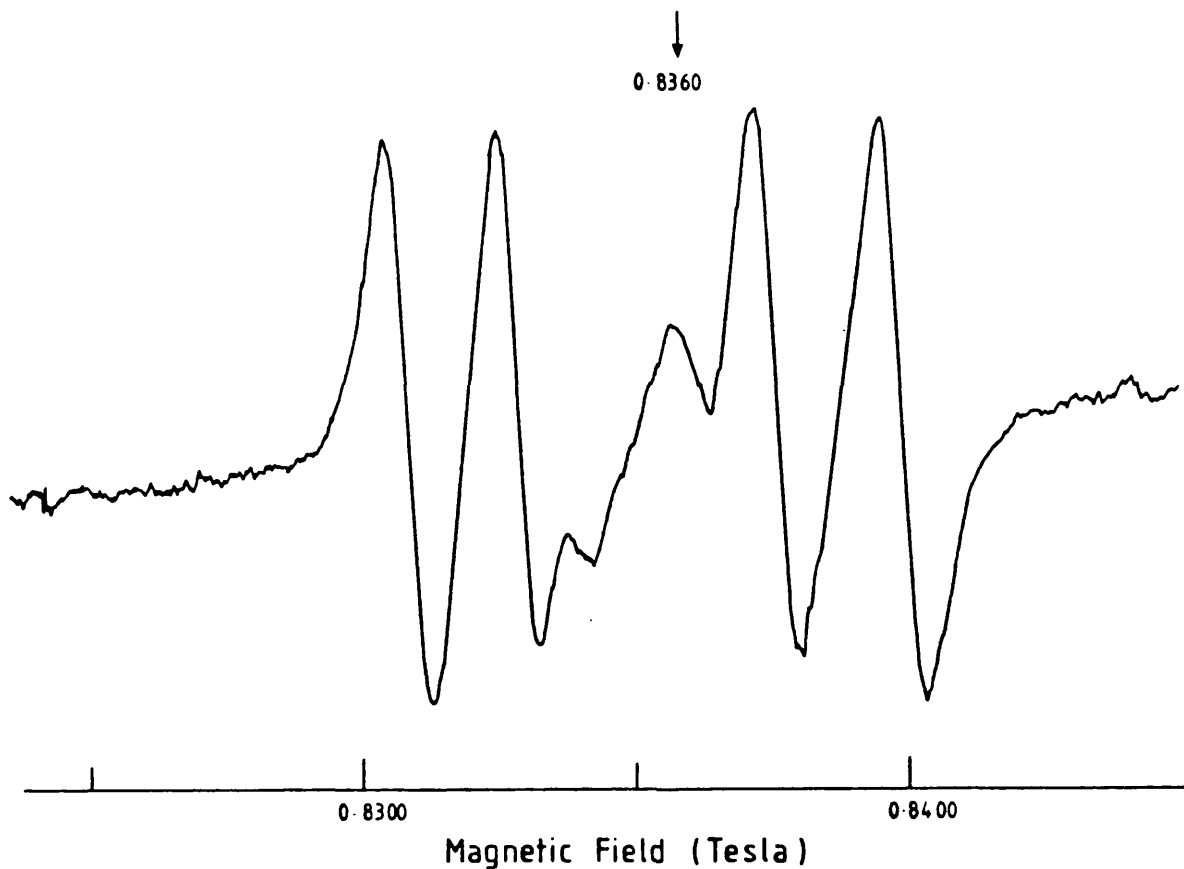


Figure V.4.6. Part of the EPR spectrum of the OH radical showing resolved Λ -doublets of differing parities split out by the applied D.C. bias. O_2 pressure 1.0 mBar, H_2 pressure 1.5 mBar, magnetic field 0.8300 ± 0.0125 T, frequency 9162 MHz, scan time 5.0 min, time constant 1.0 s, modulation frequency 100 kHz.

SECTION V.4 - EXPERIMENTAL

This proved unsuccessful even though a wide range of conditions were employed. The products of 2450 MHz discharge (50 Watts) of O_2 and H_2 were passed into the cavity in attempt to observe signals arising from the $SeCl$ radical on reaction with OH radicals. Sufficient $SeCl_2$ was added to "titrate" away the OH signals (which were being monitored on the oscilloscope) and the reactants were measured to be in the following ratio O_2 (1.3 mBar) : H_2 (1.8 mBar) : Se_2Cl_2 (0.8 mBar). Even though a wide range of conditions were employed this proved unsuccessful.

V.5 RESULTS AND DISCUSSION

The modified Zeeman cavity is simpler to assemble, sturdier and its resonant frequency can altered substantially by inserting a quartz cylinder of different length. The modified cavity has a Q of 12 000 which is an improvement on the previous design by a factor of approximately twenty. The two port mixing system allows reaction to occur inside the cavity and the addition of the laser port-hole allows for a new method of generating radicals by either direct thermal heating of solids, heating and subsequent deposition of "active" surfaces or by the photosensitisation of gases by irradiating sulphur hexafluoride, SF_6 (Chapter IV). The two port end piece does not however generate strong atom signals due to the small internal diameter of the inlet ports.

(i) - (vi) THE ATOM SYSTEMS:

The "discharge" end piece produces atom signals which are as strong as (if not stronger than) any published spectra at relatively low pressures for reaction with either solids or

SECTION V.5 - RESULTS AND DISCUSSION

mixing with other gases in abstraction type reactions.

(vii) - (viii) THE HYDROXYL RADICAL (OH) AND THE SULPHUR MONOXIDE RADICAL (SO) SYSTEMS:

The two port end piece produces OH and SO signals which are of reasonable strength, but their intensity may be being inhibited due to the small internal diameter of the lower discharge port.

(ix) METHOXY RADICAL (CH_3O) SYSTEM:

The LMR spectrum of CH_3O^{36} was observed by mixing the products of a 2450 MHz discharge of CF_4 with CH_3OH . This system is also known to generate HO_2 and HCO both of which have been detected by EPR^{30,32}. CH_3O^{38} and its sulphur analogue, the methyl thiyl radical CH_3S^{39} , have been detected by microwave spectroscopy. Both were generated by the same method excepting that in the case of CH_3S , CH_3SH was the precursor from which the proton was abstracted. The signal to noise ratio (S/N) of the observed spectra together with the frequency dependence of the signal strength³⁷ suggested that EPR signals from the CH_3O radical should be on the verge of detectability under optimum conditions, however any EPR transitions would have originated from the magnetic sublevels of the lowest rotational state consequently the population difference would not have been quite so favourable and this may have been sufficient to frustrate this attempt.

(x) THE FLUROSULPHITE RADICAL (FSO_3) SYSTEM:

The proton abstraction reaction of the fluorine atom in the generation of polyatomic radicals is a well known system for

SECTION V.5 - RESULTS AND DISCUSSION

producing such radicals within microwave spectrometers.³⁸⁻⁴² Since the EPR spectrometer's sensitivity is comparable to a microwave spectrometer the FSO_3 radical, under optimum conditions, must have been on the edge of EPR spectrometer's detection limit, however the unfavourable population distribution throughout the magnetic sub-levels must have been sufficient for the radical to evade detection.

(xi) THE PHOSPHORUS OXIDE RADICAL (PO) SYSTEM:

The PO radical has been detected by LMR and microwave spectroscopies^{41,42}. The method of generation in each case was the same as the one employed within the EPR cavity which produced the five (possibly six) transient signals observed. A comparison of the observed signals positions with the calculated magnetic field positions using a computer program for a $^2\Pi$ molecule⁴⁵ based upon the molecular constants derived from the microwave and LMR data is shown in Table V.5.1.

SECTION V.5 - RESULTS AND DISCUSSION

<u>calculated</u>	<u>observed</u>	<u>obs.-calc.</u>
0.8317 ^a	0.8674	0.0357
0.8485 ^b	0.8774	0.0289
0.8571 ^a	-	-
0.8739 ^b	0.8948	0.0209
0.8816 ^a	0.9005	0.0189
0.8984 ^b	0.9036	0.0152

^a transitions split from the ^b transitions by the ³¹P hyperfine.

Table V.5.1. Table comparing the calculated unresolved Λ -doublet magnetic field positions from the PO radical with the five transient signals observed.

The difference between the predicted magnetic field positions is not constant. The quality of the observed spectrum is too poor to be able to determine reliably the phase of the transient signals. If they are first derivative in shape then they have been split out by the applied DC bias and a further six would be expected, however if they are pseudo-second derivative in shape then just six would be expected. The spectrum's non-reproducibility prevents a more detailed analysis. The weakness of the spectrum can be ascribed to two unfavourable population factors if these signals are indeed from the PO radical viz. the signals must arise from the $^2\Pi_{3/2}$ level since the $^2\Pi_{1/2}$ is essentially diamagnetic, the transitions are occurring between the magnetic sub-levels of

SECTION V.5 - RESULTS AND DISCUSSION

the ${}^2\Pi_{3/2}$ level and so distributing the molecules in this state over the four magnetic sub-levels consequently depleting the number of molecules available in which EPR transitions can occur.

(xii) THE ARSENIC OXIDE RADICAL (AsO) SYSTEM:

The AsO radical has been detected by LMR spectroscopy⁴³, and the method of generation employed was analogous to that used in the generation of the PO radical. Similarly to PO, AsO is a regular ${}^2\Pi_r$ (the ${}^2\Pi_{1/2}$ is below the ${}^2\Pi_{3/2}$). The ${}^2\Pi_{1/2}$ is diamagnetic and since the spin-orbit coupling constant increases with atomic number even fewer molecules will be available for EPR transitions to occur within; in this case then there are two unfavourable population factors which must have been sufficient to prevent the radical from being observed by EPR.

(xiii) THE SELENIUM OXIDE RADICAL (SeO) SYSTEM:

The Stark cavity produces SeO radical signals which are as intense as any published spectrum indicating that the Stark DC bias power supply works well.

(xiv) THE SELENIUM NITIDE RADICAL (SeN) SYSTEM

The same arguments concerning the population of detectable states in the case of AsO can be applied to the SeN radical which also possesses a regular ${}^2\Pi_r$ ground state and these factors may have been sufficient for the radical to evade detection by EPR even though it has been detected by LMR spectroscopy⁴⁴.

SECTION V.5 - RESULTS AND DISCUSSION

(xiii) THE SELENIUM CHLORIDE RADICAL (SeCl) SYSTEM:

The SeF radical has been detected by EPR²², but the next analogous radical incorporating the next heaviest halogen, SeCl, appears to be previously undetected by microwave or LMR spectroscopies. OH radicals can be generated in relatively high concentrations and on admission of Se_2Cl_2 into the system the OH radicals were "titrated" away and elemental selenium was deposited inside the cavity indicating that reaction was occurring. The mechanism of the reaction is at present unclear but it is likely that SeCl is an intermediate in the reaction pathways, however not in a sufficiently high concentration to be detectable by EPR by this method of generation. The reaction between H atoms and Se_2Cl_2 is probably a chlorine atom abstraction by the proton resulting in the formation of HCl. Elemental selenium is also deposited in this reaction and H atoms are "titrated" away so SeCl is probably an intermediate in the reaction pathways, however not in a sufficiently high concentration to be detectable by EPR by this method of generation.

V.6 CONCLUSIONS

EPR spectroscopy over the past forty years has had some remarkable successes in the detection of free radicals and atoms, in the gas phase, and in many cases has preceded the microwave spectra of these radicals, notably SF and SeF. However, it is now very much a "second-string" detection system to LMR spectroscopy whose sensitivity is approaching that of optical spectroscopy. The data which can be derived from EPR spectra can complement those derived from LMR and microwave spectroscopies and the added sensitivity of LMR

SECTION V.6 - CONCLUSIONS

spectroscopy facilitates the optimising of new radical generation systems to possibly within EPR spectroscopy's detection limits, as in the case of the HO_2 radical, so providing new candidates for detection.

The modified Zeeman cavity is as good as if not better than any other published Zeeman cavity design and on the basis of the (S/N) ratios of the atomic spectra observed, utilising the discharge end piece, the system produces a relatively high concentration of radicals for reaction inside the cavity. The previously undetected (by EPR spectroscopy) PO radical has been tentatively observed under the same conditions which yielded its microwave spectrum, but the observed spectrum was non-reproducible. A further increase in the EPR spectrometer's sensitivity is required or the implementation of a micro-computer signal averaging system similar to that employed in the S_2 work, may truly establish PO as the carrier of this spectrum.

A future candidate for detection by EPR spectroscopy might be the sulphur analogue of the SeCl radical which was attempted viz. SCl. This radical should be produced in the same manner as the SeCl radical is believed to be produced excepting that it will require the reaction of H atoms or OH radicals with S_2Cl_2 . The free radical products of these reactions could be detected by either the modified Zeeman cavity or the Stark cavity and it may be a slightly more favourable candidate for detection than the SeCl radical since the EPR spectrum of the SF radical is considerably more intense than the SeF EPR spectrum²².

IV.7 REFERENCES

1. Y.Beers, A.G.Hill & A.Roberts,
Phys. Rev., 70, 112 (1946).
2. R.Beringer & J.G.Castle, Phys. Rev., 75, 1963 (1949).
3. R.Beringer & J.G.Castle, Phys. Rev., 75, 868 (1949).
4. R.L.Brown & H.E.Radford, Phys. Rev., 147, 7 (1966).
5. R.Beringer & J.G.Castle, Phys. Rev., 80, 114 (1950).
6. R.Beringer & E.B.Rawson, Phys. Rev., 87, 228 (1952).
7. E.B.Rawson & R.Beringer, Phys. Rev., 88, 677 (1952).
8. M.A.Heald & R.Beringer, Phys. Rev., 96, 645 (1954).
9. H.G.Dehmelt, Phys. Rev., 99, 527 (1955).
10. H.E.Radford, V.Beltran-Lopez & V.W.Hughes,
Phys. Rev., 123, 153 (1961).
11. V.Beltran-Lopez & H.G.Robinson,
Phys. Rev., 123, 161 (1961).
12. J.S.M.Harvey, R.A.Kamper & K.R.Lea,
Proc. Phys. Soc., B76, 976 (1960).
13. J.S.MacKenzie & N.Vanderkooi,
Advan. Chem. Ser.36, 98 (1962).
14. H.E.Radford, Phys. Rev. Lett., 122, 114 (1961).
15. C.C.MacDonald, J. Chem. Phys., 39, 2587 (1963).
16. H.E.Radford, J. Chem. Phys., 40, 2732 (1964).
17. A.M.Falick, B.H.Mahan & R.J.Myers,
J. Chem. Phys., 42, 1837 (1965).
18. A.Carrington & D.H.Levy, J. Chem. Phys., 44, 1298 (1966).
19. S.Aditya & J.E.Willard, J. Chem. Phys., 44, 833 (1966).
20. R.L.Brown, J. Chem. Phys., 44, 2827 (1966).
21. A.Carrington, D.H.Levy & T.A.Miller,
Proc. Roy. Soc. A293, 108 (1966).
22. A.Carrington, G.N.Currie, P.N.Dyer, D.H.Levy &

SECTION V.7 - REFERENCES

- T.A.Miller, Chem. Commun., 13, 641 (1967).
23. H.E.Radford & K.M.Evenson, Phys. Rev., 168, 70 (1968).
24. A.Carrington, G.N.Currie, D.H.Levy & T.A.Miller,
Mol. Phys., 17, 535 (1969).
25. A.Carrington, A.R.Fabris, B.J.Howard & N.J.D.Lucas,
J.Chem.Phys., 49, 5545 (1968).
26. A.Carrington, A.R.Fabris & N.J.D.Lucas,
Mol. Phys. 16, 195 (1969).
27. N.W.Ressler, R.H.Sands & T.E.Stark,
Phys. Rev., 184, 102 (1969).
28. A.Carrington & B.J.Howard, Mol. Phys., 18, 225 (1970).
29. W.G.Zijlstra, J.M.Henrichs, J.H.M.Moog &
J.D.W. Van Voorst, Chem. Phys. Letts., 7, 553 (1970).
30. I.C.Bowater, J.M.Brown & A. Carrington,
J. Chem. Phys., 54, 4957 (1971).
31. F.D.Wayne, P.B.Davies & B.A.Thrush,
Mol. Phys., 28, 989 (1974).
32. C.E.Barnes, J.M.Brown, A.Carrington, J.Pinkstone,
T.J.Sears & P.J.Thistlewaite,
J. Mol. Spec., 72, 86 (1978).
33. C.E.Barnes, J.M.Brown & H.E.Radford,
J. Mol. Spec., 84, 179 (1980).
34. C.P.Poole, "Electron Spin Resonance: a Comprehensive
Treatise on Experimental Techniques", Interscience
Publishers, a Division of John Wiley & Sons,
New York, London, Sydney (1967).
35. A.Carrington, D.H.Levy & T.A.Miller,
Rev. Sci. Inst., 38, 1183 (1967).
36. H.E.Radford & D.K.Russell,
J. Chem. Phys., 66, 2222 (1977).

SECTION V.7 - REFERENCES

37. P.98, "High Resolution Spectroscopy" by J.M.Hollas,
Published by Butterworths (1982).
 38. Y.Endo, S.Saito & E.Hirota,
J. Chem. Phys., 81, 122 (1984).
 39. Y.Endo, S.Saito & E.Hirota, IMS Ann. Report, 34 (1984).
 40. Y.Endo, C.Yamada, S.Saito & E.Hirota,
J. Chem. Phys., 79, 1605 (1983).
 41. Y.Endo, C.Yamada, S.Saito & E.Hirota,
IMS Ann. Report, 30 (1984).
 42. Y.Endo, S.Saito & E.Hirota IMS Ann. Report, 31 (1984).
 43. H.Uehara, Chem. Phys. Letts., 84, 539 (1981).
 44. K.Hakuta & H.Uehara, Proceedings of the
14th International Symposium on Free Radicals,
Sanda, Japan (1979).
 45. D.K.Russell, (unpublished results).
-

SECTION VI.1 - INTRODUCTION

CHAPTER VI - DETECTION BY INFRARED DIODE LASER ABSORPTION SPECTROSCOPY

VI.1 INTRODUCTION

In this Chapter infrared diode laser absorption spectroscopy (IDL) as a detection system for radicals and atoms in the gas phase is examined. The technique is firstly reviewed, indicating significant observations where relevant. An indication of the experiments performed using this method of detection then follows along with the results obtained from these experiments. An account of the majority of the original work contained in this Chapter has been published in the Journal of Chemical Physics²².

VI.2 REVIEW

The first transient species to be observed by IDL spectroscopy was the chlorine monoxide radical, ClO^1 . The observed spectrum consisted of both the ^{35}ClO and the ^{37}ClO isotopic species in their $^2\Pi_{3/2}$ and the higher $^2\Pi_{1/2}$ levels. The next transient radical to be detected by IDL spectroscopy was the carbon monosulphide radical, $\text{CS}^{2,3}$. The spectrum contained absorptions from the fundamental and the first three "hot" bands of the radical.

The first transient atom to be detected by IDL spectroscopy was the chlorine atom, Cl , and this spectrum exhibited absorptions due to the hyperfine splitting and due to the ^{35}Cl and ^{37}Cl nuclei⁴. The first triatomic transient radical to be detected was the nitrogen difluoride radical, NF_2 , in both its ν_1 and ν_3 bands⁵. The carbon analogue of this radical, the difluorocarbene radical, CF_2 , was observed by IDL spectroscopy shortly afterwards⁶. The next diatomic

SECTION VI.2 - REVIEW

radical to be observed was the nitrogen monosulphide radical, NS, in both its ${}^2\Pi_{3/2}$ and ${}^2\Pi_{1/2}$ levels⁷. The next two atoms to be detected were the fluorine and the helium (in a meta stable state) atoms^{8,9}, and it was their fine structure transitions in each case that were observed.

The ν_2 band of the elusive and very important polyatomic radical, CH_3 , was observed by IDL spectroscopy and the data derived from its spectra confirmed that the radical was indeed planar in the gas phase¹⁰. The earlier observation of the CF_2 radical was complimented by the observation of the singly fluorinated and chlorinated species, CF and CCl^{11,12}. The observed CCl spectra contained absorptions due to both the C^{35}Cl and the C^{37}Cl isotopic species and a few lines from the "hot" band ($2 \leftarrow 1$) of the C^{35}Cl . The CF spectrum contained not only transitions from the paramagnetic ${}^2\Pi_{3/2}$ but also some from ${}^2\Pi_{1/2}$ due to the mixing of these levels.

The symmetric triatomic, the boron dioxide, BO_2 and the asymmetric hydroperoxyl radical, HO_2 , were observed using IDL spectroscopy^{13,14}. Absorptions due to the both ${}^{11}\text{BO}_2$ and ${}^{10}\text{BO}_2$ isotopic species were observed in both their ${}^2\Pi_{1/2}$ and ${}^2\Pi_{3/2}$ levels. In addition, "hot" band ($2 \leftarrow 1$) absorptions from the ${}^{11}\text{BO}_2$ isotopic species were also observed. Absorptions from the ν_3 band of HO_2 were the absorptions which were actually detected.

The next new transient triatomic bands to be observed were the ν_1 and ν_3 bands of the carbonyl fluoride radical, FCO. The ν_1 band of F^{13}CO was also observed and this enabled FCO to be identified as the carrier of the spectrum¹⁵. The first gas phase spectrum of the linear boron oxychloride radical, ClBO, was reported using IDL laser spectroscopy. The

SECTION VI.2 - REVIEW

ν_3 bands were also observed for $^{35}\text{Cl}^{11}\text{B}^{16}\text{O}$, $^{37}\text{Cl}^{11}\text{B}^{16}\text{O}$ and $^{35}\text{Cl}^{10}\text{B}^{16}\text{O}^{16}$. The fluorine monoxide radical, FO, in its paramagnetic $^2\Pi_{3/2}$ level was the next diatomic to be observed employing IDL spectroscopy¹⁷, and from the data derived from its spectrum the magnitude of the dipole moment was established as being relatively small explaining why the radical had proved undetectable by microwave spectroscopic techniques previously.

The fluorinated analogue to the CH_3 radical, the trifluoromethyl radical, CF_3 , was observed and from the data derived from its ν_3 band it was established that the radical, in contrast to CH_3 , had pyramidal symmetry¹⁸. Preliminary work on the phosphorus monochloride, PCl, and the silicon nitride radicals, SiN, has been reported^{19,20}. Both the P^{35}Cl and the P^{37}Cl isotopic species have been observed the former also in its "hot" band ($2 \leftarrow 1$).

Absorptions from the ν_3 band of the nitrate radical, NO_3 , have also recently been observed²¹, for both the $^{14}\text{NO}_3$ and $^{15}\text{NO}_3$ isotopic species. Finally, both the fundamental and the "hot" band ($2 \leftarrow 1$) absorptions of the silicon hydride radical, SiH, have been detected by IDL spectroscopy²², and are described in the next section.

VI.3 EXPERIMENTAL

Vibration-rotation transitions of the SiH radical were searched for using IDL spectroscopy and the method employed to generate SiH for detection by infrared diode laser absorption spectroscopy (IDL) was the electrical plasma discharge decomposition of silane, SiH_4 , in either helium, He, argon, Ar, or hydrogen, H_2 . This method utilised a 1.5 m

SECTION VI.3 - EXPERIMENTAL

long, 35 mm internal diameter water cooled discharge tube, with co-axial electrodes, driven by a 6 kV current stabilised power supply. Typical operating conditions for maximum SiH absorption intensities were 2.5 kV and 60 mA through a flowing H₂ plasma containing 10% SiH₄ at a total pressure of several mBar. SiH could also be detected in Ar/SiH₄ and He/SiH₄ discharges, but pure SiH₄ discharges were found to be quite unstable without the addition of a buffer gas. The tube was terminated by CaF₂ windows and both tube and end windows occasionally had to be cleaned to remove silicon deposits. The SiH absorptions only dropped in intensity by a factor of two when a pure H₂ discharge was run in the silicon-coated tube. Presumably under these conditions SiH (or Si) is sputtered from the amorphous silicon surface. As well as reducing any problems from thickening wall deposits, running the discharge in this manner resulted in almost total suppression of background SiH₄ absorptions.

Figure VI.3.1 shows the experimental arrangement of the absorption cell and the diode laser spectrometer. A multiple-pass arrangement was used with a system of White-type mirrors which gave up to twenty traversals of the laser beam through the plasma. The laser was then directed to a 1/2 m monochromator for mode selection, and finally into a InSb detector. A striped geometry diode supplied by Laser Analytics (Spectra-Physics Inc.) was used to cover the central region of the SiH spectrum (1870-1980 cm⁻¹). Absolute calibration was carried out using accurately measured lines in N₂O²³, NO²⁴ and standard Ge etalons.

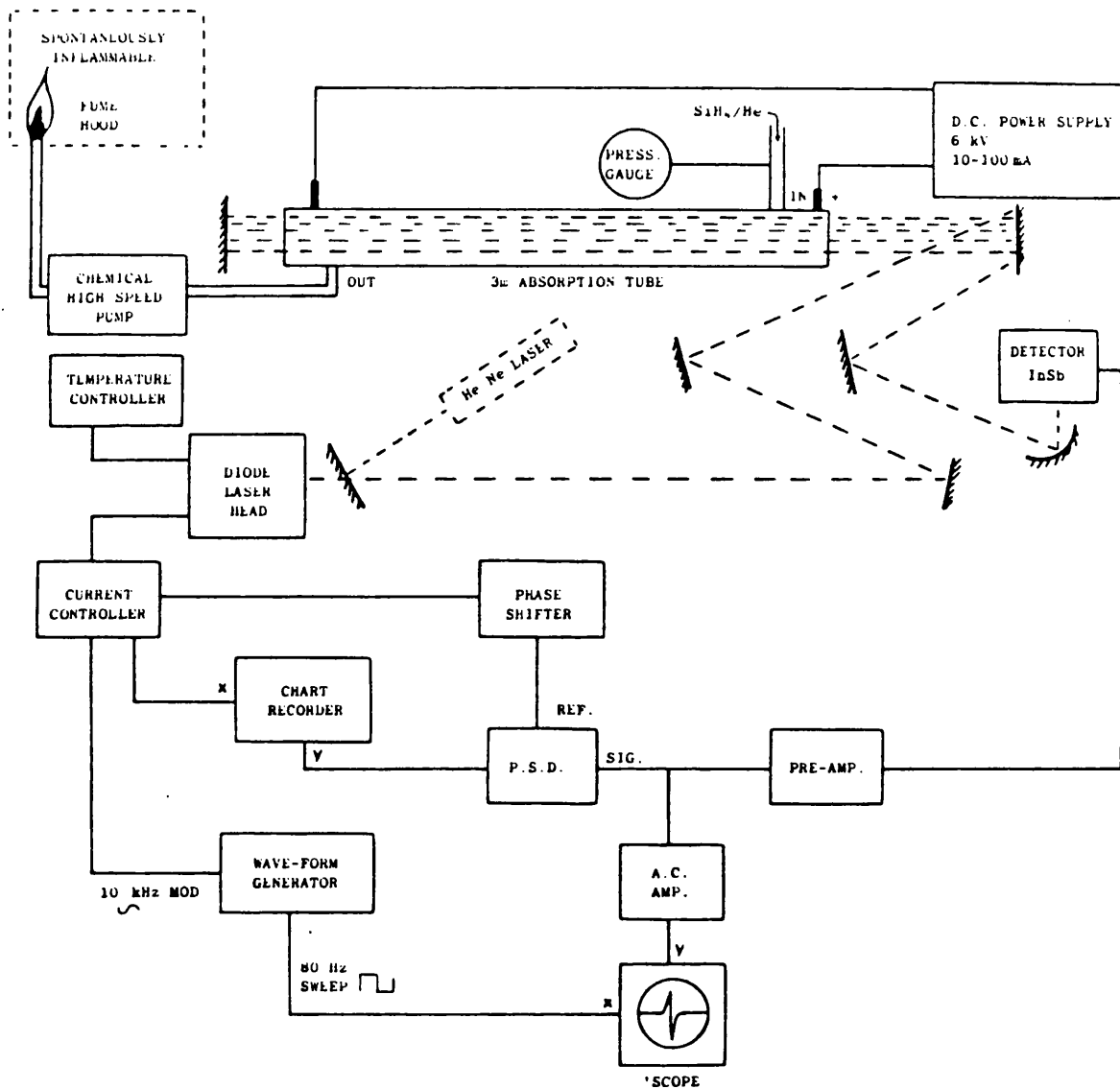


Figure VI.3.1. A schematic block diagram of the experimental arrangement of the absorption cell and infrared diode laser spectrometer.

SECTION VI.4 - RESULTS AND DISCUSSION

VI.4 RESULTS AND DISCUSSION

Although final recording of the spectra used 10 kHz source modulation and phase sensitive detection, many of the transitions could be seen in real time on the oscilloscope (absorption on the strongest lines was 5% for twenty passes of the discharge tube). This greatly aided their optimisation and reduced the search problem. The main experimental difficulty in recording and calibrating these spectra arose due to temperature fluctuations of the diode laser cold finger (an early Air Products Inc. device).

Seven Λ -doublets in the fundamental band of SiH were detected using the above technique (these are shown in Table VI.4.1).

SECTION VI.4 - RESULTS AND DISCUSSION

J	\pm^*	R_1^c	R_2^c	P_1^c	P_2	Q_1	Q_2
0.5	e	1990.601				1970.415 ^a	
0.5	f	1990.686				1970.218 ^a	
1.5	e	2003.630	2008.377	1949.475		1969.943 ^d	1970.603 ^a
1.5	f	2003.698	2008.397	1949.378		1969.564 ^e	1970.588 ^b
2.5	e	2016.320	2022.147	1934.935	1931.605 ^b	1969.069 ^d	1969.414 ^a
2.5	f	2016.368	2022.184	1934.851	1931.583 ^b	1969.538 ^d	1969.360 ^a
3.5	e	2028.664	2035.336	1919.958 ^e	1914.952 ^b	1967.788 ^d	1967.776 ^d
3.5	f	2028.690	2035.389	1919.890 ^e	1914.907 ^b	1967.141 ^d	1967.360 ^a
4.5	e	2040.650	2047.938	1904.531	1897.950 ^c	1966.080 ^d	1965.699 ^d
4.5	f	2040.650	2048.008	1904.485	1897.882 ^e	1965.361 ^d	1965.442 ^d
5.5	e	2052.251	2059.955	1888.655 ^e	1880.624 ^c	1963.944 ^d	1963.190 ^d
5.5	f	2052.232	2060.044	1888.632 ^e	1880.528 ^c	1963.202 ^d	1962.767 ^d
6.5	e	2063.450	2071.396	1872.335	1862.988 ^c	1961.365 ^d	1960.265 ^d
6.5	f	2063.412	2071.498	1872.335	1862.865 ^c	1960.642 ^d	1959.630 ^d
7.5	e	2074.225		1855.581		1958.351 ^d	
7.5	f	2074.168		1855.607	1844.898 ^c	1957.692 ^d	1956.029 ^d
8.5	e	2084.558		1838.408		1954.884 ^d	
8.5	f	2084.475		1838.460		1954.334 ^d	
9.5	e	2094.295					
9.5	f	2094.201					

* $v=0$ level parity

^a Present measurements (uncertainty ± 0.005 cm^{-1}).

^b Brown and Robinson²⁵.

^c Knights *et al.*²⁶.

^d From combination differences.

^e Line detected in present work, but not accurately calibrated.

Table VI.4.1. SiH (1-0) data set (cm^{-1})

Some of these are R- and P-branch lines were already accurately measured in the FTIR study²⁶. In addition, three hot band (2 \leftarrow 1) Λ -doublets have also been identified [$R_1(5.5)$, $Q_2(4.5)$,

SECTION VI.4 - RESULTS AND DISCUSSION

$Q_2(2.5)]$, by comparison either with the data of Knights et al., or with the study of Singh and Vanlandingham²⁷. In the latter study, combination differences of the extensive optical data available for SiH were used to generate calculated SiH $1 \leftarrow 0$ and $2 \leftarrow 1$ infrared vibration-rotation schemes. These have proved to be accurate to about $\pm 0.2 \text{ cm}^{-1}$.

The aim of our experiments was the observation and measurement of low J Q-branch lines of the fundamental band. This was necessary for an experimental determination of the parity labelling (e,f) for the R- and P-branch lines measured in the previous studies. Once this had been achieved combination differences could be used to predict, to an accuracy limited only in the precision of the present data set, the positions of all the other Q_1 - and Q_2 -branch lines up to $J = 8.5$ and $J = 7.5$ respectively. This calculation however makes the assumption that the \pm parity ordering given by Brown, Curl and Evenson²⁸ for the $\nu = 0$ vibrational level also applies to the $\nu = 1$ vibrational level.

Figure VI.4.1 is a frequency scan through the $Q_1(0.5)$ and the $Q_2(1.5)$ components and shows the resolved Λ -doubling. Assignment of the $Q_2(1.5)$ doublet (which is incorrectly labelled $Q_2(0.5)$ in the work of Knights et al.²⁶) was based upon the previous measurement by Brown and Robinson²⁵ using mid-infrared LMR. The calibration of the $Q_2(2.5)$ Λ -doublet was then used to assign the e and f labels for the linked R- and P-branch lines in the FTIR work²⁶.

The $Q_1(0.5)$ Λ -doublet has not previously been observed and so initial assignment was based on the predictions of Singh and Vanlandingham²⁷. Confirmation of the assignment was made by observation of the $Q_1(1.5)$ Λ -doublet at a measured position in

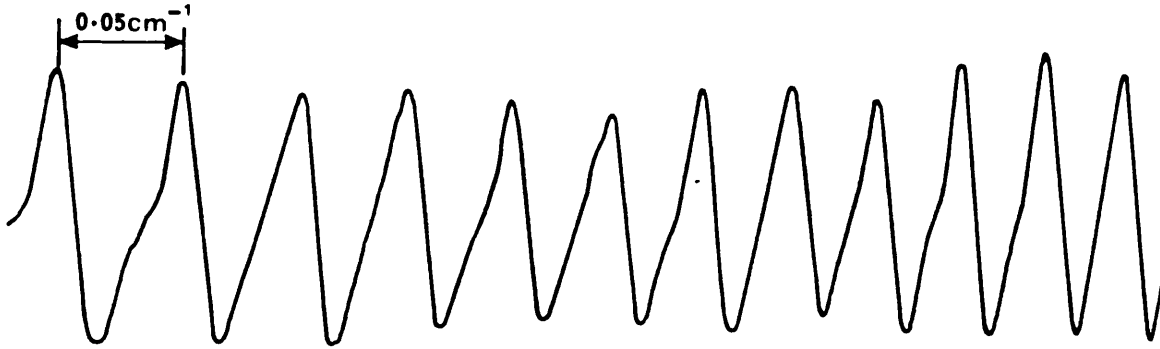
SECTION VI.4 - RESULTS AND DISCUSSION

excellent agreement with that calculated from the linking transitions $R_1(0.5)$, $P_1(0.5)$ and $Q_1(0.5)$.

The present state of the SiH data set is shown in Table VI.4.1, which gives the lines determined from these experiments, those of Knights *et al.*²⁶ and those of Brown and Robinson²⁵. The e and f transition parity labels are also indicated, together with the Q-branch transitions calculated from combination differences.

In addition to the transient absorptions which were identified as originating from either the fundamental or first excited hot band of SiH, three less intense absorptions were also observed and the positions of these are shown in the Figure VI.4.2 relative to the $R_1(5.5)$ hot band Λ doublets of SiH. It can be seen from this figure that they occur between 1978 and 1979 cm^{-1} . The molecular parameters derived from the

Etalon calibrant at $5.2 \mu\text{m}$



SiH

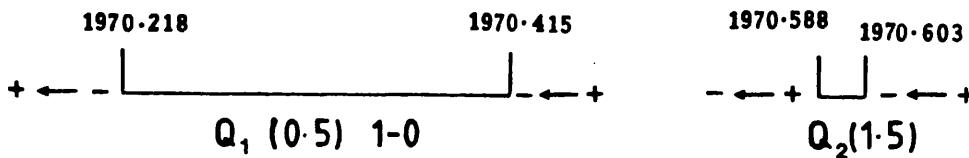
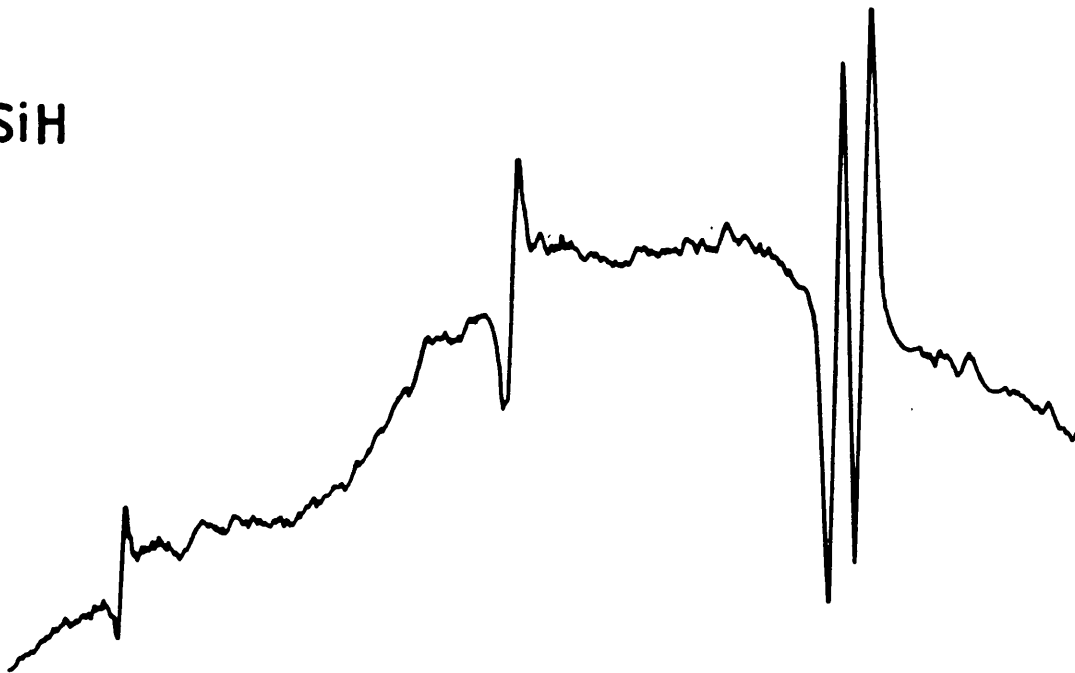


Figure VI.4.1. A frequency scan through the $Q_1(0.5)$ and $Q_2(1.5)$ components of SiH. H_2 pressure 4.0 mBar, SiH_4 pressure 0.4 mBar, time constant 1.0 s, scan time 180.0 s.

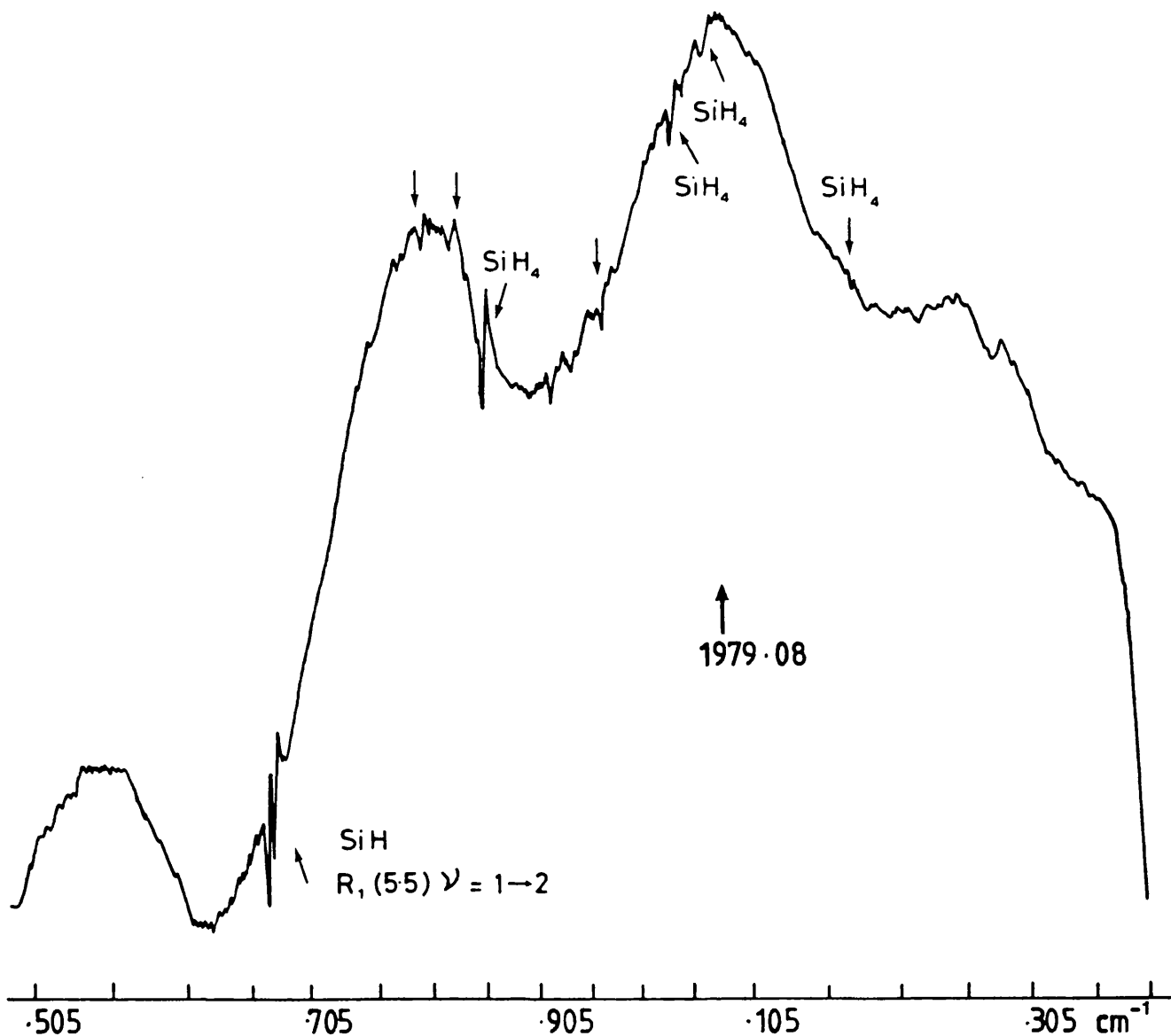


Figure VI.4.2. A frequency scan through the $R_1(5.5) (2 + 1)$ hot band showing the three transient absorptions tentatively assigned to the SiH_2 radical. He pressure 17.0 mBar, SiH_4 pressure 2.0 mBar, time constant 0.3 s, scan time 180.0 s.

SECTION VI.4 - RESULTS AND DISCUSSION

extensive optical work on the silylene radical, SiH_2^{29-32} , provided the data for a computer program³³ to predict the transition frequencies and relative strengths (based upon an estimated effective temperature within the absorption tube) of this radical. The graphical output (Figure VI.4.3) from the program indicated that the SiH_2 radical exhibited some of its most intense transitions within the 1978 and 1979 cm^{-1} region and on this basis the three transient absorptions are tentatively assigned to the SiH_2 radical.

VI.5 ANALYSIS

A computer program (NAI2PIV) was written (Appendix III) initially to predict the transition frequencies of the SiH radical based upon data derived from the optical³⁰⁻³², mid-infrared LMR and far infrared molecular parameters. This program also predicted the relative strengths of the transitions based upon an estimated temperature within the discharge tube and produced a graphical representation at a specified wavenumber resolution and minimum relative strength. Typical outputs from this program are shown in Figure VI.5.1 and Figure VI.5.2 The latter of these two figures contains the predicted transition frequencies of the Q-branch transitions which were observed and calibrated.

The program was later extended after the acquisition of the Q-branch data to calculate a statistical fit of the observed data set shown in Table VI.4.1, but it did not attempt to fit the combination difference data. The program on fitting between its predicted transition frequencies and those observed subsequently generated a root mean square error (RMS) which was an indication of the quality of the fit. This procedure was

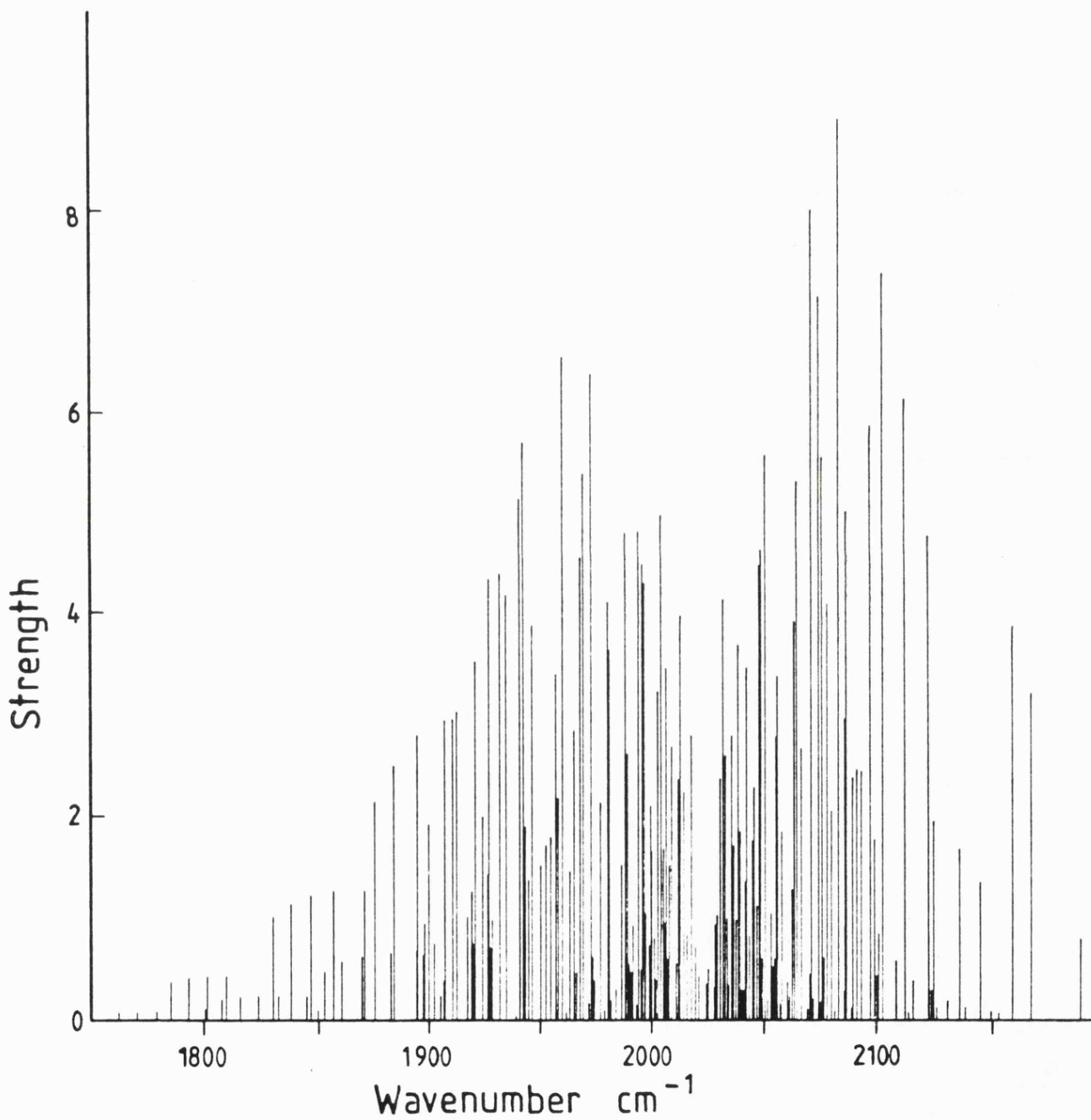
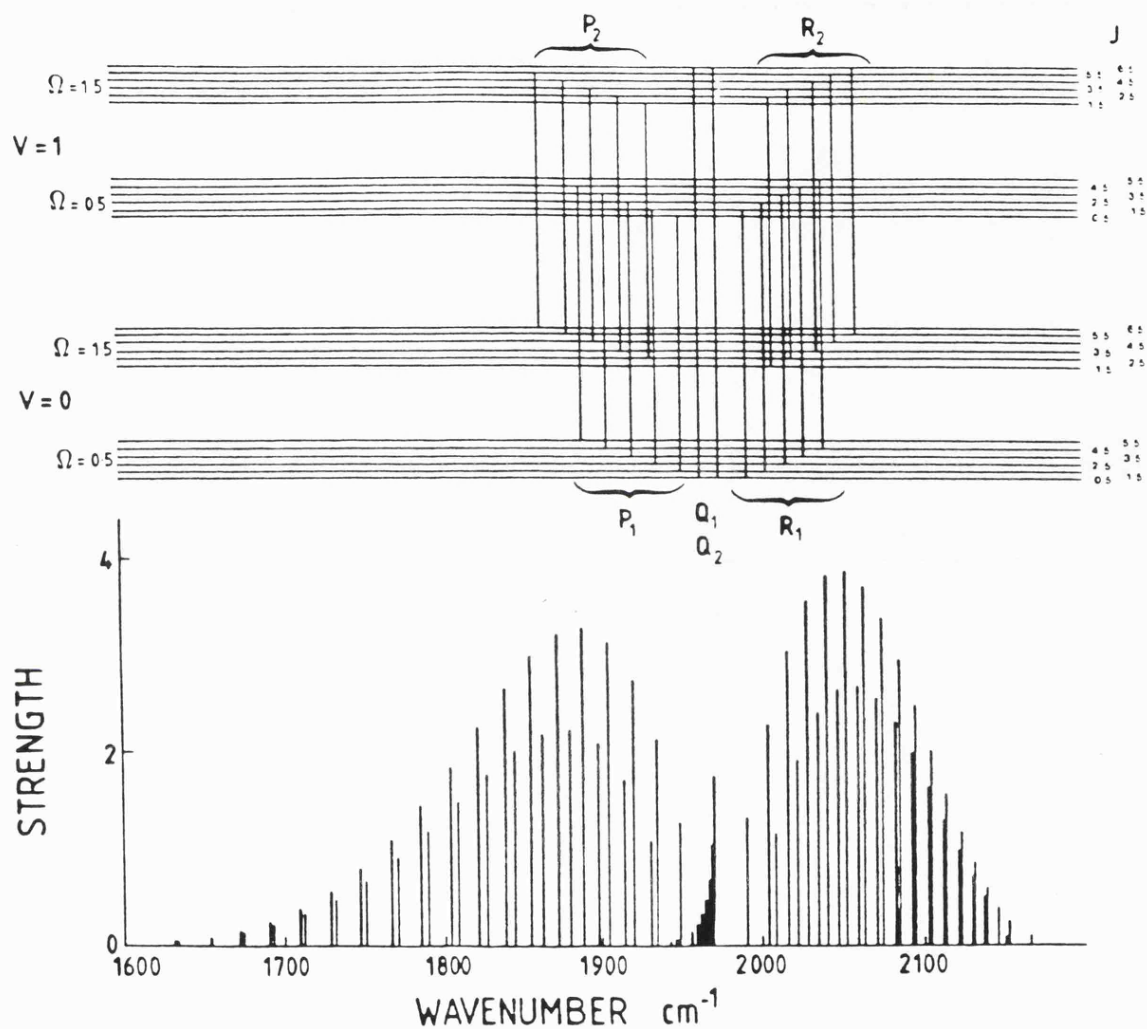
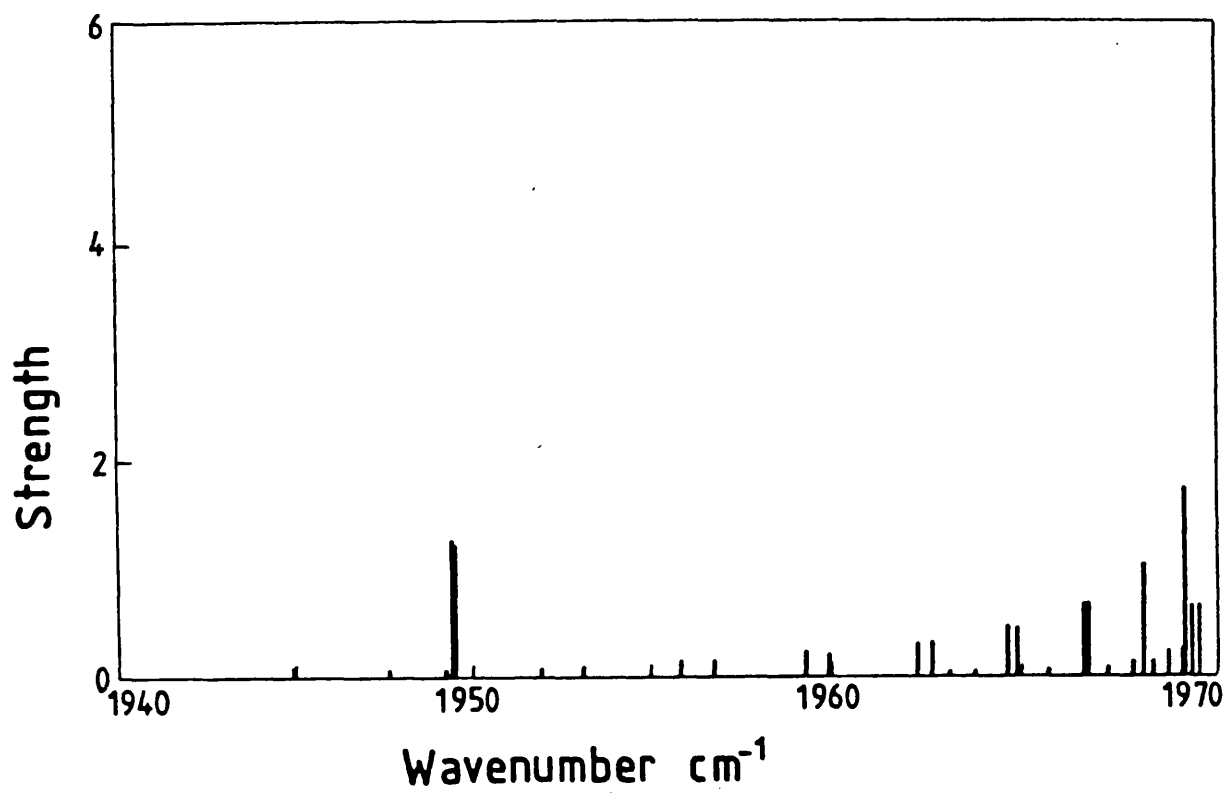


Figure VI.4.3. The graphical output from the asymmetric rotor program predicted the transition frequencies and the relative intensities of the SiH_2 radical.



SiH stretch $V=0 \rightarrow V=1$ at 698.15K

Figure VI.5.1. The graphical output of the NAI2PIV program predicting the transition frequencies and the relative intensities of the SiH radical.



SiH Q₁, Q₂ branches at 698.15K

Figure VI.5.2. The graphical output of the NAI2PIV program predicting transition frequencies and the relative intensities of the SiH Q branches.

SECTION VI.5 - ANALYSIS

attempted on the data contained in Table VI.4.1. (with the exception of the combination difference data) and an RMS error of the order of 0.07 cm^{-1} was calculated based upon the molecular parameters quoted in the two LMR papers^{28,29}. Since the uncertainty of the data contained in Table VI.4.1 is of the order of 0.005 cm^{-1} an acceptable RMS error would be either less than or equal to this value. The main source of the deviation between the predicted transition frequencies and those observed appears to be due to the Λ -doubling transition frequencies of the higher rotational levels. The source of this discrepancy may be due to the experimental accuracy of the FTIR transitions since these have an inferior precision to those observed by IDL and LMR spectroscopies. However work is still in progress in attempt to improve this fit.

VI.6 CONCLUSIONS

The SiH work presented in this Chapter shows that a silane plasma discharge is a rich source of SiH radicals. The preliminary results described in this Chapter yield a number of accurate predictions both from combination differences and from the computer program for future laboratory searches and for astrophysical searches and these also complement the mid-infrared LMR results, which are of potentially higher resolution (Lamb dip spectra). These initial studies with a less sensitive spectrometer suggest that many more transitions in SiH should be detectable and the technique has tentatively also produced transitions arising from SiH_2 , and could be extended to SiH_3 and SiH^+ the latter by the application of an A.C. discharge modulation technique.

SECTION VI.7 - REFERENCES

VI.7 REFERENCES

1. R.T.Menzies, J.S.Margolis, E.D.Hinkley & R.A.Toth,
App. Opt., 16, 523 (1977).
2. C.Yamada & E.Hirota, J. Mol. Spec., 74, 203 (1979).
3. T.R.Todd & W.B.Olson, J. Mol Spec., 74, 190 (1979).
4. P.B.Davies & D.K.Russell,
Chem. Phys. Letts., 67, 440 (1979).
5. P.B.Davies, B.J.Handy & D.K.Russell,
Chem. Phys. Letts., 68, 395 (1979).
6. P.B.Davies & D.K.Russell, J. Mol. Struc. 60, 201 (1980).
7. K.Matsumara, K.Kawaguchi, K.Nagai, C.Yamada & E.Hirota,
J. Mol. Spec., 84, 68 (1980).
8. A.C.Stanton & C.E.Kolbe, J. Chem. Phys., 72, 6637 (1980).
9. K.Nagai, K.Tanaka & E.Hirota,
J. Phys. B, (To be published).
10. C.Yamada, E.Hirota & K.Kawaguchi,
J. Chem. Phys., 75, 5256 (1981).
11. C.Yamada, K.Nagai & E.Hirota,
J. Mol. Spec., 85, 416 (1981).
12. K.Kawaguchi, K.Nagai, C.Yamada, Y.Hamada & E.Hirota,
J. Mol. Spec., 86, 136 (1981).
13. K.Kawaguchi, E.Hirota & C.Yamada,
Mol. Phys., 44, 509 (1981).
14. K.Nagai, C.Yamada, Y.Endo & E.Hirota,
J. Mol. Spec., 85, 416 (1981).
15. K.Nagai, C.Yamada, Y.Endo & E.Hirota,
J. Mol. Spec., 90, 249 (1981).
16. K.Kawagachui, Y.Endo & E.Hirota,
J. Mol. Spec., 93, 381 (1982).
17. A.R.W.McKellar, C.Yamada & E.Hirota,

SECTION VI.7 - REFERENCES

- J. Mol. Spec., 97, 425 (1983).
18. C.Yamada & E.Hirota, J. Chem. Phys., 78, 1783 (1983).
19. H.Kanamori, C.Yamada, K.Kawaguchi, J.E.Butler & E.Hirota,
IMS Ann. Rev., 32 (1984).
20. C.Yamada & E.Hirota, IMS Ann. Rev., 33 (1984).
21. T.Ishiwata, I.Tanaka, K.Kawaguchci & E.HIrota,
J. Chem. Phys., 82, 2196 (1985).
22. P.B.Davies, N.A.Isaacs, S.A.Johnson & D.K.Russell,
J. Chem. Phys., 83, 2060 (1985).
23. J.P.M.Schmitt, J. Non-Cryst. Solids, 59, 649 (1983).
24. N.Hata, A.Matsuda & K.Tanaka,
J. Non-Cryst. Solids 59, 667 (1983).
25. J.M.Brown & D.Robinson, Mol. Phys., 51, 883 (1984).
26. J.C.Knights, J.C.P.Schmitt, J.Perrin & G.Guelachvili,
J. Chem. Phys., 76, 3414 (1982).
27. P.D.Singh & F.G.Vanlandingham,
Astron. Astrophys., 66, 87 (1976).
28. J.M.Brown, R.F.Curl & K.M.Evenson,
J. Chem. Phys., 81, 2884 (1984).
29. I.Dubois, G.Herzberg & R.D.Verma,
J. Chem. Phys., 47, 4262 (1967).
30. I.Dubois, Can. J. Phys., 46, 2485 (1968).
31. I.Dubois, G.Duxbury & R.N.Dixon,
J. Chem. Soc. (Faraday Trans.), 71, 756 (1975).
32. J.F.O'Keefe & F.W.Lampe,
Appl. Phys. Lett., 42, 217 (1983).
33. S.D.Cope & D.K.Russell, (unpublished results).
-

SECTION VII.1 - INTRODUCTION

CHAPTER VII - DETECTION BY MILLIMETER WAVE MAGNETIC RESONANCE

(MMR) SPECTROSCOPY

VII.1 INTRODUCTION

In this Chapter millimeter wave magnetic resonance (MMR) spectroscopy as a detection system for free radicals and atoms in the gas phase is examined. The technique is firstly developed employing an IMPATT oscillator as a source of millimeter wave radiation, indicating problems and solutions associated with the construction and operation of the spectrometer. An account of an experiment performed using this detection system then follows along with the results obtained from this experiment. Finally, the Chapter is concluded with an indication as to how the spectrometer's sensitivity can be improved and with an alternative method of generating species for detection by this technique. A preliminary account of this work has been accepted for publication in the Review of Scientific Instruments⁵

VII.2 DEVELOPMENTAL

A commercial IMPATT (IMPact ionisation Avalanche Transit Time) oscillator model ATMO 280S was purchased from Plessey Microwave Electronics. Such oscillators operate on a double drift silicon diode mounted in a high Q cavity and exhibit limited mechanical and electronic tuning ranges. This particular model had a maximum output of approximately 10 mW, an electrical tuning range of 1000 MHz and a mechanical tuning range from 131-138 GHz. The oscillator had the mode structure typical of such resonant sources: graphs of the variation of power output and output frequency vs. mechanical tuning (i.e. cavity size) are shown in Figure

SECTION VII.2 - DEVELOPMENTAL

VII.2.1(a), (b).

The source exhibited good AM and FM noise characteristics⁶, and is small and convenient to use. The only drawback found during its operation is its delicacy: a well designed power supply is essential for protection against mains transients, since exceeding the maximum rating even for periods as brief as 1.0 μ s can prove fatal to the device. This point was unfortunately made "crystal" clear by the IMPATT oscillator failing three times even when the power supply was on its minimum settings necessary for the IMPATT oscillator to oscillate. Even after rigorous testing of our system at Plessey's laboratory no apparent source of device failure due to transients could be detected. On failure of the device for the fourth time the power supply came under suspicion. On testing as described below, the power supply originally supplied by Plessey (Model ATSM 200) proved to be inadequate. A zener diode circuit which matched the IMPATT's characteristics was constructed and connected to the original power supply and the whole was connected to a storage oscilloscope (Farnell Digital Storage Oscilloscope model DTS 12P). The oscilloscope was programmed to record any transient voltage spikes as brief as 1.0 μ s which the power supply allowed through on to the zener diode.

Figure VII.2.2 shows a typical plotted trace from the storage oscilloscope whilst the power supply was connected and it quite evident from this trace that voltage spikes greater than 1.0 V were being allowed on to the IMPATT oscillator!. It became apparent from the results of these tests that the power supply was completely inadequate for

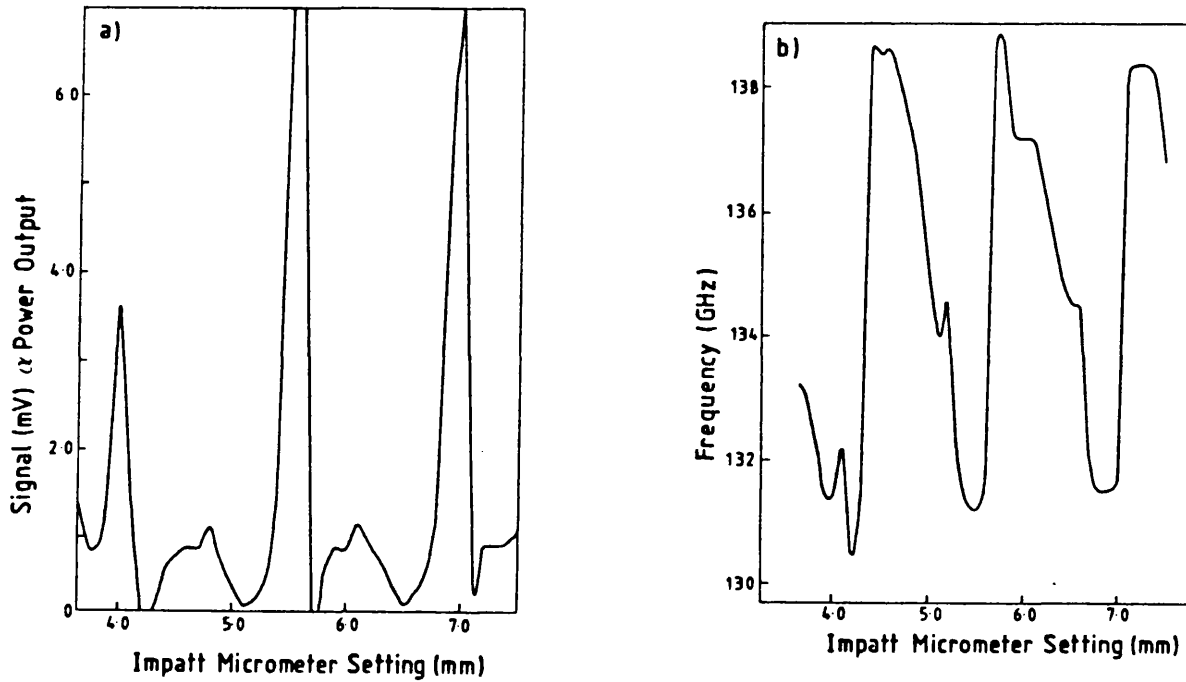


Figure VII.2.1. The Variation of (a) power and (b) frequency of the output of the IMPATT oscillator as a function of cavity size. In (a), the output of the oscillator is measured as the detector voltage: peak power corresponds to approx. 10 mW. In (b), the frequency is measured using the wavemeter and is accurate to ± 0.1 GHz.

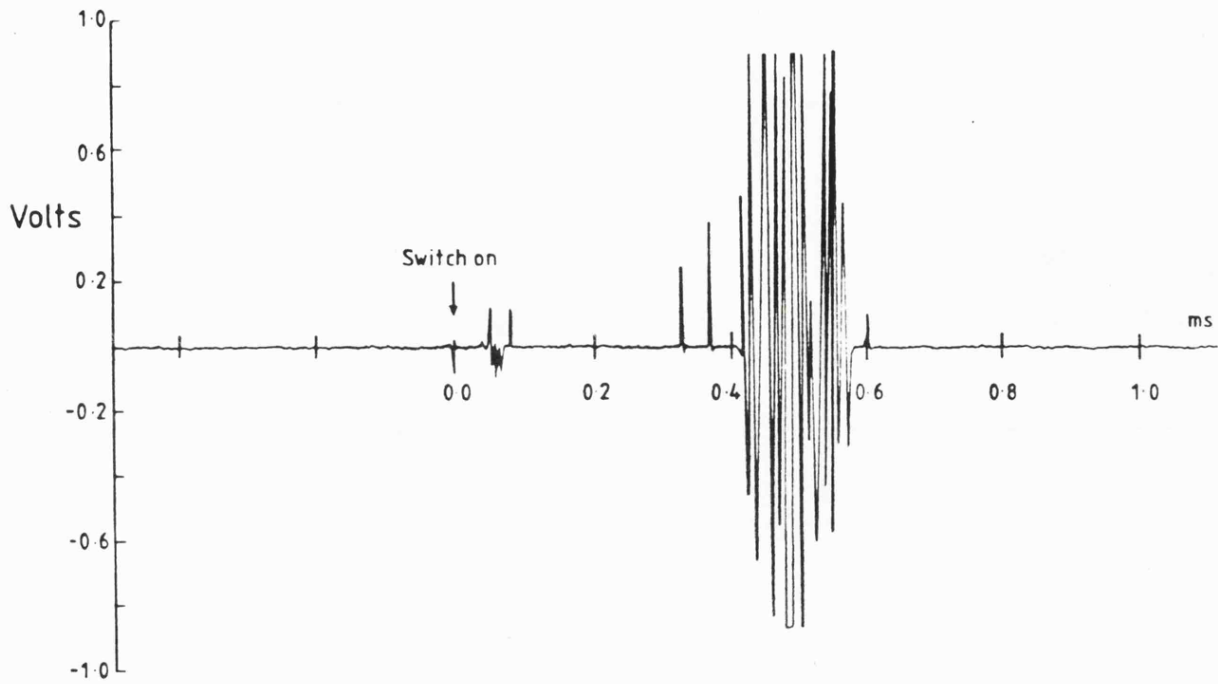


Figure VII.2.2. Typical plotted trace from the storage oscilloscope whilst the IMPATT power supply was connected to the zena diode circuit.

SECTION VII.2 - DEVELOPMENTAL

operation with the IMPATT oscillator under these operating conditions. It appeared that high frequency transients were able to pass through components external to the actual power supply and Plessey are considering withdrawing the model completely as a consequence of the data collected on the original power supply. Plessey supplied a different model (Model ATSM 301) which appeared to be satisfactory under identical test conditions with the zener diode circuit. It also proved essential to mount an isolator on the oscillator to prevent "pulling" of its output frequency by resonant external components.

Figure VII.2.3 shows the reasonably conventional design of the spectrometer. This configuration was suitable for tuning the cavity into resonance and for spectrum acquisition. The majority of the microwave components (attenuator, wave meter, directional coupler, slide-screw tuner and crystal detector) were commercial units purchased from Flann Microwave Ltd., and the isolator was purchased from Hughes Aircraft Corporation. It should be noted that at these wavelengths (2 mm) many components, including waveguide bends and twists, have non-negligible insertion losses, and the spectrometer design represents the optimal configuration. Signal recovery was carried out using conventional commercial electronics (largely Brookdeal) with a band/notch filter, pre-amplifier and lock-in amplifier output to a chart recorder or oscilloscope. Sweep through the oscillator for signal or mode display purposes was provided by modulation of the IMPATT oscillator input voltage. Molecular absorption signals were modulated at 5 kHz by a pair of Helmholtz coils (diameter 11 cm) mounted directly on to the pole caps of

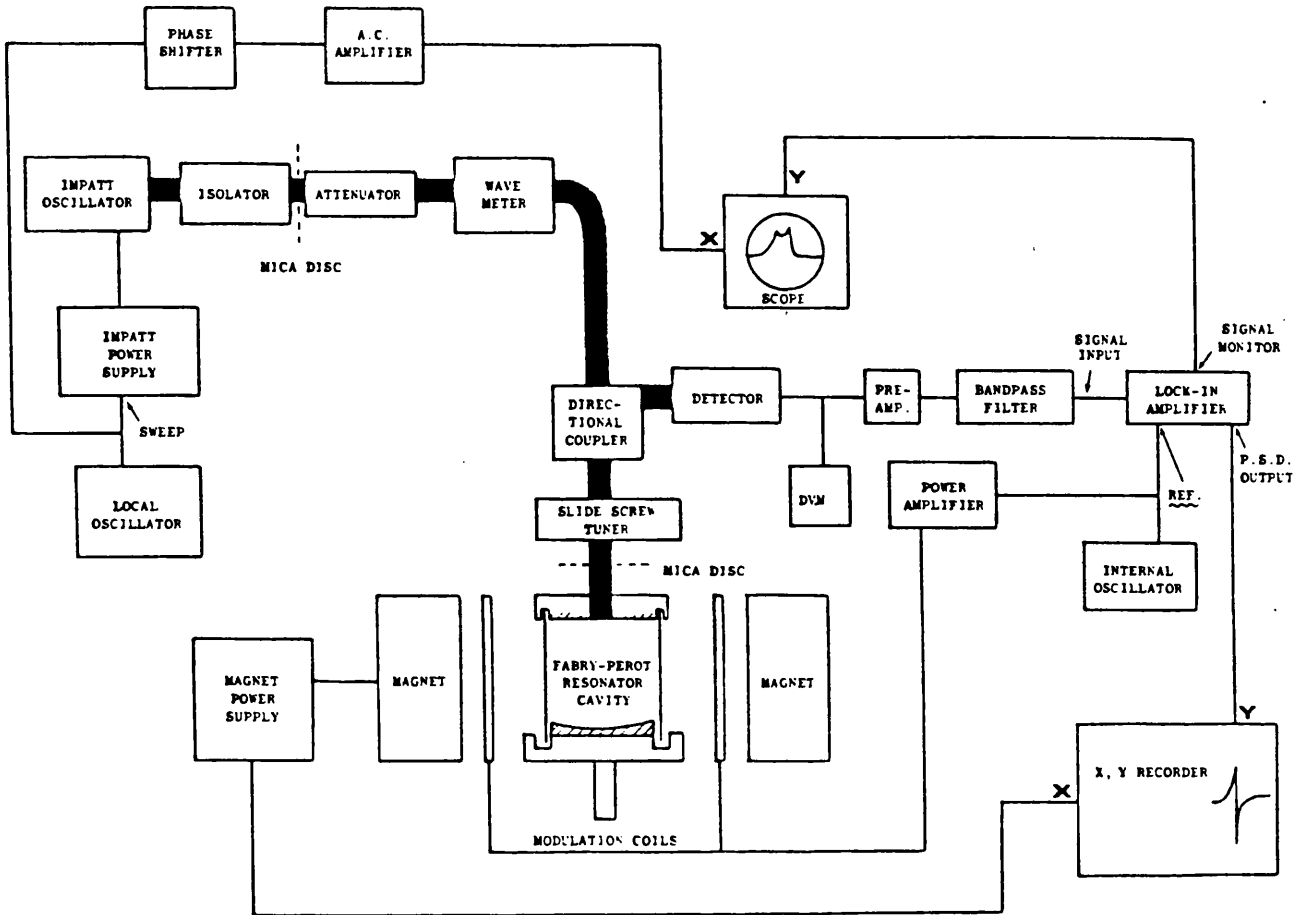


Figure VII.2.3. Schematic diagram of the millimeter wave spectrometer - for details see text.

SECTION VII.2 - DEVELOPMENTAL

a Varian V4102 electromagnet capable of supplying 0.9 T: the modulating field could be varied over the range 0.0 - 0.5 mT.

Several different cavities were constructed predominantly of the semi-confocal Fabry-Perot design. The first of these had the curved mirror on the top of the cavity with the holes of varying sizes up to the open end of the waveguide located in its centre. The plane movable mirror was located at the bottom. This arrangement proved to be difficult to construct due to the silver soldering of the waveguide. A millimeter wave horn was purchased from Flann and silver soldered on the waveguide and mounted in a housing which had a very thin plate in the top piece such that the whole formed the plane mirror. The curved mirror was then located on the movable rotating shaft in the bottom end piece. This arrangement did not allow enough power through. The plate was then drilled with a mesh of holes to allow more power through, but this did not produce a satisfactory Q. A transmission cavity was designed and constructed such that both mirrors had open ends of waveguides in their centres, but this did not produce sufficient power storage to generate any sort of Q.

The final spectrometer cavity design (Figure VII.2.4) was of the Fabry-Perot semi-confocal type, with a mirror separation of 5 cm (or about 25 wavelengths) and a radius of curvature of 24 cm for the bottom mirror. The fixed plane top mirror was constructed out of non-magnetic brass and the curved movable bottom mirror from copper, both being electro-plated with gold for chemical protection, since gold sputtering or no protection proved to be inadequate and seriously degraded the Q. Radiation was coupled in and out of

Dimensions - mm

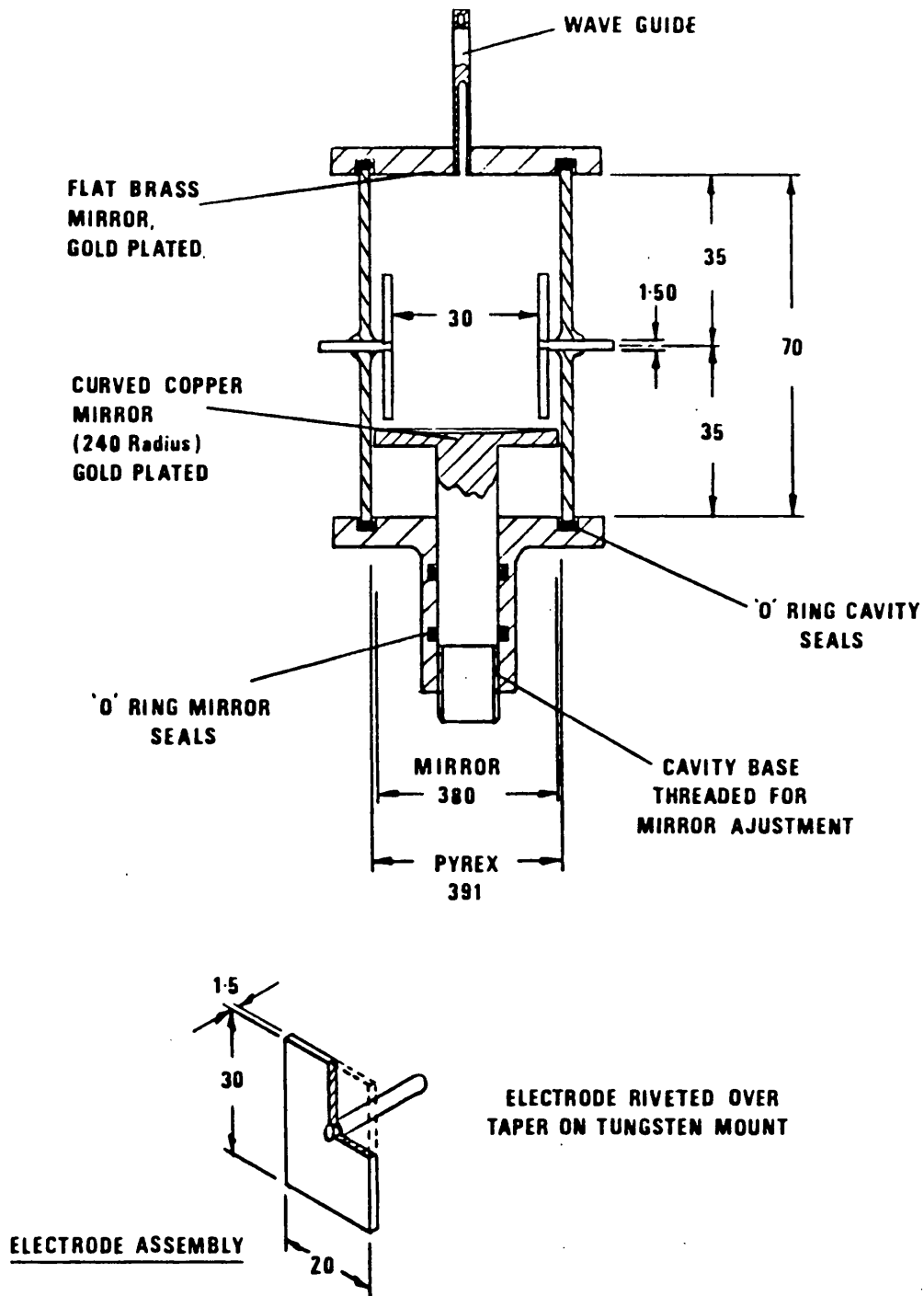


Figure VII.2.4. Scale drawing of the Fabry-Perot cavity used in the spectrometer. Not shown are the inlet and outlet ports to Pyrex vacuum assembly and the power supply used to drive the DC discharge.

SECTION VII.2 - DEVELOPMENTAL

the cavity through the open end of the waveguide mounted in the centre of the plane mirror: in the balance between obtaining a high cavity Q (i.e. utilising the smallest possible coupling hole) and high power collection (i.e. utilising the largest possible hole) this proved to be the best possible solution.

The radius of curvature of the mirror was optimised using a computer program (QCALC, Appendix IV) based upon the power profiles across the mirror given by Kogelnik and Li⁷, and the cavity Q was calculated to be 13 000, in reasonable agreement with the observed value of 10 000. This value was obtained by plotting the signal on the detector as the IMPATT power supply was electrically tuned through the cavity mode dip and the half way points of this dip taken as its width. This value was then converted into a frequency from the calibration graphs supplied with the IMPATT oscillator and divided by the oscillating frequency to obtain the value for the Q . This yields an effective pathlength of 4 m. To prevent excessive pick-up of noise via eddy currents induced in the waveguide by the modulating field, and to protect the IMPATT oscillator from the electric discharge (Figure VII.2.4), it proved necessary to insert mica isolation discs between the components at the points shown in Figure VII.2.3.

In practice the IMPATT oscillator was tuned to provide high power output: this was measured directly using a DVM to monitor the output from the detector with the slide screw tuner set to provide 100% reflection of the incident power. After withdrawal of the slide-screw tuner, the cavity was tuned into resonance by means of the movable bottom mirror. No frequency locking was required, since the IMPATT source

SECTION VII.2 - DEVELOPMENTAL

proved stable over the period required for spectrum acquisition. In its present configuration, the spectrometer is limited by detector noise, as indicated by negligible increase in detector output noise on direct irradiation by the full output power of the IMPATT oscillator. The sensitivity of the spectrometer could thus clearly be improved by using a superior commercially available detector such as the G965D supplied by Alpha Industries Inc. The current Flann detector (Model 2851) has a reported sensitivity of 20 mV/mW whilst the Alpha version reports a sensitivity of 200 mV/mW.

VII.3 EXPERIMENTAL

The millimeter wave magnetic resonance spectrometer in spectrum acquisition mode as described in Section VII.2 was set up with the relevant glassware, similar to that used with the EPR cavity (Section V.3). Oxygen, O₂, was flowed through the vacuum system at a measured pressure of 3.0 mBar and the magnetic field set to scan in 0.1 T intervals from 0.05 T. The modulation supplied to the Helmholtz coils was set to 4 kHz and at a magnetic field of 0.6670 T a signal of first derivative line shape was obtained on the chart recorder.

VII.4 RESULTS AND DISCUSSION

Figure VII.4.1 shows the first result obtained employing the spectrometer as described in Section VII.2, and (to the author's knowledge) the first high resolution spectroscopic observation utilising a millimeter wave IMPATT oscillator as a source. This signal arises from the $m_j=0 \leftrightarrow m_j=-1$ magnetic component of the $N=1, J=0 \leftrightarrow J=1$ transition of the O₂ molecule

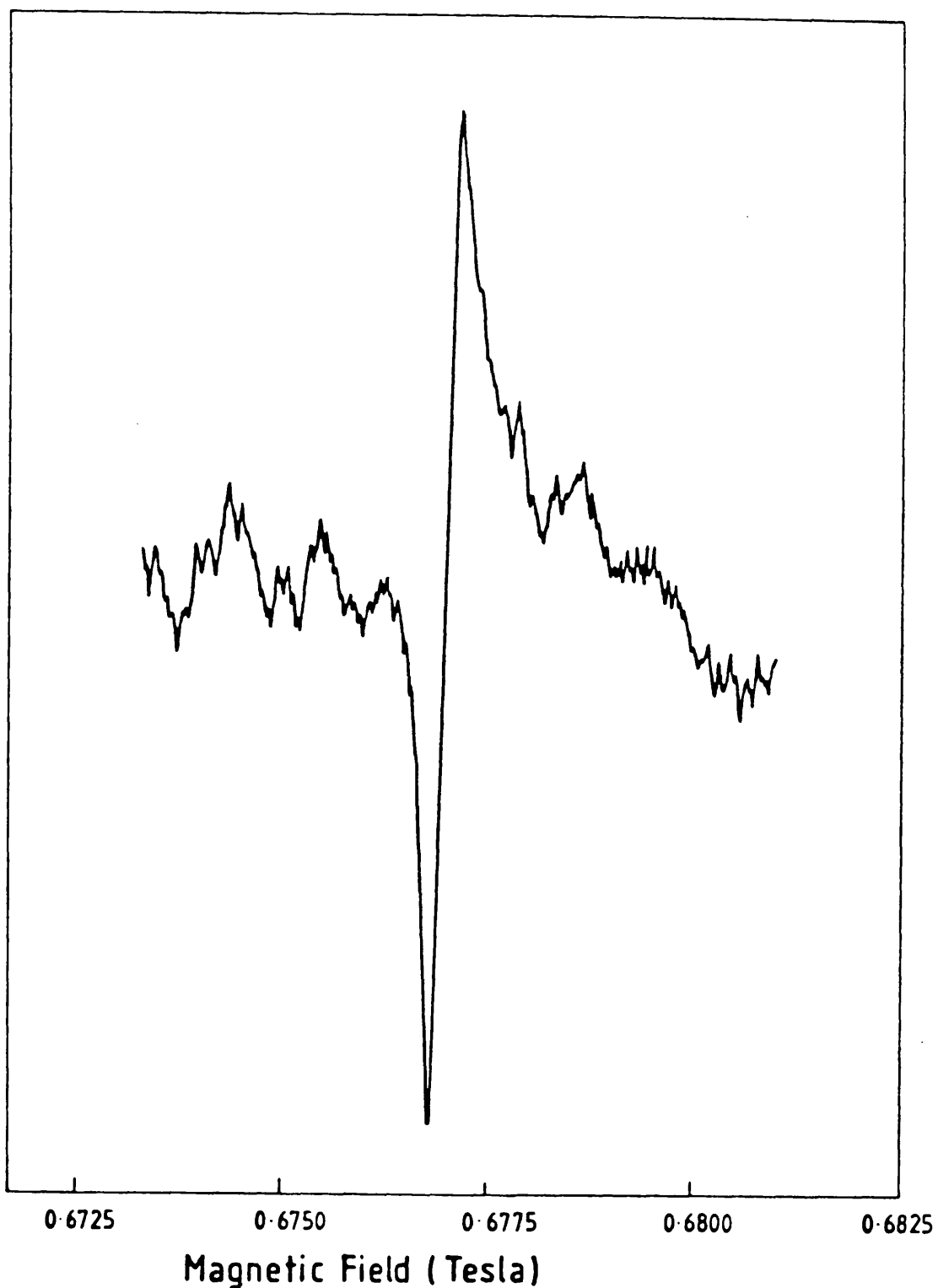


Figure VII.4.1. Millimeter wave magnetic resonance spectrum of the $m_j = 0 + m_j = -1$ component of the $N = 1, J = 0 + 1$ transition in O_2 . Pressure of $O_2 = 3.0$ mBar, sweep time = 2.5 mT min^{-1} , time constant 3 s; modulation frequency = 4.0 kHz; IMPATT oscillator frequency = 131.6 ± 0.1 GHz.

SECTION VII.4 - RESULTS AND DISCUSSION

(zero field frequency 118.75 GHz⁸), tuned into resonance with the IMPATT oscillator set at 131.6 GHz by means of a magnetic field of 0.677 T. While the S/N ratio of the spectrum is not impressive at 15:1 it should be noted that this represents an intrinsically weak magnetic dipole transition (1000 times weaker than an electric dipole transition). With the added sensitivity of the Alpha Industries Inc. detector and a more favourable candidate for detection this should be considerably improved.

VII.5 CONCLUSIONS

In Chapters III and VI electrical glow discharges have been investigated as sources of short-lived species. Electrodes have been installed (Figure VII.2.3) to provide a DC discharge operating parallel to the magnetic field within the spectrometer cavity. Such a discharge has been used with considerable success in IDL, microwave and LMR spectroscopies⁹⁻¹⁵, and has considerable potential as a source of free radicals and ions in the millimeter wave magnetic resonance spectrometer cavity. The noise characteristics of this discharge have proved excellent at its operating frequencies confirming its potential as a radical source.

The sensitivity of the spectrometer could be improved by using a superior commercially available detector such as the G965D supplied by Alpha Industries Inc. The millimeter wave resonance spectrometer's tuning range of 131-138 GHz and the added tuning of the magnetic field (up to approximately 20 GHz for 1.0 T), on paramagnetic species allows an approximate spectrometer range to be specified. Any

SECTION VII.5 - CONCLUSIONS

paramagnetic species with tunable transition(s) within the range 110-160 GHz should be detectable with the spectrometer provided a detectable concentration can be generated. Table VII.5.1 shows a list of possible candidates.

Species	Transition Frequency /GHz	Reference
NS	115 - 117	16
S ₂	125	17
SO	127	18
SeO	115	19
SiF	120 - 121	20
HO ₂	119 - 136	21
PH ₂	143	22
PO ₂	116 - 141	23
CH ₃ O	137 - 141	24

Table. VII.5.1. Table showing transient species potentially detectable by the millimeter wave magnetic resonance spectrometer.

SECTION VII.5 - CONCLUSIONS

Although this thesis has discussed either atoms or radicals it seems pertinent here to mention that since the DC discharge as a means of generating species does not impair the spectrometer's detection system the distinct possibility of detecting ions inside the cavity arises. This has been achieved successfully using LMR spectroscopy¹¹⁻¹⁵, and providing a sufficient concentration can be generated the millimeter wave resonance spectrometer shows considerable potential in this area.

VII.6 REFERENCES

1. A.F.Krupnov, in "Modern Aspects of Microwave Spectroscopy", edited by G.W.Chantry, Academic Press, London 1979, p.217.
2. W.Gordy, in "Handbook of Physics" (2nd edition), edited by E.U.Condon and H.Odishaw, McGraw-Hill, New York 1967, Ch.VI.
3. For example, D.K.Russell, in "Electron Spin Resonance", edited by P.B.Ayscough (Specialist Periodical Reports), The Chemical Society, London 1983, p1.
4. K.M.Evenson, Proceedings of the British Radio Frequency Group Spring Meeting, Cambridge (1984).
5. N.A.Isaacs & D.K.Russell, Rev. Sci. Inst., (In Press) (1986).
6. Plessey Microwave Electronics, Fig.3, Publication No. 6116 (1984).
7. H.Kogelnik & T.Li, App. Optics, 5, 1550 (1966).
8. R.S.Anderson, C.M.Johnson & W.Gordy, Phys. Rev., 83, 1061 (1951).
9. P.B.Davies, N.A.Isaacs, S.A.Johnson & D.K.Russell, J. Chem. Phys., 83, 2060 (1985); N.A.Isaacs & D.K.Russell unpublished results.
10. T.A.Dixon & R.C.Woods, Phys. Rev. Lett., 34, 61 (1975).
11. R.C.Woods, T.A.Dixon, R.J.Saykally & P.G.Szanto, Phys. Rev. Lett., 35, 1269 (1975).
12. R.J.Saykally, T.A.Dixon, T.G.Anderson, P.G.Szanto & R.C. Woods, Astrophys. J., 205, L101 (1976).
13. R.J.Saykally & K.M.Evenson, Phys. Rev. Lett., 43, 515 (1979).
14. D.Ray, K.G.Lubic & R.J.Saykally,

SECTION VII.6 - REFERENCES

- Mol. Phys., 46, 217 (1982).
15. D.C.Hovde, E.Schafer, S.E.Strahan, C.A.Ferrari, R.Ray,
K.G.Lubic & R.J.Saykally, Mol. Phys., 52, 245 (1984).
16. T.Amano, S.Saito, E.Hirota & Y.Morino,
J. Mol. Spec., 32, 97 (1969).
17. S.Saito, Y.Endo & E.Hirota,
J. Chem. Phys., 82, 2947 (1985).
18. H.M.Picket, & T.L.Boyd, J. Mol. Spec., 75, 53 (1979).
19. C.R.Parent & P.J.M.Kuijpers,
J. Chem. Phys., 40, 425 (1979).
20. M.Tanimoto, S.Saito, Y.Endo & E.Hirota,
J. Mol.Spec., 100, 205 (1983).
21. Y.Beers & C.J.Howard, J. Chem. Phys., 63, 4212 (1975).
22. Y.Endo, S.Saito, E.Hirota & T.Chikaraishi,
J. Mol. Spec., 77, 222 (1979).
23. K.Kawaguchi, S.Saito & E.Hirota,
J. Chem. Phys., 82, 4893 (1985).
24. Y.Endo, S.Saito & E.Hirota,
J. Chem. Phys., 81, 122 (1984).
-

GENERAL CONCLUSIONS

GENERAL CONCLUSIONS

Since the advent of the laser for the generation and detection of transient species, high resolution spectroscopy has become a growth area of scientific research. The laser provides high resolution spectroscopists with a relatively powerful and in some cases tunable source with which to detect these species, in concentrations which are relatively small, due to their inherent reactivities. This had led to proof of existence of a number species, which were postulated as the products of "curly arrows", after the break up of their precursors, and the spectra obtained provided sufficiently detailed data to establish their structures and molecular geometries. Other species which have been generated terrestrially have also been shown to exist in interstellar space as stable species in their own right.

It has become apparent that to obtain high resolution spectra of these transient species the overriding condition is the generation of a sufficiently high steady state concentration, which can be detected by the high resolution spectroscopic technique being employed. In Chapter II the most widely used device for this purpose, the microwave discharge, was shown to be an excellent method of generating these species. It does however have certain disadvantages when employed with microwave frequency detection systems in that its emission of noise precludes it functioning directly in the detection zone and as a consequence has to be positioned "upstream". This has proved to be a serious flaw in the generation of very short-lived transients in that their steady state concentrations have depleted to such a degree as to render them undetectable.

GENERAL CONCLUSIONS

In an attempt to circumvent this problem the electric glow discharge, as was demonstrated in Chapter III, has been installed in high resolution spectrometers to generate transients. Again this has proved to be a fruitful method of generating detectable concentrations with the added bonus of producing them in a variety of excited states. This method however also has a similar disadvantage to the microwave discharge in that it also generates an unacceptable level of "noise" when employed with microwave detection systems. However, it has been shown that it is possible utilise this transient generation method in the millimeter wave region of the electromagnetic spectrum.

One method for the generation of very short-lived transient species which does not produce excessive amounts of plasma related noise is photolysis by a carbon dioxide laser with an associated photosensitisation agent. It has been observed that the previous two methods interfere with microwave detection systems whereas this method does not. Preliminary results on this transient species generation scheme were presented in Chapter IV, and they suggest that it is a viable method provided the pathlength of the photolysis zone can be increased and the kinetics of the system under consideration can be established to ascertain whether a detectable steady state concentration can be established. Work is still very much in progress in this field to find even more efficient methods of generating transient species for high resolution spectroscopic detection.

Once a detectable steady state concentration has been achieved (with respect to the sensitivity of the particular

GENERAL CONCLUSIONS

high resolution spectroscopic technique being employed) the spectrum of the transient species under consideration can be observed. The information which the spectrum conveys depends upon which high resolution spectroscopic technique is being used. In Chapter V, electron paramagnetic resonance spectroscopy, was examined as a means of detecting transient paramagnetic radicals and atoms. Although the technique has achieved some remarkable successes in the past its sensitivity has now been surpassed by laser magnetic resonance and infrared diode laser spectroscopies and as a consequence the EPR spectra of transient species in the future are likely to have been detected, optimised and characterised by either of the above mentioned spectroscopic techniques previously. The EPR spectra of such species will however serve to complement either the LMR or IDL spectra obtained.

Chapter VI demonstrates this point clearly in the detection of the silicon hydride radical by both LMR spectroscopy in both the far-infrared and mid-infrared regions of the electromagnetic spectrum and by IDL spectroscopy whereas the radical's EPR spectrum is as yet undetected. The incidence of the number of recent papers reporting new IDL spectra of transient species is indicative of the power and flexibility of the technique: more are sure to follow.

The dearth of relatively powerful sources in the millimeter wave region of the electromagnetic spectrum has long proved to be a major handicap in the detection of many transient species' rotational transitions. Chapter VII reported a new millimeter wave source being incorporated in a

GENERAL CONCLUSIONS

magnetic resonance spectrometer which goes some way to plugging this gap as it shows considerable potential in the detection of transient species as its theoretical sensitivity approaches that of LMR spectroscopy.

The generation and high resolution spectroscopic detection of transient species in the gas phase has become, and will remain, an active field of scientific research as more and more chemical processes are found to be controlled by the concentration and nature of the transient species dictating the concentration and nature of the products.

APPENDIX I - EQUIPMENT AND CHEMICALS

APPENDIX I - EQUIPMENT AND CHEMICALS

CHAPTER II

Microwave Discharge:	Electro-Medical Supplies Microtron 200.
High Speed Pump:	Edwards High Vacuum E2M40.
Needle Valves:	Edwards High Vacuum LBIB Needle Valves.
Pressure Gauge:	Edwards High Vacuum Pirani 1001.
Pressure Heads:	Edwards High Vacuum PRH10.
EPR Spectrometer:	As Below.
Elemental Iodine:	BDH Laboratory Reagents.
Tetrafluoromethane:	British Oxygen - Special Gases.
Molecular Oxygen:	British Oxygen.

CHAPTER III

DC Power Supply for the EPR and MMR:	Constructed in this Laboratory.
EPR:	As Below.
High Speed Pump etc:	As Above.
DC power Supply for the IDL:	KSM Type HV I 6000-1.
Molecular Oxygen:	As Above.
Tetrafluoromethane:	As Above.
Elemental Sulphur:	BDH Laboratory Reagents.
Helium:	British Oxygen.
Silane:	British Oxygen - Special Gases.
Hydrogen:	British Oxygen.
Argon:	British Oxygen.

APPENDIX I - EQUIPMENT AND CHEMICALS

CHAPTER IV

Zinc Selenide Windows

and Lens:	Davin Optical Ltd. and Specac Ltd.
Univ. of Cambridge CO ₂ laser:	Apollo 550.
Univ. of Leicester CO ₂ laser:	Edinburgh Instruments PL-4.
Laser Power Meter:	Coherent Model 201.
Digital Multimeter:	ITT Instruments Services Thurlby Model 1503 HA.
EPR Spectrometer:	As Above.
Infrared Spectrometer:	Perkin Elmer 580B.
Microwave Discharge:	As Above.
High Speed Pump etc:	As Above.
Chopper:	Brookdeal Electronic Ltd. Model 9479.
Laser Gas Mixture:	British Oxygen - Special Gases.
1,1-Dimethylsilacyclobutane:	Courtesy of Dr.I.M.T.Davidson.
Sulphur Hexafluoride:	British Oxygen - Special Gases.
Vinyldimethylcarbinoxydi- methylsilane:	Courtesy of Dr.I.M.T.Davidson.
Dihydridosilacyclobutane:	Courtesy of Dr.I.M.T.Davidson..
Methyl Iodide:	BDH Laboratory Reagents.
Acetone:	BDH Laboratory Reagents.
Acetaldehyde:	BDH Laboratory Reagents.
Iron Pentacarbonyl:	Courtesy of Dr.R.D.W.Kemmit, Univ. of Leiceter.
Molecular Oxygen:	As Above.
Elemental Sulphur:	As Above.
Argon:	As Above.
Tetrafluorohydrazine:	Courtesy of Dr.P.B.Davies,

APPENDIX I - EQUIPMENT AND CHEMICALS

Univ. of Cambridge.

Selenium(I) Chloride: Cambrian Chemicals Ltd.

CHAPTER V

Microwave EPR bridge: Constructed in this Laboratory.

EPR Control Unit: Varian Associates V4500-10A.

X-Y Chart Recorder: JJ Instruments PL 1000.

PSD: Varian Associates V4560.

Electro-Magnet Power Supply: Varian Associates

Fieldial Mark II.

Electro-Magnet: Varian V4102.

High Speed Pump etc: As Above.

Microwave Discharge: As Above.

Stark DC bias Supply: Constructed in this Laboratory.

Nitric Oxide: British Oxygen - Special Gases.

Molecular Oxygen: As Above.

Hydrogen: As Above.

Nitrogen: British Oxygen.

Chlorine: British Oxygen - Special Gases.

Tetrafluoromethane: As Above.

Hydrogen Peroxide: BDH Laboratory Reagents.

Sulphur(I) Chloride: BDH Laboratory Reagents.

Methanol: BDH Laboratory Reagents.

Fluoro-sulphuronic Acid: BDH Laboratory Reagents.

Red Phosphorus: BDH Laboratory Reagents.

Metallic Arsenic: BDH Laboratory Reagents.

Selenium(I) Chloride: As above.

APPENDIX I - EQUIPMENT AND CHEMICALS

CHAPTER VI

Infrared Diode Laser: Laser Analytics (Spectra Physics Inc.).

Diode Cold Head: Air Products CSA-202.

Temperature Controller: Oxford Instruments Digital Temperature Controller - DTC2.

Current Controller: Arthur D. Little Inc. SCPS-II.

Waveform Generator: Prosser Scientific Instruments Ltd A101.

DC power Supply for the IDL: KSM Type HV I 6000-1.

Infrared Detector (InSb): Santa Barbara.

High Speed Chemical Pump: Alcatel.

PSD: Brookdeal 9412A.

Silane: As Above.

Helium: As Above.

Argon: As Above.

Hydrogen: As Above.

Nitrogen Dioxide: British Oxygen - Special Gases.

Nitric Oxide: As Above.

CHAPTER VII

IMPATT Oscillator: Plessey Microwave Electronics Model ATMO 280S.

Defective IMPATT

Power Supply: Plessey Microwave Electronics Model ATSM 200.

Zener Diode Circuit: Constructed in this Laboratory.

Digital Storage Oscilloscope: Farnell Digital Oscilloscope Model DTS 12P.

IMPATT Power Supply: Plessey Microwave Electronics

APPENDIX I - EQUIPMENT AND CHEMICALS

Model ATSM 301.

mm-Wave Waveguide Components: Flann Microwave Ltd.
mm-Wave Isolator: Hughs Aircraft Corporation.
Band/Notch Pass Filter: Brookdeal Electronics Ltd.
Model 5010.
Pre-amplifier: Brookdeal Electronics Ltd.
Model 5006.
Lock-in Amplifier: Brookdeal Electronics Ltd.
Model 9503 SC.
Reference Oscillator: Brookdeal Electronics Ltd.
Model 5012 F
X-Y Chart Recorder: As Above.
Oscilloscope: Solatron Electronics Group Ltd.
Model CD 1400.
Helmholtz Coils: Constructed in this Laboratory.
Modulation Oscillator: Advance Electronics
LF Signal Generator Type SG 66.
Electro-Magnet: As Above.
Gold Electro-plating: Courtesy of Physics Dept.
Univ. of Leicester.
High Speed Pump etc: As Above.
Molecular Oxygen: As Above.

APPENDIX II - PROGRAM OASPECPROGRAM DESCRIPTION

This program (written in BASIC for a DEC VAX/VMS) first simulates the EPR spectrum of the oxygen atom (O) from the measured positions of the signals of the experimental spectra. The intensities of this simulated spectrum are calculated from the relevant Boltzmann distribution and angular momentum factors. The program was written to display these spectra of a given line-width (pressure) on a BBC micro computer, acting as a graphics terminal in direct output mode. As each spectrum was simulated, its width (relative to the overall spread of the spectrum) was stored. A conversion factor for each spectrum was taken to be the maximum and minimum of the overall envelope of the six signals which make up the spectrum divided by the maximum and minimum of either of the centre two signals. At low pressures (widths), when the spectrum was fully resolved, this factor was one, but as the signal width was increased the centre four signals overlapped and its value varied. The conversion factor along with the width were then written to a file NAICV.DAT.

The calculation of the conversion factor was necessary to establish the true height of a 3P_2 signal from a given experimental envelope spectrum so that its intensity could be compared to that of the measured experimental 3P_1 signal to yield the desired "effective" temperature of the O atoms. This was achieved by first plotting the width of the signal (as a percentage of the 3P_1 distance) in the simulated spectrum against the calculated conversion factor for the spectrum. Secondly, the experimental signal heights of the 3P_1 and envelope were input into the program from the file OASPEC.DAT

APPENDIX II - PROGRAM OASPEC

along with some of the other experimental parameters for reference. The width of any given experimental spectrum was then used to calculate the actual height of the 3P_2 signal which was buried under the overlapped envelope and this corrected height along with that of the 3P_1 signal were used in a rearranged Boltzmann distribution calculation to yield the "effective" temperature. This value along with the experimental parameters was then written to the screen and to a file NAITEMP.DAT for later printing.

PROGRAM OASPEC

LINES	FUNCTION
210-500	Simulates EPR O atom spectrum.
510-780	Plots the conversion factor graph.
790-1290	Reads experimental data, calculates 3P_2 height and temperature.
1300-1410	Calculates maximum and minimum of simulated spectrum.
1420-1650	Plots simulated spectrum.
1790-1810	Assigns the conversion factor.
1820-1980	Prints the experimental parameters to the file and the screen.
1990-2040	Clears the text window on the BBC.

APPENDIX II - PROGRAM OASPEC

```
100 REM PROGRAM TO PLOT OXYGEN SPECTRUM
110 PRINT<ESC>"[2<ESC>J[H"
120 INPUT "DO YOU WANT TO CALCULATE THE CONVERSION FACTORS
(Y/N)";Y$
130 DIM X1(2000),Y1(2000),X2(2000),Y2(2000),W1(1000),C(1000),
C1(50)
140 DIM Y3(2000),M1(1000),M2(1000),M3(1000),M4(1000),P1(1000),
P2(1000)
150 DIM A(6),W(6),X(6),Y(6),X3(2000),Y5(1000),D5(50),H1(50),
H2(50),H3(50)
160 DIM T(50),W5(50),W6(50),O(50),S(50),P(50)
165 DIM Y11(2000),Y12(2000),Y13(2000),Y14(2000),Y15(2000),
Y16(2000)
170 DATA 0.33,-0.50000,0.67,-0.07554,1.0,-0.01799
180 DATA 1.0,0.03237,0.67,0.09712,0.33,0.50000
190 IF Y$="N" GOTO 510
200 OPEN "NAICV.DAT" FOR OUTPUT AS FILE E1%
210 FOR I5 =1 TO 100 STEP 10
220 W1(I5)=(I5/1000)
240 RESTORE
250 FOR I = 1 TO 6
260 READ A(I),X(I)
270 IF W1(I5)=0.0 GOTO 290
280 W(I)=(4/3/(W1(I5)^2))
290 NEXT I
310 X1(1)=(X(1)+X(2)+X(3)+X(4)+X(5)+X(6))/6
320 Y1(1)=0.0
330 M1(I5)=-1.0E+20
340 M2(I5)=+1.0E+20
350 M3(I5)=M1(I5)
```

APPENDIX II - PROGRAM OASPEC

```
360 M4(I5)=M2(I5)
370 FOR J = 2 TO 2000
375 Y1(J)=0.0
380 X1(J)=X1(1)-1.0 +(J/1000)
390 FOR K = 1 TO 6
400 Y(K)=A(K)*(X1(J)-X(K))/(1+(W(K)*((X1(J)-X(K))^2))^2
410 IF K=1 THEN Y(1)=Y(1)*EXP(-158.3/(0.69503*298.15))
420 IF K=6 THEN Y(6)=Y(6)*EXP(-158.3/(0.69503*298.15))
421 IF K=1 THEN Y11(J)=Y(K)
422 IF K=2 THEN Y12(J)=Y(K)
423 IF K=3 THEN Y13(J)=Y(K)
424 IF K=4 THEN Y14(J)=Y(K)
425 IF K=5 THEN Y15(J)=Y(K)
426 IF K=6 THEN Y16(J)=Y(K)
430 Y1(J)=Y1(J)+Y(K)
440 NEXT K
450 X3(J)=X1(J)
460 Y3(J)=Y1(J)
470 GOSUB 1300
480 NEXT J
490 GOSUB 1420
500 NEXT I5
510 REM PLOTS CV GRAPH FROM HERE
520 X5=M2
530 X6=M1
540 Y5=M2
550 Y6=M1
555 PRINT<ESC>"[2<ESC>J[H"
560 INPUT "DO YOU WISH TO PLOT THE CONVERSION FACTOR GRAPH";N$
570 IF N$="N" GOTO 2040
```

APPENDIX II - PROGRAM OASPEC

```
575 OPEN "NAICV.DAT" FOR INPUT AS FILE £1%, &
      ORGANIZATION SEQUENTIAL
580 FOR I=1 TO 100
590 INPUT £1%, W1(I);C(I)
600 W1(I)=W1(I)*100.0
610 IF W1(I) < X5 THEN X5=W1(I)
620 IF W1(I) > X6 THEN X6=W1(I)
630 IF C(I) < Y5 THEN Y5=C(I)
640 IF C(I) > Y6 THEN Y6=C(I)
650 NEXT I
660 CALL PAPER(1)
680 CALL PSPACE(0.1,0.95,0.1,0.95)
690 CALL MAP(X5,X6,Y5,Y6)
700 CALL AXES
710 CALL POSITN(W1(1),C(1))
720 FOR J=2 TO 100
730 CALL JOIN(W1(J),C(J))
740 NEXT J
745 CALL CTRMAG(15)
750 Y=Y5-(Y6/15.0)
760 CALL PCSEND(X6,Y,"PERCENTAGE WIDTH OF TRIPLET P1'S
DISTANCE",41)
770 CALL CTRORI(90.0)
780 CALL PLOTCS(X5-(X6/15.0),Y6-((Y6-Y5)/1.75),"CONVERSION
FACTOR",16)
790 K=1
795 OPEN "OASPEC.DAT" FOR INPUT AS FILE £2%, &
      ORGANIZATION SEQUENTIAL
800 GOSUB 1990
801 PRINT "O2 PRESS."
```

APPENDIX II - PROGRAM OASPEC

```

802 PRINT "(MBAR)"
803 INPUT £2%, O(K);S(K);P(K);D5(K);W6(K);H1(K);H2(K)
804 PRINT O(K)
805 PRINT"SF6 PRESS."
806 PRINT"(MBAR)"
808 PRINT S(K)
810 PRINT"LASER"
820 PRINT"POWER"
830 PRINT"(W)"
845 PRINT P(K)
860 PRINT"3P1S' DIST."
870 PRINT"(mm)"
885 PRINT D5(K)
900 PRINT"EXP. WIDTH"
910 PRINT"(mm)"
925 PRINT W6(K)
930 W5(K)=(W6(K)/D5(K))*100.0
980 REM CUTTING TO ONE DECIMAL PLACE
990 W5(K)=(INT((W5(K)*10.0)+0.5))/10.0
1000 CALL POSITN (W5(K),0.0)
1005 F=0
1010 FOR J=2 TO 100
1020 IF ABS(W5(K)-W1(J)) < 0.01 THEN F=1
1030 IF F=1 THEN CALL JOIN (W5(K),C(J))
1040 IF F=1 THEN GOSUB 1790
1050 NEXT J
1060 FOR I = 1 TO 50
1070 CALL POSITN(W5(K),C1(K))
1080 CALL JOIN(0.0,C1(K))
1090 NEXT I

```

APPENDIX II - PROGRAM OASPEC

```

1100 PRINT"3P1 HEIGHT (mm)"
1115 PRINT H1(K)
1130 PRINT"EXP. 3P2"
1140 PRINT"HEIGHT (mm)"
1155 PRINT H2(K)
1170 H3(K)=H2(K)/C1(K)
1180 PRINT
1190 T(K)=158.3/0.69503/LOG((H3(K)*0.33333333)/H1(K))
1195 T(K)=INT(T(K)+0.5)
1200 PRINT
1210 PRINT"TEMP=";T(K);"K"
1220 PRINT
1240 INPUT "MORE";Y$
1250 K=K+1
1260 IF Y$="Y" THEN GOTO 800
1270 CALL GREND
1280 IF Y$="N" THEN GOSUB 1820
1290 GOTO 2040
1300 REM SUBROUTINE TO DETERMINE YMIN AND YMAX
1310 IF Y3(J) > M1(I5) THEN M1(I5)=Y3(J)
1320 IF Y3(J) < M2(I5) THEN M2(I5)=Y3(J)
1330 IF Y14(J) > M3(I5) THEN M3(I5)=Y14(J)
1335 IF Y14(J) < M4(I5) THEN M4(I5)=Y14(J)
1370 IF J=2000 THEN P1(I5)=ABS(M3(I5))+ABS(M4(I5))
1380 IF J=2000 THEN P2(I5)=ABS(M1(I5))+ABS(M2(I5))
1395 REM ENVELOPE/RESOLVED ABOVE LINE ^
1400 IF J=2000 THEN PRINT E1%, W1(I5);", "; C(I5)
1410 RETURN
1420 REM SUBROUTINE TO PLOT SPECTRUM
1430 X1=X3(2)

```

APPENDIX II - PROGRAM OASPEC

```

1440 X2=X3(2000)
1450 Y1=M2(I5)
1460 Y2=M1(I5)
1470 LET I1 = INT(1.0)
1480 IF I5=1 THEN CALL PAPER(I1)
1490 CALL FRAME
1500 CALL PSPACE(0.1,0.95,0.1,0.95)
1510 CALL MAP(X1,X2,Y1,Y2)
1520 CALL POSITN(X3(2),Y3(2))
1530 FOR N = 2 To 2000
1540 CALL JOIN(X3(N),Y3(N))
1550 NEXT N
1551 CALL REDPEN
1552 CALL POSITN(X3(2),Y11(2))
1554 FOR N = 2 To 2000
1556 CALL JOIN(X3(N),Y11(N))
1558 NEXT N
1560 CALL POSITN(X3(2),Y12(2))
1562 FOR N = 2 To 2000
1564 CALL JOIN(X3(N),Y12(N))
1566 NEXT N
1568 CALL POSITN(X3(2),Y13(2))
1570 FOR N = 2 To 2000
1572 CALL JOIN(X3(N),Y13(N))
1574 NEXT N
1576 CALL POSITN(X3(2),Y14(2))
1578 FOR N = 2 To 2000
1580 CALL JOIN(X3(N),Y14(N))
1582 NEXT N
1584 CALL POSITN(X3(2),Y15(2))

```

APPENDIX II - PROGRAM OASPEC

```

1586 FOR N = 2 To 2000
1588 CALL JOIN(X3(N),Y15(N))
1590 NEXT N
1592 CALL POSITN(X3(2),Y16(2))
1594 FOR N = 2 To 2000
1596 CALL JOIN(X3(N),Y16(N))
1598 NEXT N
1599 CALL BLKPEN
1600 PRINT "3P2R MIN="
1601 PRINT M4(I5)
1602 PRINT "3P2R MAX="
1603 PRINT M3(I5)
1604 PRINT "3P2E MIN="
1610 PRINT M2(I5)
1620 PRINT "3P2E MAX="
1630 PRINT M1(I5)
1640 IF I5=100 THEN CALL GREND
1650 RETURN
1790 REM SUBROUTINE TO PRINT AND STORE CONVERSION FACTOR
1800 C1(K)=C(J)
1805 F=F+1
1810 RETURN
1820 REM SUBROUTINE TO PRINT THE TEMPERATURE DATA TO THE FILE
1830 PRINT"POWER","3P1'S DIST.,""EXP. WIDTH","3P1 HEIGHT","3P2
HEIGHT", &
      "TEMP."
1840 PRINT" (W) "," (mm) "," (mm) "," (mm) ","
(mm) "," (K) "
1850 PRINT"_____"", "_____"", "_____"", "_____"",
"_____"", "_____"

```

APPENDIX II - PROGRAM OASPEC

```

1860 PRINT
1870 OPEN "NAITEMP.DAT" FOR OUTPUT AS FILE £2%
1880 FOR K1= 1 TO K-1
1890 PRINT P(K1),D5(K1),W6(K1),H1(K1),H2(K1),T(K1)
1900 NEXT K1
1910 PRINT £2, "POWER", "3P1'S DIST.", "EXP. WIDTH", "3P1
HEIGHT", "3P2 HEIGHT", "TEMP."
1920 PRINT £2, " (W) ", " (mm) ", " (mm) ", " (mm) ",
" (mm) ", " (K) "
1930 PRINT £2, "_____", "_____", "_____", "_____",
"_____", "_____"
1940 PRINT £2
1950 FOR K1= 1 TO K-1
1960 PRINT £2, P(K1),D5(K1),W6(K1),H1(K1),H2(K1),T(K1)
1970 NEXT K1
1980 RETURN
1990 REM SUBROUTINE TO POKE SCREEN
2000 PRINT CHR$(12)
2010 PRINT CHR$(12)
2020 PRINT CHR$(30)
2025 PRINT "SPEC. NO."
2027 PRINT K
2030 RETURN
2040 END

```

APPENDIX III - PROGRAM NAI2PIVPROGRAM DESCRIPTION

This program was written in FORTRAN for the CDC CYBER computer. It first prompts for a set of molecular constants which must be stored on the data file SIHCONS.DAT. It then reads these constants into the program via the SUBROUTINE CONSTS. The program then sets up the quantum numbers for the P-, Q- and R-Branch vibrational-rotation levels for the first twenty rotational levels. As each set of quantum numbers for a particular level are calculated a SUBROUTINE CALC is called and the Hamiltonian matrix elements for these quantum numbers are calculated. The Hamiltonian contains the terms which describe the interactions between the various angular momenta involved (electron spin and orbital, nuclear rotational angular momentum coupled according to Hund's case (a) (spin-orbit coupling is large) in addition to contributions from rotation, centrifugal distortion and vibrations). The resultant matrix elements are set up in a two by two matrix, and this matrix is diagonalised by calling a standard NAG library routine (FO2AAF). The NAG routine then returns the eigenvalues of this diagonalisation, and these values constitute the energies of the particular level in question. These energies are then stored and used to calculate the transition frequencies. The relative strength or intensity of each transition is also calculated by using the Boltzmann factor of the levels involved in the transition (relative to the lowest energy level calculated) together with the appropriate angular momentum factors. The predicted transition frequencies and strengths can then either be displayed in tabulated form at the terminal, or plotted by calling the SUBROUTINE GRAPHIC, which writes the graphical

information to the data file SIHPIC.DAT.

The program can also fit these predicted transition frequencies to any number of observed transition frequencies which are stored on the data file SIHDATA.DAT by applying a least squares fitting procedure which is contained in the SUBROUTINE LSQRS. This fitting procedure reads the assigned quantum numbers and their transition frequency from the data file SIHDATA.DAT and calculates the energy of the levels involved in the transition by calling the SUBROUTINE CALC. The fitting is achieved by varying the molecular parameters slightly to calculate the differential coefficients of the observed transitions with respect to the varying parameters, the number and identity of which maybe specified (eg. the spin-orbit coupling constant of the first vibrational state ($v=1$) is parameter number 2), and this data is held on the data file SIHCONS.DAT after the actual values of the constants. This is done in an iterative procedure (the number of iterations is also held on the same data file). The program then prints an RMS error which indicates the quality of the fit, the final calculated transition frequencies, the matrix of eigenvectors to indicate the correlation of the calculated molecular parameters with each other, and the best fit values of these molecular parameters with their standard deviations.

PROGRAM MODULE

NAI2PIV

Calculates the quantum numbers
for the P-,Q-,R- vibration
rotational levels, calculates
the transition frequencies and
their relative strengths and

APPENDIX III - PROGRAM NAI2PIV

prints them out in tabulated form.

SUBROUTINE CALC

Sets up the terms of the Hamiltonian in the matrix, diagonalises the matrix for a given set of quantum numbers and stores the eigenvalues (energy levels).

SUBROUTINE CONSTS

Reads in the molecular constants for the v=0 and v=1 states.

SUBROUTINE GRAPHIC

Plots the transition frequencies against their relative strengths.

SUBROUTINE LSQRS

Reads in the observed transitions and their assigned quantum numbers, calculates the differential coefficients, varies the molecular constants, calculates the predicted transitions from the assigned quantum numbers best fits and prints them after the iterations.

SUBROUTINE QNOSO

Puts the assigned quantum numbers for the v=0 level in a correct form for CALC.

SUBROUTINE QNOS1

Puts the assigned quantum numbers for the v=1 level in a correct form for CALC.

APPENDIX III - PROGRAM NAI2PIV

PROGRAM NAI2PIV

IMPLICIT DOUBLE PRECISION (A-H,O-X,Z)

COMMON/CALLERS/J,IPARITY,M,IVIT,I

COMMON/CONSTS/A(2),B(2),D(2),P(2),Q(2),PD(2),QD(2),GA(2),
+H(2),V(2)

COMMON/BLOCK/AA(2,2),BB(2),W(25),PI1L(40),PI2L(40),
+PI1U(40),PI2U(40)

COMMON/QN/VO(90),JO(90),PARO(90),OHMO(90),V1(90),
+J1(90),PAR1(90),OHM1(90),FR(90),WT(90),ASSIG(90)

DIMENSION PLOWER1(20),PUPPER1(20),QLOWER1(20),QUPPER1(20)
+,RLOWER1(20),RUPPER1(20)

DIMENSION PLOWER2(20),PUPPER2(20),QLOWER2(20),QUPPER2(20)
+,RLOWER2(20),RUPPER2(20),XTION(6,60),STR(6,60)

REAL J,JO,J1,OHMO,OHM1

INTEGER VO,V1

OPEN(UNIT=9,FILE='SIHCONS.DAT',STATUS='OLD')

OPEN(UNIT=8,FILE='SIHPIC.DAT',STATUS='NEW')

OPEN(UNIT=7,FILE='SIHDATA.DAT',STATUS='OLD')

Z=1.38066E-23

T=698.15

HX=1.98648E-23

CALL CONSTS

C P-BRANCH TRANSITIONS DELTA J=-1

M=1

DO 13 L1=1,6

DO 14 L2=1,40

XTION(L1,L2)=0.0

STR(L1,L2)=0.0

14 CONTINUE

13 CONTINUE

APPENDIX III - PROGRAM NAI2PIV

```

DO 17 IVIT=1,2
DO 19 N=1,20
DO 18 IPARIT2=1,2
IF (IPARIT2.EQ.2) IPARITY=-1
IF (IPARIT2.EQ.1) IPARITY=+1
IF (IVIT.EQ.1) J=N+0.5
IF (IVIT.EQ.2) J=N-0.5
IF (IVIT.EQ.2) IPARITY=IPARITY*(-1)
CALL CALC
IF (IVIT.EQ.1) PLOWER1(M+2)=PI1L(M)
IF (IVIT.EQ.1) PLOWER2(M+2)=PI2L(M)
IF (IVIT.EQ.2) PUPPER1(M+2)=PI1U(M)
IF (IVIT.EQ.2) PUPPER2(M+2)=PI2U(M)
IF (IVIT.EQ.2) XTION(1,M+2)=PUPPER1(M+2)-PLOWER1(M+2)
IF (IVIT.EQ.1) STR(1,M+2)=EXP(-((PLOWER1(M+2)-
+14.34911303)*HX)/(Z*T))*(((J)**2)-((0.5)**2))/J)
IF (IVIT.EQ.2) XTION(4,M+2)=PUPPER2(M+2)-PLOWER2(M+2)
IF (IVIT.EQ.1) STR(4,M+2)=EXP(-((PLOWER2(M+2)-
+14.34911303)*HX)/(Z*T))*(((J)**2)-((1.5)**2))/J)
C Q-BRANCH TRANSITIONS DELTA J=0
IF (IVIT.EQ.1) J=N-0.5
IF (IVIT.EQ.2) J=N-0.5
CALL CALC
IF (IVIT.EQ.1) QLOWER1(M)=PI1L(M)
IF (IVIT.EQ.1) QLOWER2(M)=PI2L(M)
IF (IVIT.EQ.2) QUPPER1(M)=PI1U(M)
IF (IVIT.EQ.2) QUPPER2(M)=PI2U(M)
IF (IVIT.EQ.2) XTION(2,M)=QUPPER1(M)-QLOWER1(M)
IF (IVIT.EQ.1) STR(2,M)=EXP(-((QLOWER1(M)-
+14.34911303)*HX)/(Z*T))*(((2*J)+1.0)*(0.5)**2)

```

APPENDIX III - PROGRAM NAI2PIV

```

+/(J*(J+1.0))
  IF (IVIT.EQ.2) XTION(5,M)=QUPPER2(M)-QLOWER2(M)
  IF (IVIT.EQ.1) STR(5,M)=EXP(-((QLOWER2(M)-
+14.34911303)*HX)/(Z*T))*(((2*J)+1.0)*(1.5)**2)/
+(J*(J+1.0))

```

C R-BRANCH TRANSITIONS DELTA J=+1

```

  IF (IVIT.EQ.1) J=N-0.5
  IF (IVIT.EQ.2) J=N+0.5
  CALL CALC
  IF (IVIT.EQ.1) RLOWER1(M)=PI1L(M)
  IF (IVIT.EQ.1) RLOWER2(M)=PI2L(M)
  IF (IVIT.EQ.2) RUPPER1(M)=PI1U(M)
  IF (IVIT.EQ.2) RUPPER2(M)=PI2U(M)
  IF (IVIT.EQ.2.AND.J.EQ.1.5) RUPPER2(M)=0.0
  IF (IVIT.EQ.2) XTION(3,M)=RUPPER1(M)-RLOWER1(M)
  IF (IVIT.EQ.1) STR(3,M)=EXP(-((RLOWER1(M)-
+14.34911303)*HX)/(Z*T))*(((J+1.0)**2)-((0.5)**2))
+/(J+1.0)
  IF (IVIT.EQ.2) XTION(6,M)=RUPPER2(M)-RLOWER2(M)
  IF (IVIT.EQ.1) STR(6,M)=EXP(-((RLOWER2(M)-
+14.34911303)*HX)/(Z*T))*(((J+1.0)**2)-((1.5)**2))
+/(J+1.0)
  M=M+1

```

18 CONTINUE

19 CONTINUE

M=1

17 CONTINUE

DO 69 N1=1,40

DO 59 K=1,6

IF (XTION(K,N1).LT.0) XTION(K,N1)=0.0

APPENDIX III - PROGRAM NAI2PIV

```

59 CONTINUE
69 CONTINUE
    WRITE(*,987)
987 FORMAT(1X,'DO YOU WANT TO SEE THE POSITIONS AND STRENGTHS
    +(Y/N)')
    READ(*,990) PRINT
990 FORMAT(A1)
    IF (PRINT.NE.'Y') GOTO 50
    WRITE(*,7777)
7777 FORMAT(1X,/,/, ' J ',6X,' P(1) ',3X,' Q(1) ',3X,' R(1)
+ ',6X,' P(2) ',3X,' Q(2) ',3X,' R(2) ',/)
    J=0.5
    DO 49 N1=1,40,2
    WRITE (*,700) J,(XTION(I,N1),I=1,3),(XTION(I,N1),I=4,6)
    WRITE (*,800) (STR(I,N1),I=1,3),(STR(I,N1),I=4,6)
    WRITE (*,800) (XTION(I,N1+1),I=1,3),(XTION(I,N1+1),I=4,6)
    WRITE (*,900) (STR(I,N1+1),I=1,3),(STR(I,N1+1),I=4,6)
700 FORMAT(1X,F4.1,3X,3F11.3,3X,3F11.3)
800 FORMAT(1X,7X,3F11.3,3X,3F11.3)
900 FORMAT(1X,7X,3F11.3,3X,3F11.3,/)
    J=J+1.0
49 CONTINUE
50 CONTINUE
    WRITE(8,925)
925 FORMAT(1X,' BLK')
    DO 79 L3=1,6
    DO 89 L4=1,40
    WRITE(8,*) XTION(L3,L4),STR(L3,L4)
89 CONTINUE
79 CONTINUE

```

APPENDIX III - PROGRAM NAI2PIV

```

WRITE(8,975)
975 FORMAT(1X,'-1 -1',/, ' FIN')
WRITE (*,888)
888   FORMAT(1X,'DO YOU WISH TO PLOT THE POSITIONS AND
+STRENGTHS (Y/N)')
READ (*,666) YESPLOT
666   FORMAT(A1)
IF (YESPLOT.EQ.'Y') CALL GRAPHIC
CALL LSQRS
END
SUBROUTINE CALC
IMPLICIT DOUBLE PRECISION (A-H,O-X,Z)
COMMON/CALLERS/J,IPARITY,M,IVIT,I
COMMON/CONSTS/A(2),B(2),D(2),P(2),Q(2),PD(2),QD(2),GA(2)
+,H(2),V(2)
COMMON/BLOCK/AA(2,2),BB(2),W(25),PI1L(40),PI2L(40),
+PI1U(40),PI2U(40)
COMMON/QN/VO(90),JO(90),PARO(90),OHMO(90),V1(90),
+J1(90),PAR1(90),OHM1(90),FR(90),WT(90),ASSIG(90)
REAL J,JO,J1,OHMO,OHM1
INTEGER VO,V1
C   PI1 HOLDS DOUBLET PI 1/2 ENERGIES, PI2 HOLD2 DOUBLET PI
C   3/2 ENERGIES
II=IPARITY
DO 2090 K=1,2
BB(K)=0.0
DO 2090 L=1,2
2090 AA(K,L)=0.0
IJ=J-0.49
IK=II*(-1.0)**IJ

```

APPENDIX III - PROGRAM NAI2PIV

C DOUBLET PI 3/2 TERMS:

```

AA(2,2)=V(IVIT)+(0.5*A(IVIT))+B(IVIT)*((J*(J+1))-0.75)
+-D(1)*(((J**2)*(J+1)**2)-(1.5*J*(J+1)))
+-0.5*IK*QD(1)*(J+0.5)*ZOOM(J)**2
++H(1)*((J**3)*(J+1)**3)

```

C DOUBLET PI 1/2 TERMS:

```

AA(1,1)=V(IVIT)+B(IVIT)*((J*(J+1))+1.25)-GA(1)
+-D(1)*(((J**2)*(J+1)**2)+(2.5*J*(J+1)))
+-0.5*IK*(P(1)+2*Q(1))*(J+0.5)
+-0.5*IK*(PD(1)+2*QD(1))*(J+0.5)*(ZOOM(J)**2+2)
+-0.5*IK*QD(1)*(J+0.5)*ZOOM(J)**2
+-0.5*A(IVIT)
++H(1)*((J**3)*(J+1)**3)

AA(2,1)=-((B(IVIT)-GA(1))/2-2*D(1)*(J+0.5)**2)
+-0.5*IK*Q(1)*(J+0.5)-0.25*IK*(PD(1)+2*QD(1))*(J+0.5)
+-0.5*IK*QD(1)*(J+0.5)**3)*ZOOM(J)

AA(1,2)=AA(2,1)

IF (J.EQ.0.5) BB(1)=AA(1,1)

IK=II

IF (J.EQ.0.5) GOTO 7

NUM2=2

NUMO=0

CALL FO2AAF(AA,NUM2,NUM2,BB,W,NUMO)

```

7 CONTINUE

```

IF (IVIT.EQ.1) PI1L(M)=BB(1)
IF (IVIT.EQ.1) PI2L(M)=BB(2)
IF (IVIT.EQ.2) PI1U(M)=BB(1)
IF (IVIT.EQ.2) PI2U(M)=BB(2)

RETURN

END

```

APPENDIX III - PROGRAM NAI2PIV

```

FUNCTION ZOOM (R)
IMPLICIT DOUBLE PRECISION (A-H,O-X,Z)
ZOOM=SQRT((R+1.5)*(R-0.5))
RETURN
END

SUBROUTINE CONSTS
IMPLICIT DOUBLE PRECISION (A-H,O-X,Z)
COMMON/CALLERS/J,IPARITY,M,IVIT,I
COMMON/CONSTS/A(2),B(2),D(2),P(2),Q(2),PD(2),QD(2),
+GA(2),H(2),V(2)
COMMON/BLOCK/AA(2,2),BB(2),W(25),PI1L(40),PI2L(40),
+PI1U(40),PI2U(40)
COMMON/QN/VO(90),JO(90),PARO(90),OHMO(90),V1(90),
+J1(90),PAR1(90),OHM1(90),FR(90),WT(90),ASSIG(90)
CHARACTER Y*1
DO 3225 I=0,1
3010 CONTINUE
WRITE(*,3020) I
3020 FORMAT(1X,'INPUT THE VIBRATIONAL ENERGY IN CM-1
+FOR THE V(' ,I1,' ) STATE')
READ(9,3025) V(I+1)
WRITE(*,*) 'V=',V(I+1)
3025 FORMAT(F10.6)
3030 WRITE (6,3060) I
3060 FORMAT(1X,'INPUT THE SPIN-ORBIT COUPLING CONSTANT IN CM-1
+IN THE V(' ,I1,' ) STATE')
READ(9,3066) A(I+1)
WRITE(*,*) 'A=',A(I+1)
3066 FORMAT(F10.4)
WRITE (6,3080) I

```

APPENDIX III - PROGRAM NAI2PIV

```

3080 FORMAT(1X,'INPUT THE ROTATIONAL CONSTANT IN CM-1
+IN THE V( ',I1,' ) STATE')
      READ(9,3086) B(I+1)
      WRITE(*,*) 'B=',B(I+1)
3086 FORMAT(F10.6)
      WRITE (6,3100) I
3100 FORMAT(1X,'INPUT THE CENTRIFUGAL CONSTANT IN CM-1
+IN THE V( ',I1,' ) STATE')
      READ(9,3106) D(I+1)
      WRITE(*,*) 'D=',D(I+1)
3106 FORMAT(F10.8)
      WRITE (6,3120) I
3120 FORMAT(1X,'INPUT THE LAMBDA-DOUBLING CONSTANT P IN
+CM-1 IN THE V( ',I1,' ) STATE')
      READ(9,3126) P(I+1)
      WRITE(*,*) 'P=',P(I+1)
3126 FORMAT(F10.8)
      WRITE (6,3140) I
3140 FORMAT(1X,'INPUT THE LAMBDA-DOUBLING CONSTANT Q IN
+CM-1 IN THE V( ',I1,' ) STATE')
      READ (9,3146) Q(I+1)
      WRITE(*,*) 'Q=',Q(I+1)
3146 FORMAT(F10.8)
      WRITE (6,3160) I
3160 FORMAT(1X,'INPUT THE LAMBDA-DOUBLING CONSTANT PD IN
+CM-1 IN THE V( ',I1,' ) STATE')
      READ(9,3166) PD(I+1)
      WRITE(*,*) 'PD=',PD(I+1)
3166 FORMAT(F12.10)
      WRITE (6,3180) I

```

APPENDIX III - PROGRAM NAI2PIV

```

3180 FORMAT(1X,'INPUT THE LAMBDA-DOUBLING CONSTANT QD IN
+CM-1 IN THE V(' ,I1,' ) STATE')
      READ (9,3186) QD(I+1)
      WRITE(*,*) 'QD=',QD(I+1)
3186 FORMAT(F12.10)
      WRITE (6,3200) I
3200 FORMAT(1X,'INPUT THE SPIN-ROTATION CONSTANT IN CM-1
+IN THE V(' ,I1,' )STATE')
      READ (9,3206) GA(I+1)
      WRITE(*,*) 'GA=',GA(I+1)
3206 FORMAT(F10.8)
      WRITE(*,3216) I
3216 FORMAT(1X,'INPUT THE SIXTH ORDER DISTORTION TERM H
+FOR THE V(' ,I1,' ) STATE')
      READ(9,3217) H(I+1)
      WRITE(*,*) 'H=',H(I+1)
3217 FORMAT(F10.8)
      WRITE(*,3215) I
3215 FORMAT(1X,'CONSTANTS CORRECT FOR THE V(' ,I1,' )
+STATE (Y/N)')
      READ (5,3218) Y
3218 FORMAT(A1)
      WRITE(*,3218) Y
      IF (Y.NE.'Y') GOTO 3010
3225 CONTINUE
      RETURN
      END
      SUBROUTINE GRAPHIC
      COMMON/CALLERS/J,IPARITY,M,IVIT,I
      COMMON/CONSTS/A(2),B(2),D(2),P(2),Q(2),PD(2),QD(2),GA(2),

```

APPENDIX III - PROGRAM NAI2PIV

```

+H(2),V(2)
COMMON/BLOCK/AA(2,2),BB(2),W(25),PI1L(40),PI2L(40),
+PI1U(40),PI2U(40)
COMMON/QN/VO(90),JO(90),PARO(90),OHMO(90),V1(90),
+J1(90),PAR1(90),OHM1(90),FR(90),WT(90),ASSIG(90)
DIMENSION AG(100,2)
DIMENSION OPT(5)
DATA OPT/4H BLK,4H BLU,4H GRN,4H RED,4H FIN/
CALL PAPER(1)
CALL PSPACE(0.1,0.90,0.1,0.90)
C WRITE(*,55)
WRITE(*,56)
56 FORMAT(/,1X,'ENTER WAV. MIN. AND WAV. MAX. ')
READ(*,*) VAL,VLL
WRITE(*,57)
57 FORMAT(/,1X,'ENTER MIN. STR. TO BE PLOTTED ')
READ(*,*) SMIN
REWIND 8
1 READ(8,100) OP
100 FORMAT(A4)
I=1
IF (OP.EQ.OPT(1)) CALL BLKPEN
IF (OP.EQ.OPT(2)) CALL BLUPEN
IF (OP.EQ.OPT(3)) CALL GRNPEN
IF (OP.EQ.OPT(4)) CALL REDPEN
IF (OP.EQ.OPT(5)) GOTO 30
CALL MAP(VAL,VLL,0.0,10.0)
DO 10 I=1,100
READ(8,*) AG(I,1),AG(I,2)
IF (AG(I,1)+AG(I,2).EQ.-2) GOTO 20

```

APPENDIX III - PROGRAM NAI2PIV

```

IF(AG(I,1).LT.VAL.OR.AG(I,1).GT.VLL) GOTO 10
IF(AG(I,2).LT.SMIN) GOTO 10
CALL POSITN(AG(I,1),0)
CALL JOIN(AG(I,1),AG(I,2))
10 CONTINUE
20 GOTO 1
30 CONTINUE
CALL BLKPEN
CALL AXES
CALL PLOTCS(0.7*VAL+0.3*VLL,-0.8,'WAVENUMBER CM-1',17)
CALL CTRORI(1.0)
CALL PLOTCS(1.1*VAL-0.1*VLL,2.5,'STRENGTH',9)
CALL GREND
RETURN
END
SUBROUTINE LSQRS
IMPLICIT DOUBLE PRECISION (A-H,O-X,Z)
COMMON/CALLERS/J,IPARITY,M,IVIT,I
COMMON/CONSTS/A(2),B(2),D(2),P(2),Q(2),PD(2),QD(2),GA(2),
+H(2),V(2)
COMMON/BLOCK/AA(2,2),BB(2),W(25),PI1L(40),PI2L(40),
+PI1U(40),PI2U(40)
COMMON/QN/VO(90),JO(90),PARO(90),OHMO(90),V1(90),
+J1(90),PAR1(90),OHM1(90),FR(90),WT(90),ASSIG(90)
DIMENSION VV(20,20),SIGMA(20),SIGMAP(20),QQ(20),WWW(20)
DIMENSION DN(20),DD(20,20),DX(20,20),C(20)
DIMENSION IPAR(20),DI(90,20),RES(90),W1(90),W2(90)
DIMENSION PAR(20)
EQUIVALENCE (A(1),PAR(1))
CHARACTER TITLES*60,ULINE*60

```

APPENDIX III - PROGRAM NAI2PIV

```

REAL J,JO,J1,OHMO,OHM1
INTEGER VO,V1
E11=0
E12=0
E21=0
E22=0
E31=0
E32=0
WRITE(*,777)
777  FORMAT(1X,'DO YOU WANT TO SEE THE OBSERVED TRANSITIONS
+(Y/N)')
READ(*,888) YESDATA
888  FORMAT(A1)
READ(9,*) NPAR,NIT
READ(9,*) (IPAR(I),I=1,NPAR)
READ(7,444) TITLES
IF (YESDATA.EQ.'Y') WRITE(*,444) TITLES
444  FORMAT(1X,A60)
READ(7,333) ULINE
IF (YESDATA.EQ.'Y') WRITE(*,333) ULINE
333  FORMAT(1X,A60)
NN=1
222  CONTINUE
READ(7,11) SPACE,VO(NN),JO(NN),PARO(NN),OHMO(NN),V1(NN),
+J1(NN),PAR1(NN),OHM1(NN),FR(NN),WT(NN),ASSIG(NN)
IF (YESDATA.EQ.'Y') WRITE(*,12) VO(NN),JO(NN),PARO(NN),
+OHMO(NN),V1(NN),J1(NN),PAR1(NN),OHM1(NN),FR(NN),
+WT(NN),ASSIG(NN)
11  FORMAT(A1,I1,2X,F3.1,2X,A1,2X,F3.1,2X,I1,2X,F3.1,2X,A1,
+2X,F3.1,3X,F8.3,2X,F3.1,2X,A20)

```

APPENDIX III - PROGRAM NAI2PIV

```

12  FORMAT(1X,I1,2X,F3.1,2X,A1,2X,F3.1,2X,I1,2X,F3.1,2X,A1,
      +2X,F3.1,3X,F8.3,2X,F3.1,2X,A20)
      IF (FR(NN).EQ.0.0) GOTO 555
      NN=NN+1
      GOTO 222
555  NN=NN-1
      TOT=0.0
      DO 1280 I=1,NN
1280 TOT=TOT+WT(I)
      IF (NIT.EQ.0) GO TO 1660
      DO 1650 II=1,NIT
      SUMSQ=0.0
      DO 1420 I=1,NN
      CALL QNOSO
      CALL CALC
      IF (OHMO(I).EQ.0.5) E11=BB(1)
      IF (OHMO(I).EQ.1.5) E11=BB(2)
C    WRITE(*,*) 'J=',J,' IPARITY=',IPARITY,' OHMO(',I,')=',
C    +OHMO(I),' E11=',E11,' V=',(IVIT-1)
      CALL QNOS1
      CALL CALC
      IF (OHM1(I).EQ.0.5) E12=BB(1)
      IF (OHM1(I).EQ.1.5) E12=BB(2)
C    WRITE(*,*) 'J=',J,' IPARITY=',IPARITY,' OHMO(',I,')=',
C    +OHMO(I),' E12=',E12,' V=',(IVIT-1)
      E1=E12-E11
      DO 1400 JJ=1,NPAR
      DEL=0.001
      IF (PAR(IPAR(JJ)).NE.0.0) DEL=0.001*PAR(IPAR(JJ))
      PAR(IPAR(JJ))=PAR(IPAR(JJ))+DEL

```

APPENDIX III - PROGRAM NAI2PIV

```

C      WRITE(*,*) PAR(IPAR(JJ))
      CALL QNOSO
      CALL CALC
      IF (OHMO(I).EQ.0.5) E21=BB(1)
      IF (OHMO(I).EQ.1.5) E21=BB(2)
      CALL QNOS1
      CALL CALC
      IF (OHM1(I).EQ.0.5) E22=BB(1)
      IF (OHM1(I).EQ.1.5) E22=BB(2)
      E2=E22-E21
      PAR(IPAR(JJ))=PAR(IPAR(JJ))-DEL
1400  DI(I,JJ)=(E2-E1)/DEL
      RES(I)=FR(I)-E1
1420  SUMSQ=SUMSQ+RES(I)*RES(I)*WT(I)
      RMS=SQRT(SUMSQ/TOT)
      WRITE (6,1450) RMS
1450  FORMAT(1X,/, ' RMS ERROR IS ',F12.7,/)
      DO 1459 IIZ=1,NN
      IF (ABS(RES(IIZ)).LT.10.0*RMS) GO TO 1459
      WT(IIZ)=0.1*WT(IIZ)
      WRITE (6,1455) ASSIG(IIZ)
1455  FORMAT(1X, ' TRANSITION ',A9, ' HAS BEEN REDUCED IN
      +WEIGHT' )
1459  CONTINUE
      DO 1490 IL=1,NPAR
      DN(IL)=0.0
      DO 1490 JJ=1,NPAR
1490  DD(IL,JJ)=0.0
      DO 1550 IP=1,NPAR
      DO 1520 K=1,NN

```

APPENDIX III - PROGRAM NAI2PIV

```

1520 DN(IP)=DN(IP)+DI(K,IP)*RES(K)*WT(K)
      DO 1550 JJ=1,NPAR
      DO 1550 K=1,NN
1550 DD(IP,JJ)=DD(IP,JJ)+DI(K,IP)*DI(K,JJ)*WT(K)
      DO 1580 IR=1,NPAR
      DO 1580 JJ=1,NPAR
1580 DX(IR,JJ)=DD(IR,JJ)
      NUM20=20
      NUM100=100
      NUMO=0
      CALL FO4ATF(DD,NUM20,DN,NPAR,C,DI,NUM100,W1,W2,NUMO)
      DO 1610 IS=1,NPAR
1610 PAR(IPAR(IS))=PAR(IPAR(IS))+C(IS)
      WRITE (6,1630) II
1630 FORMAT(1X,///,' ITERATION NO. ',I2,/)
1650 CONTINUE
1660 WRITE (6,1670)
1670 FORMAT(1X,///,' FINAL CALCULATED FREQUENCIES',/)
      WRITE (6,1690)
1690 FORMAT(1X,' NO OBS.FREQ    CALC.FREQ    ERROR        WT
+ASSIGNMENT',/)
      SUMSQ=0.0
      DO 1755 I=1,NN
      CALL QNOSO
      CALL CALC
      IF (OHMO(I).EQ.0.5) E31=BB(1)
      IF (OHMO(I).EQ.1.5) E31=BB(2)
      CALL QNOS1
      CALL CALC
      IF (OHM1(I).EQ.0.5) E32=BB(1)

```

APPENDIX III - PROGRAM NAI2PIV

```

IF (OHM1(I).EQ.1.5) E32=BB(2)
EE=E32-E31
RES(I)=FR(I)-EE
SUMSQ=SUMSQ+RES(I)*RES(I)*WT(I)
WRITE(*,1760) I,FR(I),EE,RES(I),WT(I),ASSIG(I)
1755 CONTINUE
1760 FORMAT(1X,I4,F10.4,F11.4,F7.4,2X,F8.5,2X,A10)
RMS=SQRT(SUMSQ/TOT)
WRITE (6,1450) RMS
IF (NIT.EQ.0) GO TO 1970
CALL FO2ABF(DD,NUM20,NPAR,QQ,VV,NUM20,WWW,NUMO)
WRITE (6,1810)
1810 FORMAT(1X,/, ' QQ          SIGMA  ',/)
DO 1840 M=1,NPAR
SIGMA(M)=SQRT(SUMSQ/(QQ(M)*(NN-NPAR)))
1840 WRITE (6,1900) QQ(M),SIGMA(M)
1900 FORMAT(1X,2F15.7)
WRITE (6,1870)
1870 FORMAT(1X,/, ' MATRIX OF EIGENVECTORS ',/)
DO 1890 IT=1,NPAR
1890 WRITE (6,4001) (VV(IT,JJ),JJ=1,NPAR)
4001 FORMAT(1X,24F5.2)
DO 1930 JJ=1,NPAR
SIGM=0.0
DO 1925 IU=1,NPAR
SIGM=SIGM+VV(JJ,IU)*VV(JJ,IU)*SIGMA(IU)*SIGMA(IU)
1925 CONTINUE
1930 SIGMAP(JJ)=SQRT(SIGM)
WRITE (6,1945)
1945 FORMAT(1X,/, '          CONSTANT          STAND. DEV. ',/)

```

APPENDIX III - PROGRAM NAI2PIV

```

WRITE(*,1905)(PAR(IPAR(IV)),SIGMAP(IV),IV=1,NPAR)
1905 FORMAT(1X,F20.10,F15.10)
1970 CONTINUE
      WRITE (6,1990)
1990 FORMAT (/,' THATS IT, FOLKS - BYE!')
      RETURN
      END
      SUBROUTINE QNOSO
      IMPLICIT DOUBLE PRECISION (A-H,O-X,Z)
      COMMON/CALLERS/J,IPARITY,M,IVIT,I
      COMMON/CONSTS/A(2),B(2),D(2),P(2),Q(2),PD(2),QD(2),GA(2),
+H(2),V(2)
      COMMON/BLOCK/AA(2,2),BB(2),W(25),PI1L(40),PI2L(40),
+PI1U(40),PI2U(40)
      COMMON/QN/VO(90),JO(90),PARO(90),OHMO(90),V1(90),
+J1(90),PAR1(90),OHM1(90),FR(90),WT(90),ASSIG(90)
      REAL J,JO,J1,OHMO,OHM1
      INTEGER VO,V1
      J=JO(I)
      IF (PARO(I).EQ.'+') IPARITY=+1
      IF (PARO(I).EQ.'-') IPARITY=-1
      IVIT=VO(I)+1
      RETURN
      END
      SUBROUTINE QNOS1
      IMPLICIT DOUBLE PRECISION (A-H,O-X,Z)
      COMMON/CALLERS/J,IPARITY,M,IVIT,I
      COMMON/CONSTS/A(2),B(2),D(2),P(2),Q(2),PD(2),QD(2),GA(2),
+H(2),V(2)
      COMMON/BLOCK/AA(2,2),BB(2),W(25),PI1L(40),PI2L(40),

```

APPENDIX III - PROGRAM NAI2PIV

```

+PI1U(40),PI2U(40)
COMMON/QN/VO(90),JO(90),PARO(90),OHMO(90),V1(90),
+J1(90),PAR1(90),OHM1(90),FR(90),WT(90),ASSIG(90)
REAL J,JO,J1,OHMO,OHM1
INTEGER VO,V1
J=J1(I)
IF (PAR1(I).EQ.'+') IPARITY=+1
IF (PAR1(I).EQ.'-') IPARITY=-1
IVIT=V1(I)+1
RETURN
END

```

APPENDIX IV - PROGRAM QCALC

APPENDIX IV - PROGRAM QCALC

PROGRAM DESCRIPTION

This program (which was written in BASIC for both the CDC CYBER and DEC VAX/VMS computers) calculates the power storage factor (the Q) for a Fabry-Perot semi-confocal resonator based upon the formulae of Kogelnik and Li. The program initially prompts for a set of cavity dimensions and the wavelength of the radiation under consideration and these variables are then used in the formulae to calculate the beam sizes (in centimeters) at each of the mirrors, and the percentage loss both from the edges of the mirrors and through the coupling hole. The values of these parameters for each of the mirrors are then printed to the terminal along with the Q of a cavity of the input dimensions.

PROGRAM QCALC

LINES	FUNCTION
100-340	Input the cavity dimensions.
350-500	Calculates the beam waists, percentage loss at each mirror and the Q.
502-590	Prints the results in tabulated form.

APPENDIX IV - PROGRAM QCALC

```

00100 PRINT"EFFECTIVE Q CALCULATION PROGRAM"
00110 PRINT"-----"
00120 PRINT
00130 PRINT
00140 PRINT"INPUT THE RADIUS OF CURVATURE OF THE MIRROR WITH"
00150 PRINT"THE COUPLING HOLE IN IT (M) ";
00160 INPUT R1
00170 PRINT
00180 PRINT"INPUT THE RADIUS OF CURVATURE OF THE OTHER MIRROR
(M) ";
00190 INPUT R2
00200 PRINT
00210 PRINT"INPUT THE DIAMETER OF THE MIRROR WITH THE COUPLING
HOLE IN IT (M) ";
00220 INPUT C1
00230 PRINT
00240 PRINT"INPUT THE DIAMETER OF THE OTHER MIRROR (M) ";
00250 INPUT C2
00260 PRINT
00270 PRINT"INPUT THE AREA OF THE COUPLING HOLE (M^2) ";
00280 INPUT A1
00285  $A1=A1/2$ 
00287  $A1=SQR(A1/3.142)$ 
00290 PRINT
00300 PRINT"INPUT THE LENGTH OF THE SPACE BETWEEN THE TWO
MIRRORS (M) ";
00310 INPUT D
00320 PRINT
00330 PRINT"INPUT THE WAVELENGTH OF THE RADIATION (M) ";
00340 INPUT L

```

APPENDIX IV - PROGRAM QCALC

```

00350 C1=C1/2
00360 C2=C2/2
00370 W1=SQR(((L*R1/3.142)^2)*((R2-D)/(R1-D))*(D/(R1+R2-D)))
00380 W2=SQR(((L*R2/3.142)^2)*((R1-D)/(R2-D))*(D/(R2+R1-D)))
00400 X1=1-EXP(-2*(A1^2)/W1)
00405 Y1=X1*100
00410 X2=EXP(-2*(C1^2)/W1)
00415 Y2=X2*100
00420 X3=EXP(-2*(C2^2)/W2)
00425 Y3=X3*100
00430 Q=(2*3.142*D)/(L*(X1+X2+X3+X4))
00470 B1=2*SQR(W1)*100
00500 B2=2*SQR(W2)*100
00502 PRINT
00504
PRINT"-----"
00506 PRINT"!          PROPERTY          ! MIRROR WITH HOLE ! OTHER
MIRROR !"
00508
PRINT"!-----!-----!-----!"
00510 PRINT"!          !          !"
!"
00512 PRINT"! BEAM WAIST (CM) !      ";B1"      !      ";B2"      !"
00514 PRINT"!          !          !"
!"
00516 PRINT"! EDGES LOSS (%)      !      ";Y2"      ! ";Y3"      !"
00518 PRINT"!          !          !"
!"
00520 PRINT"! HOLE LOSS (%)      !      ";Y1"      !      -      !"
00522 PRINT"!          !          !"

```

APPENDIX IV - PROGRAM QCALC

!"

00524

PRINT"-----"

00526 PRINT

00527 PRINT" EFFECTIVE Q = ";Q

00528 PRINT

00529 PRINT

00530 PRINT" ANOTHER CALCULATION (Y/N) ";

00540 INPUT Y\$

00550 PRINT

00560 PRINT

00570 IF Y\$="Y" GOTO 00100

00580 STOP

00590 END

THE GENERATION AND HIGH RESOLUTION SPECTROSCOPIC DETECTION
OF FREE RADICALS IN THE GAS PHASE

Ph.D. Thesis submitted by Neil Alan Isaacs in February
1986

The assignment and analysis of high resolution spectra of transient species in the gas phase leads to the unambiguous identification of the carrier of the spectra. Such spectra can only be observed provided a detectable steady state concentration, depending on the particular spectroscopic technique being employed, can be generated. The first half of this thesis is concerned with three methods of producing detectable concentrations by utilising (i) microwave discharge, (ii) electrical discharge, (iii) carbon dioxide laser photolysis with an associated photosensitiser, sulphur hexafluoride. The high resolution electron paramagnetic resonance spectra of iodine and fluorine atoms and the sulphur monoxide and nitrogen difluoride radicals serve as examples of species produced by these methods and some characteristics of the laser photolysis technique are described in Chapter IV.

The advent of the infrared semiconductor diode laser and also a solid state millimeter wave source (an IMPATT oscillator, in conjunction with the technique of magnetic resonance) has led to the development of more sensitive high resolution spectroscopic techniques. High resolution spectra of the important silicon monohydride radical have been observed using the former technique and the experiments and subsequent analysis are described in Chapter VI. The millimeter wave magnetic resonance spectrometer designed and constructed by the author is described in Chapter VII, together with the millimeter wave magnetic resonance spectrum of the oxygen molecule, the first spectrum to be observed by this new technique.
